Development of a predictive cellular model to assess biomaterial-modulated immunoresponses of macrophages *in vitro*

Dissertation

der Mathematisch-Naturwissenschaftlichen Fakultät

der Eberhard Karls Universität Tübingen

zur Erlangung des Grades eines

Doktors der Naturwissenschaften

(Dr. rer. nat.)

vorgelegt von

Sören Segan

aus Troisdorf

Tübingen

2020

Gedruckt mit Genehmigung der Mathematisch-Naturwissenschaftlichen Fakultät der Eberhard Karls Universität Tübingen.

Tag der mündlichen Qualifikation:	06.05.2021
Dekan:	Prof. Dr. Thilo Stehle
1. Berichterstatter:	Prof. Dr. Ulrich Rothbauer
2. Berichterstatter:	Prof. Dr. Peter Loskill

CONTENT

FIGURES

TABLES

ABBREVATIONS

AB	antibody
CB	chromobody
CD	cluster of differentiation
CMV	cytomegalovirus
CRISPR	clustered regularly interspaced short palindromic repeats
DAPI	4′,6-diamidino-2-phenylindole
EDTA	ethylenediaminetetraacetic acid
EF1-α	elongation factor 1 alpha
ELISA	enzyme linked immunosorbent assay
FACS	fluorescence activated cell sorting
FBGC	foreign body giant cells
FBR	foreign body reaction
FCS	fetal calf serum
GAPDH	glyceraldehyde 3-phophate dehydrogenase
GFP	green fluorescent protein
IDO	indoleamine-pyrrole 2,3-dioxygenase
IF	immunofluorescence
IFN	interferon
IL	interleukin
NOS2	nitric oxid synthase 2
PBMCs	peripheral blood mononuclear cells
PEM	polyelectrolyte multilayer
$phalloidin_{AF555}$	Phalloidin Alexa Fluor 555
PMA	phorbol 12-myristate 13-acetate
RFP	red fluorescence protein
ROS	reactive oxygen species
S.D.	standard derivation
SDS-PAGE	sodium dodecyl sulfate polyacrylamide gel electrophoresis
SEM	Scanning electron microscopy
TBST	Tris-buffered saline with Tween20
TEMED	N′-tetramethylethylenediamine
TG2	transglutaminase 2
VEGF	vascular endothelial growth factor
V_H	variable domain of heavy chain
VHH	variable domain of heavy-chain-only antibody
V_L	variable domain of light chain
w/v	weight per volume

1 ZUSAMMENFASSUNG

Biomaterialien sind aus der medizinischen Praxis nicht mehr wegzudenken. Implantate und medizinische Geräte wie Gefäßprothesen, Herzklappen, Zahnimplantate oder Herzschrittmacher und Biosensoren verbessern die Lebensqualität von Patienten, indem sie natürliche Funktionen übernehmen oder ersetzen. Trotz ihrer breiten und erfolgreichen Anwendung bei Patienten löst die Implantation von Medizinprodukten Entzündungsreaktionen aus. Da das Ausmaß der induzierten Immunreaktionen den Langzeiterfolg von Implantaten erheblich beeinflusst, ist es für das Design und die Entwicklung neuartiger Biomaterialien von besonderem Interesse, diese Wirts-Material-Reaktionen vorherzusagen. Durch den Einsatz von *in vitro* Tests auf der Basis menschlicher Zellen kann eine prädiktive Aussage über die Reaktionen nach der Implantation getroffen werden. Es fehlen jedoch Studien, die den Einfluss spezifischer Oberflächeneigenschaften in dieser Hinsicht untersuchen. Zudem wird die Beurteilung von Immunreaktionen auf Biomaterialien bisher hauptsächlich durch Endpunkt-Assays erfüllt, was im Widerspruch zu den räumlich dynamischen Veränderungen der Entzündung im menschlichen Körper steht.

Es wird postuliert, dass die Oberflächeneigenschaften von Biomaterialien nicht nur den entzündlichen Phänotyp von Makrophagen beeinflussen, sondern dass dieser Phänotyp sich auch in der zellulären Morphologie und der Organisation des Zytoskeletts widerspiegelt. In dieser Dissertation wurde ein Makrophagenmodell auf der Basis der monozytären Zelllinie THP-1 entwickelt, um Biomaterial-induzierte Reaktionen zu beurteilen. Nach chemischer Stimulation spiegelte sich der entzündliche Makrophagen-Phänotyp in morphologischen Veränderungen wider. Allerdings konnten Biomaterial-induzierte Veränderungen in der Morphologie der Makrophagen nicht mit der Entzündungsreaktion in Verbindung gebracht werden. Dennoch konnte mit Hilfe eines auf der Organisation des Aktin-Zytoskelett basierenden Readouts eine tendenzielle Korrelation zur Zytokinsekretion gezeigt werden. Um diese Veränderungen in lebenden Zellen nachzuverfolgen, wurde ein Aktin-spezifischer Biosensor (Aktin-Chromobody) stabil in THP-1-Zellen eingebracht. In einer proof-or-principle Studie wurde die stabile THP-1_Aktin-CB-Zelllinie verwendet, um den Effekt der Hydrophobizität auf die Entzündungsreaktion, die Makrophagenmorphologie und die Zytoskelettorganisation in lebenden Zellen zu verfolgen.

Zusammengefasst wurde in dieser Dissertation mit der Entwicklung eines THP-1 Zellen abgeleiteten Makrophagenmodells ein robustes und empfindliches Zellmodell zur *in vitro*

Bestimmung von Immunreaktionen auf Biomaterialien etabliert und umfangreich auf verschiedensten Biomaterialien getestet. Während die Morphologie der Makrophagen nicht direkt mit dem entzündlichen Phänotyp in Zusammenhang zu stehen scheint, deuten charakteristische Veränderungen des Aktin-Zytoskeletts daraufhin, dass sich der Polarisationszustand der Makrophagen prinzipiell über eine optische Nachverfolgung bestimmen lässt. Die hier gemachten Untersuchungen zeigen aber auch, dass ein optischer Nachweis die biochemische Bestimmung von Entzündungsfaktoren wie z.B. Zytokinen nicht ersetzen kann.

2 ABSTRACT

Biomaterials have become indispensable in medical practice. Implants and medical devices such as vascular grafts, heart valves, dental implants, or pacemakers and biosensors improve patients' quality of life by replacing or substituting natural functions. Despite their broad and successful application in patients, implantation of medical products triggers inflammatory responses. Since the extend of the induced immune reactions significantly affects the long-term success of implants, it is of particular interest for the design and development of novel biomaterials to predict these host-material reactions. By employing *in vitro* tests based on human cells, a predictive statement can be made regarding the host responses following implantation. However, to date the assessment of immune reactions to biomaterials is mainly fulfilled by endpoint assays, which contradicts the spatial dynamic changes of inflammation in the human body.

It is postulated that biomaterial surface properties not only affect the inflammatory phenotype of macrophages but that this phenotype is also reflected by the cellular morphology and cytoskeleton organization. In this dissertation, a macrophage model based on the monocytic cell line THP-1 was developed to assess biomaterial-induced responses. Upon chemical stimulation, the inflammatory macrophage phenotype was reflected by morphological changes. However, biomaterial-induced changes in macrophage morphology could not be linked to the inflammatory response. Nevertheless, employing a readout based on actin cytoskeleton formations a trend correlation to the cytokine secretion could be shown. To allow to trace these changes in living cells, the previously described actin-chromobody was stably introduced into THP-1 cells. For illustrating a possible application, the stable THP-1_actin-CB cell line was used to monitor the effect of hydrophobicity on the inflammatory response, macrophage morphology and cytoskeleton organization in living cells.

Taken together, the THP-1 derived macrophage model provides a robust and sensitive tool to determine immune responses to biomaterials *in vitro*. While macrophage morphology does not seem to be directly related to the inflammatory phenotype, actin cytoskeleton organization indicated the macrophage polarization state. Replacement of cytokine measurement as well as the application of a high throughput approach are not possible.

3 INTRODUCTION

3.1 Biomaterials

Biomaterials are substances that have been "…engineered to take a form which, alone or as part of a complex system, is used to direct, by control of interactions with components of living systems, the course of any therapeutic or diagnostic procedure, … " (Williams, 2009). Humankind 's use of biomaterials dates to antiquity when all kinds of natural materials were used. Prosthesis fashioned from wood as well as artificial teeth of stone can be found in egyptian mummies (Patel & Gohil, 2012). Over the centuries, naturally derived materials began to be replaced by manufactured materials, such as iron and gold (Saini, Singh, Arora, Arora, & Jain, 2015). Since the early parts of the twentieth century, the first biomaterials as we know them today were applied: metals (titanium alloys, cobalt-chrom, gold, etc.), ceramics (alumina, zirconia, etc.), and polymers (polyurethane, polymethylmetacrylate, etc.) were used to manufacture implants. These advancements in the field of materials led to an increased functionality and higher reproducibility of biomaterials, resulting in a broad range of applications. Biomaterials have become indispensable in medical practice today. Implants and medical devices such as vascular grafts, heart valves, lenses, dental implants or pacemakers and biosensors improve patients' quality of life by replacing or substituting natural functions. Thus, it is not surprising that the global market for biomaterials has been estimated at 106.5 billion dollars in 2019 (www.grandviewresearch.com), which is only set to grow further due to an ageing population.

Over the past decades, the design of biomaterials has evolved fundamentally, a development which is still ongoing (Hench & Polak, 2002). Given the limited knowledge of materials science and biological interactions, the first generation of biomaterials, such as classical metal implants, focused on achieving physical properties matching those of the replaced tissue. Commonly, these materials were designed to be 'inert' and not to interact with the host, thus preventing biological rejection (Hench, 1980). Although the design of the first generation of biomaterials was often the result of fortunate accidents (Ratner & Bryant, 2004), the design principle of biological inertness still applies to some implants used today. Nevertheless, advances in understanding foreign body reactions in the 1980s and 1990s significantly changed the way biomaterials were designed and utilized. The development of second generation biomaterials shifted the emphasis on materials that elicit a specific biological response (Hench & Thompson, 2010). Examples of this type of material

are bioactive glasses, ceramics, glass ceramics and composite materials. Bioactive ceramics such as hydroxyapatite have been shown to bond to bone tissue and promote bone formation (Ducheyne, 1994). By the end of the 1990s, the clinical use of these materials in orthopedic and dental applications was already well established. Another category of second generation biomaterials are resorbable polymers. By resorption of the biomaterial, the foreign material is replaced by regenerating tissue (Hench, 1980). Despite the clinical success of bioinert, bioactive and resorbable implants in the developed world, skeletal prostheses and artificial heart valves still have limited survivability rates of two thirds and less within 10 to 25 years (Hench & Thompson, 2010; Schoen, Levy, & Piehler, 1992). Ageing populations and increasing costs for the revision of failed implants therefore led to the design of third generation biomaterials in the early twenty-first century. For third generation biomaterials, emphasize shifted even more towards a biologically based approach. Their design is based on the stimulation of specific cellular responses at the molecular biology level. To this end, the concepts of bioactive and resorbable materials have been combined. One example of this approach is the modulation of cellular responses, such as proliferation and differentiation, by introducing molecular modifications to polymer systems which induce specific interactions with cellular receptors. On the other hand, bioactive materials are being developed with the aim to stimulate tissue regeneration by gene activation (Hench & Thompson, 2010). In the last decade, research has led to the fourth generation of biomaterials, so called biomimetic or smart materials. Investigation of materials is currently ongoing with the aim of mimicking the microenvironment of extracellular matrix in natural tissues (Sachot et al., 2015).

In summary, biomaterials used today can be classified into three categories based on their interaction with the surrounding tissue: ‘inert‘ materials that cause no or minimal response, bioactive materials that interact with the surrounding tissue, and biodegradable materials that dissolve after initial incorporation into the tissue. The evolution of biomaterials was accompanied by a change in the focus of research. While the academic focus was initially on materials science and classical engineering sciences, modern biomaterials science is a multidisciplinary field with a strong emphasis on biology.

3.2 Macrophages

3.2.1 Origin

Macrophages (Greek: Macro – 'Large'; Phage – 'to eat') are immune cells originally identified by Élie Metchnikoff in the 19th century as phagocytic cells that contribute substantially to innate immune defense (Tauber, 2003). Besides the immune response against pathogens, macrophages are involved in tissue development, homeostasis and repair by clearing cell debris and apoptotic cells (Ginhoux, Schultze, Murray, Ochando, & Biswas, 2016; Mosser & Edwards, 2008). To fulfil their role as sentinels, macrophages are equipped with a broad repertoire of perceptual tools, such as scavenger receptors, pattern recognition receptors (PRRs), cytokine receptors and adhesion molecules. Generic responses of macrophages include activities associated with their sophisticated lysosomal compartment with specific proteases and bactericidal activity, the production of different growth factors, and the provision of cytokines and antigen presentation for orchestration of the inflammatory response (Varol, Mildner, & Jung, 2015).

For many years macrophages were classified as a part of the mononuclear phagocyte system (MPS) described by van Furth and Cohn (1968): It was assumed that tissue-specific macrophages in adulthood originate exclusively from bone-marrow derived blood monocytes (van Furth et al., 1972). However, recent studies in adult tissue have demonstrated the capacity of macrophages to self-renew. Moreover, certain macrophage populations establish during embryonic development before circulating monocytes are present (Ginhoux & Jung, 2014). This led to the revised concept of the MPS, which is based on macrophages of two distinct origins. Most macrophages develop prenatally and persist in the adult tissue through longevity with limited proliferation. In pathological, homeostatic, and inflammatory conditions, they also develop from tissue-infiltrating monocytes to complement the classical tissue-resident immune response. The lifespan of these monocyte-derived macrophages is generally limited (Varol et al., 2015).

3.2.2 M1 and M2 macrophages

The activation of macrophages occurs through a multitude of temporally and spatially dynamic signals that are typically induced by innate immune cells. To effectively adjust to these endogenous stimuli, macrophages display different polarization states with distinct effector activities. In addition, the macrophage phenotype can dynamically switch from one to another depending on the

encountered environmental signals. This plasticity is an important hallmark of these cells. Similar to the T helper cell nomenclature (T_h1 and T_h2), macrophages can be roughly grouped into classically activated (M1) and alternatively activated (M2) macrophages (Mills, Kincaid, Alt, Heilman, & Hill, 2000). This classification is based on a set of specifically expressed markers for M1 and M2 activation (Table 1). However, marker expression widely varies depending on the stimuli, cellular substrate (cell line or primary cells), cell origin (murine or human), and in the *in vivo* or *in vitro* context (Atri, Guerfali, & Laouini, 2018).

Classically activated M1 macrophages are generally associated with a pro-inflammatory response to defend the host against pathogens. *In vitro*, the M1 phenotype occurs by stimulation with granulocyte/macrophage colony-stimulating factor (GM-CSF), or IFN-γ and/or Toll-like receptor (TLR) ligands (such as LPS). In order to guide inflammatory responses, M1 macrophages produce a number of pro-inflammatory cytokines and chemokines, such as IL-1β, TNF-α, IL-6, IL-8, MCP-1, and MIP-1 β. They are further characterized by the expression of cell activation markers (CD80, MHCII), microorganism phagocytosis and high antigen presentation capacity (Atri et al., 2018). To identify M1 activation in murine macrophages, nitric oxide synthase 2 (NOS2) represents a commonly used marker (Martinez et al., 2013).

On the other hand, alternatively activated M2 macrophages inhibit anti-inflammatory responses and are involved in repair mechanisms, homeostasis and wound healing. Furthermore, they play a role during parasitic, helminthic, and fungal infections. Based on the encountered stimuli, the M2 phenotype can be divided into four different subtypes with the common feature of IL-10 secretion: M2a, M2b, M2c. Treatment with IL-4 and IL-13 leads to the activation of the M2a phenotype. Its expression profile encompasses elevated levels of anti-inflammatory cytokines (IL-10, IL-1Ra), transglutaminase 2 (TGM2) and surface markers (CD206, CD163), among others (Martinez & Gordon, 2014). Murine M2a macrophages also can be characterized by the expression of Arginase-1 (Martinez et al., 2013). Another M2 category is represented by M2b macrophages which is activated by immune complexes or LPS. Characteristic for this phenotype is the production of IL-10 and pro-inflammatory cytokines, such as IL-1β and IL-6 (Rőszer, 2015). Finally, M2c macrophages are activated by IL-10 and glucocorticoids. CD163, IL-10 and TGF-β are characteristic expression markers for this subset (Atri et al., 2018).

Despite the validity of the M1/M2 paradigm for *in vitro* studies, it has been acknowledged that it only represents the extremes of the macrophage polarization *in vivo*. Macrophages most likely continuously undergo polarization in both directions (Xu, Zhao, Daha, & van Kooten, 2013). This continuum is a central factor in inflammatory reactions and their resolution.

Table 1: Overview of the macrophage polarization states.
Data are adopted from (Atri et al., 2018; Martinez & Gordon, 2014; Martinez et al., 2013; Rőszer, 2015)

Phenotype	Induction	Marker expression	Cytokine/Chemokine secretion
M1	LPS IFN-γ GM-CSF	CD86 CD80 MHC-II IDO Murine markers: iNos	IL-1β IL-8 IL-6 TNF-α
M2a	IL-4 IL-13	CD163 CD206 MHC-II TG-2 Murine markers: Ym1 FIZZ1 Arginase-1	IL-10 TGF-β IL-1Ra
M2b	immuncomplexes LPS	CD86 MHC-II	IL-1β IL-6 IL-10
M2c	IL-10 glucocorticoids	CD163 CD206	IL-10 TGF-β

3.3 Immune responses to biomaterials

Despite scientific efforts to improve implantable materials and the broad, successful application of biomaterials, all implants cause adverse reactions in the patient's body. Ideally, permanent implants remain in the patient's body for their entire lifetime without causing adverse side effects, while resorbable materials degrade into harmless and non-toxic components. However, this is usually not the case as implanted biomaterials trigger undesired immune reactions resulting in the so-called foreign body reaction. The foreign body reaction describes a series of inflammatory events and wound healing responses to biomaterials that lead to fibrosis and are orchestrated by the immune system. Historically, the immune system is known for defending the body against bacterial and viral infections. However, it has been shown that foreign bodies such as implanted biomaterials also elicit an immune response. Successful integration and performance of implants is highly dependent on the extent of the inflammatory reaction.

Inflammatory responses occur immediately after surgical implantation of biomaterials as a result of tissue injury. Disruption of the vascular tissue at the implantation site results in immediate blood contact with the biomaterial. Within seconds, a protein layer adsorbs to the biomaterial surface (Anderson & McNally, 2011). Proteins adsorbing to the biomaterial include components of the coagulation system, the complement cascade and other plasma proteins (albumin, fibronectin, fibrinogen, vitronectin, and gammaglobulins). Adsorbed plasma proteins are crucial for the adhesion and activation of immune cells on biomaterials in the following hours and days, since these processes occur predominantly through the interaction of adhesion receptors with the adsorbed proteins. Hence, the type, amount and conformation of the proteins adsorbed on the surface are crucial determinants for the resulting immune reaction (Anderson, Rodriguez, & Chang, 2008). The composition of the protein layer depends on the biomaterial surface properties and on dynamic processes of protein adsorption and dissociation at the biomaterial surface (known as the Vroman effect) (Anderson & McNally, 2011). Tissue injury also leads to the activation of platelets and the subsequent release of tissue factors resulting in the activation of the extrinsic coagulation cascade (Brown, Sicari, & Badylak, 2014). The initiation of the intrinsic coagulation cascade may occur upon biomaterial surface activation of Factor XII (Zhuo, Siedlecki, & Vogler, 2006). As a result, an initial fibrin clot forms at the implant interface, the so called transient provisional matrix. The provisional matrix accommodates numerous factors (chemoattractants, cytokines, growth factors and other bioactive molecules) that promote or inhibit subsequent immune cell proliferation and activation. Furthermore, infiltration of immune cells to the implant side is stimulated by the activation of the complement system in response to biomaterial surface contact (Nilsson, Ekdahl, Mollnes, & Lambris, 2007) and release of danger signals (such as heat shock proteins, HMGB1, ATP, and urid acid) in response to tissue injury (Franz, Rammelt, Scharnweber, & Simon, 2011).

Following the initial formation of the provisional matrix, acute and chronic inflammation occur successively. Acute inflammation is a relatively short-term process that resolves within days. The purpose of acute inflammation is the elimination of foreign materials, predominantly by phagocytosis. This phase is mainly characterized by the recruitment of granulocytes, predominantly neutrophils, to the site of injury. Granulocyte migration from blood to the implant side is triggered by several factors, such as histamine release in association with mast cell degranulation and chemoattractants which are released from activated platelets, endothelial cells, and injured tissue cells (Franz et al., 2011; Zdolsek, Eaton, & Tang, 2007). Interactions of cellular

adhesion receptors with the biomaterial-adsorbed proteins activate neutrophils, causing a phagocytic response and degranulation. Secretion of proteases and reactive oxygen species leads to the degradation of the biomaterial and surrounding tissue (Franz et al., 2011). Furthermore, activated neutrophils synthesize different immunoregulatory signals, such as interleukin-8 (IL-8), whose primary target are neutrophils themselves. Activated neutrophils also secrete MCP-1 and MIP-1 β. These chemokines specifically cause immigration and activation of monocytes, macrophages, and lymphocytes (Yamashiro et al., 2001). As acute inflammation subsides, neutrophils undergo apoptosis due to a lack of further activation signals and are replaced by macrophages (Gilroy, 2004).

Chronic inflammation occurs as the inflammatory stimuli persist at the implantation site and is associated with the presence of monocytes and macrophages. This stage may last from a few days to several months or years. Circulating monocytes are recruited to the biomaterial, become activated through interactions with the adhered proteins (such as fibrinogen), and differentiate into macrophages (Sheikh, Brooks, Barzilay, Fine, & Glogauer, 2015; Shen, Garcia, Maier, & Horbett, 2004). Due to the different macrophage subsets with distinct functions and their plasticity (comprehensively described in section 3.2.2), macrophages play a central role in orchestrating the subsequent reactions throughout immune responses following implantation.

At first, macrophages attaching to the foreign biomaterial display a pro-inflammatory M1 phenotype. Activated macrophages adhering to the biomaterial surface secrete pro-inflammatory cytokines such as IL-8, MCP-1 and MIP-1 β, which foster the invasion of additional immune cells (Jones et al., 2007). Additionally, they release reactive oxygen species (ROS) and degrading enzymes to phagocytize the foreign material (Lynn, Kyriakides, & Bryant, 2010). Since the biomaterial is too large to be internalized, macrophages fuse to so called foreign body giant cells (FBGCs) in an attempt to increase their phagocytic functionality. The induction of macrophage fusion is mediated through the cytokines IL-4 and IL-13, which are secreted by activated mast cells and T helper cells (DeFife, Jenney, McNally, Colton, & Anderson, 1997; Kao, McNally, Hiltner, & Anderson, 1995; McNally & Anderson, 1995). Moreover, macrophage fusion is promoted by vitronectin adhered to the biomaterial surface (McNally, Jones, Macewan, Colton, & Anderson, 2008). If FBGCs are unable to phagocytize the foreign material, they undergo a process referred to as frustrated phagocytosis. This phenomenon describes the reduced phagocytic activity along with an enhanced degradation capability following macrophage fusion (Xia et al., 1994). Nevertheless,

macrophages fused to FBGCs persist at the implant side, thus forming a cellular barrier between the tissue and the implant (Anderson, 2000). The fusion to FBGCs is typically associated with a phenotype switch from a pro-inflammatory to a more anti-inflammatory state. This transition is reflected in the profile of secreted cytokines. FBGCs predominantly release anti-inflammatory factors, such as IL-10, TGF-β, and IL-1RA. However, macrophages still produce pro-inflammatory agents ROS, MCP-1, RANTES and degradative enzymes following fusion (Franz et al., 2011). Ultimately, fibroblasts are recruited to the implantation site through the secretion of pro-fibrotic factors VEGF and TGF- β of activated immune cells (macrophages, T-cells, mast cells) (Mariani, Lisignoli, Borzi, & Pulsatelli, 2019). The arrival of fibroblasts at the injury site marks the initiation of the wound healing process. Along with endothelial cells, fibroblasts form granulation tissue around the implanted material. Proliferation of endothelial cells from pre-existing blood vessels results in the formation of novel blood vessels, a process known as angiogenesis (Anderson & McNally, 2011). To repair the damaged tissue around the implant, fibroblasts synthesize collagens. This process generally results in the fibrotic encapsulation of the material (Ratner & Bryant, 2004), thus isolating the implant from the surrounding tissue to maintain the organisms' safety. The fibrotic capsule in coincidence with FBGCs is called the foreign body reaction (FBR) and marks the end stage of the inflammatory and wound healing responses following biomaterial implantation (**Figure 1**).

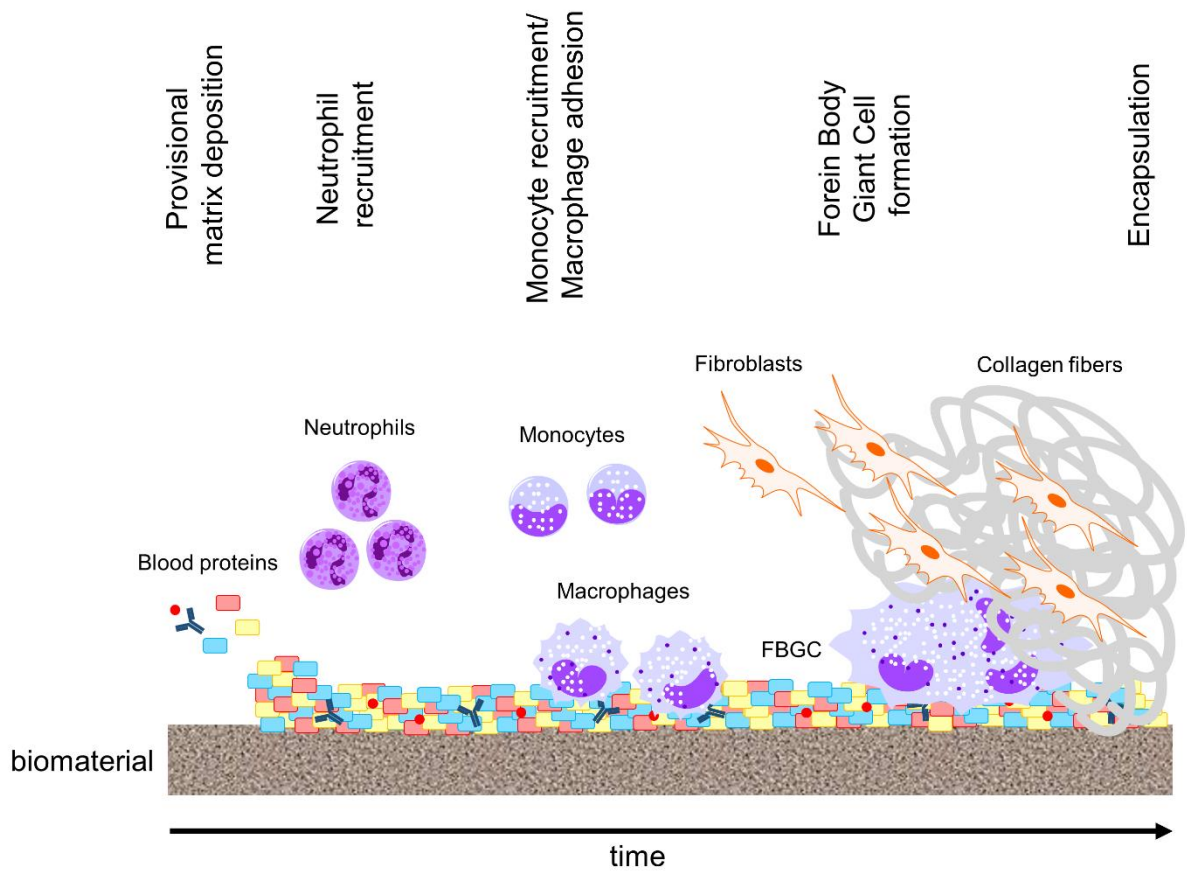

Figure 1: Immune response towards biomaterials generally results in the development of the foreign body reaction.
Upon implantation, protein adsorption to the implant surface immediately occurs. This process ultimately results in the so called transient provisional matrix, which orchestrates recruitment and activation of immune cells. Within hours, neutrophils enter the implantation site where they mediate the degradation of the biomaterial. In the next days, monocytes which differentiate into macrophages replace neutrophils. Limited by size and degradability, macrophages fail to phagocytose the biomaterial and fuse to so called foreign body giant cells (FBGCs). Mediators secreted by FBGCs attract fibroblasts. Activated fibroblasts produce collagen, thereby leading to the fibrotic encapsulation of the implant and inhibiting the interaction with the surrounding tissue. (modified from Mariani et al. (2019))

The extent of the foreign body response primarily influences the performance of the implant. Persistent chronic inflammation leads to excessive biomaterial encapsulation, accompanied by the continuous release of ROS and degradative enzymes. The combination of these two may jeopardize the functioning of the implanted material. Therefore, successful biomaterial integration with minimal fibrous encapsulation requires the resolution of the pro-inflammatory environment. The ratio of the anti-inflammatory response to the pro-inflammatory response is therefore crucially.

3.4 Modulating immune responses to biomaterials

Functionality and long-term survival of medical devices or implants depend strongly on the extent of the foreign body reaction elicited. Since the second generation of biomaterials, the development of materials provoking desired cellular responses has been driven forward. With growing knowledge about the induced reactions following biomaterial implantation and wound healing, the field of biomaterial engineering has also begun to address the idea of immune modulation. Ideally, biomaterial modifications induce immune cell responses that promote wound healing and improved implant integration without altering the function of the implant. In several studies, the potential of biomaterials to modulate elicited immune reactions has been demonstrated (Barth, Waterfield, & Brunette, 2013; Bartneck, Schulte, et al., 2010; Hamlet, Alfarsi, George, & Ivanovski, 2012; Paul et al., 2008). Design strategies used to achieve such biomaterials are based on alterations of surface properties, either passively using physicochemical features (surface chemistry and surface topography) or actively by incorporating molecules or matrices that systematically influence cell behavior.

3.4.1 Immunomodulation by surface chemistry

As previously described (section 3.3), the layer of adsorbed proteins on the biomaterial surface is crucial for the subsequent immune reactions to the implant. Type, quantity, and confirmation of proteins strongly depend on the biomaterial's chemistry. By modifying the surface chemistry, protein adsorption is modulated, subsequently affecting the adhesion and activation of immune cells. Indeed, surface wettability (hydrophobicity and hydrophilicity) and chemical moieties have been shown to affect protein expression and cytokine responses of macrophages in various studies. For example, hydrophilic titanium surfaces have been shown to enhance the expression of anti-inflammatory markers of macrophages compared to hydrophobic ones. Furthermore, adsorption and conformation of the proteins fibronectin and fibrinogen were controlled by surface hydrophilicity (Lv et al., 2018). Further studies have also observed a correlation between titanium surface hydrophilicity and down-regulated pro-inflammatory responses or elevated anti-inflammatory responses of macrophages (Hamlet et al., 2012; Hotchkiss et al., 2016). Nevertheless, immunomodulatory effects can also be obtained by chemical groups. It has been shown that hydrophobicity is not the sole factor for conformational changes of adsorbed proteins, but that also terminal groups also play an important role (Sivaraman, Fears, & Latour, 2009). Another study

reported that chemical moieties affect the macrophage phenotype: While nanorods with amino groups induced an anti-inflammatory M2-phenotype, carboxyl terminated rods led to a pro-inflammatory M1 phenotype (Bartneck, Keul, et al., 2010).

3.4.2 Immunomodulation by surface topography

Another passive surface alteration is the variation of roughness, texture, and geometry. Manufacturing processes themselves, such as blasting, acid etching and injection molding, already allow the introduction of topographical features. As with surface chemistry, surface topography has been reported to influence protein adsorption. Accordingly, it has been shown that surface nanostructures have important implications for the adsorption of proteins (Scopelliti et al., 2010). Various studies have also reported that topographic features direct cell responses: micro- or nanoscale topographic features can be used to modulate myofibroblast differentiation (Myrna et al., 2012), control keratocyte alignment (Kilic, Girotti, Rodriguez-Cabello, & Hasirci, 2014) and influence endothelial cell migration (Le Saux, Magenau, Bocking, Gaus, & Gooding, 2011). Micropatterned structures can further be exploited to induce specific immune responses. For example, it has been shown that microstructured topographies on polyvinylidene fluoride induce an inflammatory reaction (Paul et al., 2008). Another study revealed the induction of an anti-inflammatory macrophage response on cylindrical posts, whereas macrophages cultured on regular grooves displayed a pro-inflammatory phenotype (Bartneck, Schulte, et al., 2010). Regarding the influence of geometry, scaffolds with pore diameters of 30-40 µm shifted the macrophage phenotype towards the anti-inflammatory M2 state (Madden et al., 2010). Accordingly, it has been shown that increasing pore size correlated with increased expression of the anti-inflammatory marker arginase-1, while expression of the pro-inflammatory marker inducible nitric oxide synthase decreased (Garg, Pullen, Oskeritzian, Ryan, & Bowlin, 2013). Finally, roughness should also be addressed. The cultivation of murine macrophages on rough epoxy substrates increased the expression of MCP-1 and MIP-1α compared to smooth substrates (Barth et al., 2013).

3.4.3 Immunomodulation using bioactive molecules

More recent methods focus on the functionalization of biomaterials by incorporating bioactive molecules (adhesion sites, growth factors, anti-inflammatory mediators) that enable specific biological responses. This approach is applied at both the protein and the gene level.

To direct immune cell responses, the functionalization of biomaterials with specific integrin binding sites represents a powerful strategy. Fibronectin-derived oligopeptides RGD (arginine-glycine-aspartate) and PHSRN (proline-histidine-serine-arginine-asparagine) have been shown to mediate specific cell activation. Incorporation of these domains on biomaterial surfaces initiated intracellular signal pathways through interaction with integrin adhesion sites, mediating macrophage adhesion and function (Kao & Lee, 2001; Kao & Liu, 2001). Additionally, surface coatings utilizing polyethylene glycol (PEG) is a technique which prevents protein adsorption and thus the subsequent activation of immune cells (VandeVondele, Voros, & Hubbell, 2003). The advantage of combining these two approaches is the prevention of unspecific cell-material interactions with simultaneous activation of specific cell responses (Franz et al., 2011).

The use of anti-inflammatory factors represents another method to render the biomaterial-induced immune response. Chemokines and cytokines are key regulators of the inflammatory response because they directly modulate immune responses. Anti-inflammatory cytokines and chemokines such as IL-4 and IL-10 play a fundamental role in tissue repair and regeneration, making them an attractive tool for immune modulation. Following implantation of a scaffold that allowed localized and sustained IL-10 delivery using a gene therapy-based approach, a decreased inflammatory response was observed (Gower et al., 2014). Furthermore, it has been reported that the delivery of IL-4 conjugated scaffolds or hydrogels induced an anti-inflammatory macrophage phenotype and tissue repair in rat models (Mokarram, Merchant, Mukhatyar, Patel, & Bellamkonda, 2012; Spiller et al., 2015). Another example of anti-inflammatory mediators are glucocorticoids. These are immunosuppressive drugs that inhibit the synthesis of inflammatory mediators (including cytokines, chemokines, prostaglandins, ROS, proteolytic enzymes) and promote anti-inflammatory cytokine release (Franz et al., 2011). The coupling of glucocorticoids to biomaterials led to reduced biomaterial-induced inflammation, as shown by the absence of immune cells and fibrous capsule. However, this treatment also resulted in reduced VEGF secretion, which prevented angiogenesis and consequently delayed wound healing (Morais, Papadimitrakopoulos, & Burgess, 2010). A permanent control of immune responses at the implant side has been described by the application of NO-releasing coatings (Hetrick, Prichard, Klitzman, & Schoenfisch, 2007). Another study confirmed these results: the continuous release of NO reduced recruitment and activation of inflammatory cells (Gifford et al., 2005).

Although growth factors (VEGF, PDGF, GM-CSF, TGF-β) predominantly target tissue cells, they can nevertheless be considered as immunomodulatory agents. For example, fibroblasts have been shown to inhibit the MIP-1α production by activated macrophages (Oshikawa, Yamasawa, & Sugiyama, 2003). By modulating tissue cell responses by means of incorporated growth factors on the biomaterial surface, activity of immune cells may be controlled indirectly.

3.4.4 Immunomodulation using artificial or acellular ECM

While functionalization of biomaterials is usually based on a single signal, the cellular response in the natural environment is controlled by various bioactive factors. The extracellular matrix (ECM) provides cells with biochemical and biomechanical signals that regulate migration, differentiation and proliferation, thus making it an attractive tool for the development of biomaterials with physiological functions.

To mimic the physiology of ECM, natural and synthetic hydrogels are attractive matrices. Hydrogels are three-dimensional polymeric structures with a high water absorption capacity, thus resembling soft tissue (Hoffman, 2002). Hydrogels synthesized from synthetic polymers like polyethylene glycol (PEG) are usually bio-inert. Incorporation of growth factors and other bioactive molecules, presentation of specific adhesion sites, etc. have been applied to render synthetic scaffolds bio-interactive (Franz et al., 2011). In contrast to synthetic hydrogels, naturally derived hydrogels already have similar properties to the ECM. Frequently used polymers in these hydrogels are ECM proteins (collagen, fibrin, gelatin) and polysaccharides (GAGs, dextran, alginate, chitosan) (Geutjes et al., 2006). Most commonly, naturally derived hydrogels do not induce chronic inflammation. However, origin and sterilization method have the potential to elicit detrimental host responses (Valentin, Badylak, McCabe, & Badylak, 2006).

Coatings with extracellular matrix proteins have also been exploited to regulate the immune cell response to biomaterials. As an example, GAGs have been reported to bind cytokines and chemokines (Witt & Lander, 1994). The binding of the anti-inflammatory cytokine IL-10 by sulfated GAGs resulted in enhanced activity on immune cells (Salek-Ardakani, Arrand, Shaw, & Mackett, 2000). Furthermore, GAGs like chondroitin sulfate and hyaluronic acids may act as immunosuppressants. Chondroitin sulfate has been found to not only prevent ROS damage by reducing free radicals (Campo et al., 2003), but to also reduce nuclear translocation of the transcription factor NF-κB, which mediates various pro-inflammatory pathways (Franz et al.,

2011). On the other hand, hyaluronic acids (HA) elicit different immune responses depending on their molecular size (Stern, Asari, & Sugahara, 2006). Under physiological conditions, large HA polymers can be found that have anti-inflammatory properties and thus promote tissue integrity (Franz et al., 2011). When tissue is injured, these HA polymers are split into smaller fragments that serve as pro-inflammatory mediators. Various studies have demonstrated the activation of inflammatory cytokine production in immune cells by low molecular weight HA (Termeer et al., 2002; Yamawaki et al., 2009). Therefore, HA coatings of biomaterials might be a double-edged sword.

Lastly, decellularized ECM scaffolds can be utilized in order to induce specific immune responses. Both the structural and functional properties of the decellularized ECM support numerous cellular processes that have been associated with wound healing processes and tissue remodeling (Badylak, Freytes, & Gilbert, 2009; Turner & Badylak, 2015). Among the affected cellular processes are shifts in macrophage polarization. Accordingly, the transplantation of acellular scaffolds resulted in a predominant anti-inflammatory M2 response (Badylak & Gilbert, 2008; Brown, Valentin, Stewart-Akers, McCabe, & Badylak, 2009). Nevertheless, tissue origin, decellularization and modification processes majorly define the immunogenicity of the scaffold (Mariani et al., 2019).

3.5 The role of actin cytoskeleton in macrophages

The cytoskeleton is an essential structure of an interconnected network of filamentous polymers and regulatory proteins present in the cytoplasm of all cells. It carries out broad cellular functions ranging from cell shape, cellular movement, and intracellular organization to intracellular signaling, cellular division and intracellular transport (Huber, Boire, Lopez, & Koenderink, 2015). In eukaryotes, the cytoskeleton is composed of three main types of cytoskeletal polymers: (i) microtubules, which form long and cylindrical polymers of α/β tubulin with a diameter of 23 nm (ii) intermediate filaments, which are heterogeneous polymers consisting of different proteins like vimentin, keratin, lamin, and desmin with a diameter of roughly 10 nm, and (iii) actin filaments, which are composed of two twisted helices with a diameter of 6 nm (Huber et al., 2015; Jekely, 2014).

Actin is one of the most abundant cellular proteins (Pollard & Borisy, 2003). In mammals, actin is encoded by six different genes. Four of them are specifically expressed in muscles (α-actinin-1, α-actinin-2, α-actinin-3, γ-actin-2) whereas the other two (β-actin, and γ-actin-1) are also present in non-muscular cells (Herman, 1993). Actin is an ATPase that can take two forms: monomeric actin (G-actin) and filamentous actin (F-actin). The transition between G-actin and F-actin allows filament assembly and disassembly in cells. It is regulated through ATP hydrolysis and a set of regulatory proteins, including Arp 2/3 complex, profilin, capping protein, cofilin, and ADF (Pollard & Borisy, 2003; Wegner & Isenberg, 1983). Participation of the actin cytoskeleton has been demonstrated for many cellular processes associated with immune responses, including migration (Yin & Hartwig, 1988), adhesion (Yin & Hartwig, 1988), phagocytosis (Oliver & Berlin, 1982), cellular shape (Lehto, Hovi, Vartio, Badley, & Virtanen, 1982), and secretion (Tapper, 1996). Macrophages show distinct cytoskeleton arrangements as opposed to the stress fibers in mesenchymal cells (McWhorter, Davis, & Liu, 2015). Instead, macrophages form distinct cylindrical adhesion structures, known as podosomes. They consist of an actin-rich core surrounded by actin regulators and an outer ring rich of vinculin and talin (Linder & Aepfelbacher, 2003). Functionally, they play a key role in adhesion, mechanosensing and migration (Van Audenhove, Debeuf, Boucherie, & Gettemans, 2015). Thus, podosomes may enable macrophages mechanotransduction mechanism distinct from most tissue cells, allowing them to respond accordingly to the surrounding substrate. Differences in actin organization between M1 and M2 macrophages were observed in several studies. In this context, it has been reported that M2 macrophages form podosomes, while M1 macrophages were devoid of podosomes (Cougoule et al., 2012). Another study observed clustering of actin around the nucleus in M1 macrophages compared to M2 macrophages in which actin was present at the periphery of the cells (Vereyken et al., 2011). As mentioned above, actin cytoskeleton is also involved to determine the cellular shape. Upon M1 or M2 polarization macrophages undergo morphological changes. In particular, M1 macrophages have been observed to adopt a circular morphology, while M2 macrophages exhibit an elongated morphology (McWhorter, Wang, Nguyen, Chung, & Liu, 2013).

3.6 Visualization tools for actin cytoskeleton

The visualization of the actin cytoskeleton in fixed cells is well established for decades. Initially, antibody-based immunofluorescence staining was used to visualize fixed actin structures (Lazarides & Weber, 1974). The gold standard for the staining of the actin cytoskeleton in fixed cells is nowadays phalloidin, a derivate of phallotoxin which binds F-actin. Fluorescent labeling enables the use as an imaging tool. However, cytotoxicity and low membrane permeability limit the application of phalloidin to fixed samples (Melak, Plessner, & Grosse, 2017). Thus, dynamical changes of actin structures cannot be traced. Moreover, fixation and permeabilization methods possibly introduce artifacts, which subsequently lead to distorted results. To overcome these drawbacks, intracellular expressed fluorescent fusion proteins have been widely employed. This approach was used extensively to study dynamics of actin (Clark, Dierkes, & Paluch, 2013; Doyle & Botstein, 1996; Koestler et al., 2009). However, the large molecular weight of fluorescent tags like GFP (approximately 27 kDa) can interfere with the characteristics and functionality of actin, thus preventing proper localization and interaction with associated proteins (Doyle & Botstein, 1996; Wu & Pollard, 2005). To combine the advantages of immunofluorescence staining techniques and fluorescent proteins, several intracellular binding molecules have been developed over the last decades in order to visualize endogenous actin in living cells.

3.6.1 Visualization of actin dynamics using actin-binding domains

The application of intracellularly expressed binding molecules which have been fused to fluorescent proteins (intrabodies) is widespread. They serve as attractive tools to visualize spatiotemporal dynamics of endogenous structures in living cells without affecting the native constitution or manipulation of the gene locus of the protein. One prominent example of such intrabodies for the visualization of actin is LifeAct, a 17 amino acid peptide derived from the actin binding protein (Abp140) from yeast. While several studies described the successful application to trace actin dynamics (Riedl et al., 2008; Riedl et al., 2010; Suarez et al., 2015), overexpression has been shown to result in severe actin remodeling (Spracklen, Fagan, Lovander, & Tootle, 2014). Another actin binding peptide is F-tractin which comprises 43 amino acids and is derived from the actin-binding domain of the rat protein inositol-trisphosphatase 3-kinase A (Schell, Erneux, & Irvine, 2001). However, the larger size compared to LifeAct represents a major drawback, since the size may result in interferences with endogenous actin binding proteins. Accordingly, F-tractin

expression has been shown to alter the organization and morphology of the actin cytoskeleton (Belin, Goins, & Mullins, 2014).

Lastly, the cell-permeable chemically synthesized probe SiR-actin can be utilized to trace actin structures in living cells (D'Este, Kamin, Gottfert, El-Hady, & Hell, 2015). It is based on the F-actin binding toxin Jasplakinolide. In contrast to the previously described peptide-based approaches, there is no need for genetic manipulation or overexpression. Nevertheless, structural similarities to Jasplakinolide may result in stabilizing effects (Melak et al., 2017).

3.6.2 Visualization of actin dynamics using chromobodies

Although some intrabodies (such as the previously described LifeAct and F-tractin) are based on non-antibody scaffolds like aptamers (Wang, Xiao, Zhang, & Wong, 2018), peptides (Riedl et al., 2008), monobodies (Gross et al., 2013), or designed ankyrin repeat proteins (Vigano et al., 2018), the majority of intrabodies are derived from immunoglobulins (IgGs). Full-length IgG molecules are composed of two heavy chains (~ 50 kDa) and two light chains (~ 25 kDa), each comprising a constant domain (C_H and C_L) and the variable domain (V_H or V_L), which mediates the specific antigen binding (Janeway Jr, Travers, Walport, & Shlomchik, 2001). Due to their large size of ~150 kDa and the reducing environment of the cytosolic compartment which inhibits correct folding and disulfide bridge formation, IgGs cannot be applied for intracellular applications in living cells. Nevertheless, these restrictions can be circumvented by the generation of so-called single chain variable fragment (scFv): Fusion of the V_H and V_L domain via a flexible peptide linker, commonly comprising $(Gly_4/Ser)_3$ repeats, results in a ~28 kDa binding molecule (Bird et al., 1988). However, hydrophobic residues on the surface of V_Hs and V_Ls can still restrict intracellular functionality of scFvs due to low expression rates or aggregation (Cattaneo & Biocca, 1999).

More recently, heavy chain only antibodies have been discovered alongside conventional antibodies in camelids (Hamers-Casterman et al., 1993). They consist of two identical heavy chains with two constant domains (C_H2 and C_H3, but no C_H1), a hinge region and a variable domain (V_HH). The lack of the C_H1 domain is explained by a G to A point mutation which causes the elimination of the C_H1 exon during splicing (Nguyen, Hamers, Wyns, & Muyldermans, 1999). Since heavy chain only antibodies are devoid of light chains, antigen binding is mediated by a single domain (V_HH, also referred to as nanobody). Due to their small size of 13 - 15 kDa, high solubility, and tolerance of salt concentrations, temperature and pH conditions (Rothbauer et al., 2008),

nanobodies are attractive tools for biomedical research (Muyldermans, 2013). Furthermore, intramolecular disulfide bridges are not generally necessary for the correct folding of nanobodies, thus enabling the selection and application of nanobodies to trace and manipulate endogenous targets in living cells (reviewed in Kaiser, Maier, Traenkle, Emele, and Rothbauer (2014)). For visualization of endogenous proteins, nanobodies have been genetically fused to fluorescence proteins. Subsequently, these DNA-encoded constructs are expressed in mammalian cells. Due to their chimeric structure, these constructs are referred to as chromobodies (CBs). The successful application of the CB technology was first shown with a GFP binding CB which was fused to RFP. Co-expression of this GFP-CB with different GFP-labeled proteins demonstrated specific labeling of its antigens (Rothbauer et al., 2006). During the last few years, CBs against a variety of different targets have been developed. Applying the CB technology nuclear components (β-catenin, PCNA, PARP1) and cytoskeletal components (lamin, vimentin, and actin) were visualized in living cells. The actin-chromobody (actin-CB) was originally selected against mammalian β-actin but was shown to also stain F-actin in other species (Melak et al., 2017; Panza, Maier, Schmees, Rothbauer, & Sollner, 2015; Periz et al., 2017). One such example is the generation of actin-CB expressing zebrafishes which were raised from embryos to adulthood, thus demonstrating that the CB is not interfering with developmental stages. Moreover, following the CB signal, actin was visualized in different cell types including macrophages, epidermal cells or embryonic muscle fibers (Panza et al., 2015). Since actin dynamics are not affected by the expression of the actin-CB, it offers an excellent tool for visualizing actin dynamics in living cells.

3.7 Aim and objectives

Design and development of biomaterials that induce appropriate immune responses in the host are absolutely essential to ensure implant functionality without occurrence of adverse side effects. Hence, a thorough understanding of the relationship between material properties and the associated cellular response is required to achieve such materials. To date, the gold standard to assess biomaterial-induced effects following implantation are time consuming and cost-intensive animal models. Moreover, physiological differences between species may result in distorted results. *In vitro* test systems based on human cell line derived macrophages thus present a promising alternative.

Analysis of biomaterial-induced immune responses *in vitro* is generally performed by immunoassays, flow cytometry, immunofluorescence staining, or Western blotting. Nevertheless, these assays are still time consuming and limited to endpoint findings thus not allowing the assessment of dynamic changes over time. Overcoming these drawbacks, the CB technology allows an optical monitoring of spatiotemporal dynamics in living cells. Observations that macrophage polarization is associated with morphological changes led to the hypothesis that actin-CB can be utilized to trace morphological changes in macrophages to predict the elicited immune responses.

The aim of this work was to develop a cellular model based on macrophages derived from the monocytic cell line THP-1 to quantify immunological and morphological responses to biomaterials. To further monitor morphological changes dynamically, a novel THP-1 cell line expressing the actin-CB was generated, thereby attempting to predict the immune response from the morphologies observed.

4 MATERIAL AND METHODS

4.1 Material

4.1.1 Chemicals and solutions

Chemical/Solution	Manufacturer
2-Propanol	Carl Roth GmbH & Co. KG, Karlsruhe, Germany
Acrylamide Bisacrylamide	Carl Roth GmbH & Co. KG, Karlsruhe, Germany
Ammonium persulfate (APS)	Carl Roth GmbH & Co. KG, Karlsruhe, Germany
β-Mercaptoethanol	Carl Roth GmbH & Co. KG, Karlsruhe, Germany
DAPI (4,6-diamiddino-2-phenylindole)	Roche Diagnostics GmbH, Mannheim, Germany
DMSO ≥99 %	Carl Roth GmbH & Co. KG, Karlsruhe, Germany
DNAse I	Applichem GmbH, Darmstadt, Germany
Ethanol, absolute grade	Sigma-Aldrich Chemie GmbH, Munich, Germany
Ethanol, denatured	Carl Roth GmbH & Co. KG, Karlsruhe, Germany
Fetal Bovine Serum (FBS)	Thermo Fisher Scientific, Schwerte, Germany
Formaldeyde (37%)	Applichem GmbH, Darmstadt, Germany
G418	Thermo Fisher Scientific, Schwerte, Germany
Hoechst33258	Thermo Fisher Scientific, Schwerte, Germany
IFN-γ	Miltenyi Biotec B.V. & Co. KG, Bergisch Gladbach, Germany
IL-4	Miltenyi Biotec B.V. & Co. KG, Bergisch Gladbach, Germany
IL-13	Miltenyi Biotec B.V. & Co. KG, Bergisch Gladbach, Germany
LPS O55:B5	Merck Millipore, Darmstadt, Germany
Milkpowder, Blotting Grade	Carl Roth GmbH & Co. KG, Karlsruhe, Germany
NP-40	Carl Roth GmbH & Co. KG, Karlsruhe, Germany
PageRuler™ Prestained Protein Ladder Plus	Fermentas GmbH, St.Leon-Rot, Germany
Penicillin Streptomycin	Thermo Fisher Scientific, Schwerte, Germany
Phenylmethanesulfonylfluoride (PMSF)	SERVA Electrophoresis GmbH, Heidelberg, Germany
Phalloidin Alexa Fluor 555	Santa Cruz, Dallas, USA
Phosphate Buffered Saline (PBS), 1x	Thermo Fisher Scientific, Schwerte, Germany
Phorbol-12-myristat-13-acetat (PMA)	Sigma-Aldrich Chemie Gmbh, Munich, Germany
Pierce™ BCA Protein Assay Kit	Thermo Fisher Scientific, Schwerte, Germany
Ponceau S	Sigma-Aldrich Chemie Gmbh, Munich, Germany
Protease Inhibitor Mix M	SERVA Electrophoresis GmbH, Heidelberg, Germany
Roswell Park Memorial Institute (RPMI) 1640	Thermo Fisher Scientific, Schwerte, Germany
Sodium dodecyl sulfate (SDS)	Carl Roth GmbH & Co. KG, Karlsruhe, Germany
TransIT-2020 Transfection Reagent	VWR International GmbH, Darmstadt, Germany
Trypsin-EDTA (0.25%), phenol red	Thermo Fisher Scientific, Schwerte, Germany

4.1.2 Devices

Device	Manufacturer
Autoklave VX-95	Systec GmbH, Wettenberg, Germany
Axiovert 200M	Zeiss AG, Oberkochen, Germany
BD FACSMelody	Becton, Dickinson and Company, Heidelberg, Germany
CASY TT Cell Counter System	OLS OMNI Life Science GmbH & Co. KG, Bremen, Germany
Centrifuge 5415R	Eppendorf AG, Hamburg, Germany
Centrifuge 5424	Eppendorf AG, Hamburg, Germany
Centrifuge 5702	Eppendorf AG, Hamburg, Germany
Centrifuge 5810R	Eppendorf AG, Hamburg, Germany
Centrifuge Universal 2S	Hettich GmbH & Co KG, Tuttlingen, Germany
CO_2 -Incubator CB150	Binder GmbH, Tuttlingen, Germany
Elektrophoresis Chamber	Bio-Rad Laboratories GmbH, München, Germany
GFL water bath 1002	GFL Gesellschaft für Labortechnik mbH, Burgwedel, Germany
GFL water bath 1083	GFL Gesellschaft für Labortechnik mbH, Burgwedel, Germany
High-content microscope MetaXpressXL system	Molecular Devices, Biberach, Germany
Light microscope TMS-F	Nikon, Duesseldorf, Germany
Microscope Axiovert 200M	Zeiss AG, Oberkochen, Germany
PHERAstar plate reader	BMG Labtech, Offenburg, Germany
Pipet HandyStep	Brand GmbH & Co KG, Wertheim, Germany

Device	Manufacturer
Pipets 10 µL, 20 µL, 100 µL, 200 µL, 1000 µL	Brand GmbH & Co KG, Wertheim, Germany
Pipettboy	Integra BioSciences, Fernwald, Germany
PowerPac Basic Power Supply	Bio-Rad Laboratories GmbH, München, Germany
Semi-Dry transfer cell	Bio-Rad Laboratories GmbH, München, Germany
Steril hood	BDK GmbH, Sonnenbühl-Genkingen, Germany
Steril hood	CARLO ERBA Reagents GmbH, Emmendingen, Germany
Thermomixer comfort	Eppendorf AG, Hamburg, Germany
Typhoon TRIO	GE Healthcare Life Sciences

4.1.3 Consumables

Consumable	Manufacturer
µClear 96-well microplate	Greiner Bio-One, Frickenhausen, Germany
µ-Plate 24 Well Black	Ibidi GmbH, Gräfelfing, Germany
Amersham Protan 0,45 µm Nitrocellulose	GE Healthcare, Uppsala, Sweden
Blotting Paper Grad 703	Bio-Rad Laboratories GmbH, Munich, Germany
Cell Culture Flasks T-25, T-75, T-125	Corning GmbH, Wiesbaden, Germany
Falcon Tubes (15 and 50 mL)	Sarstedt AG & Co., Nümbrecht, Germany
Falcon-Tubes 15mL und 50mL	Greiner Bio-One, Frickenhausen, Germany
Multiwell plate: 6, 12, 24, 96 well	Corning GmbH, Wiesbaden, Germany
Nitrocellulose membrane	Bio-Rad Laboratories GmbH, Munich, Germany
Parafilm	Brand GmbH & Co. KG, Wertheim, Germany
Pipettes (5 mL. 10 mL, 25 mL, 50 mL)	Sarstedt AG & Co., Nümbrecht, Germany
Pipettetips (10 µL, 20 µL, 200 µL, 1000 µL, 1250 µL)	Starlab GmbH, Hamburg, Germany
Reaction tube 1.5 mL / 2 mL	Sarstedt AG & Co., Nümbrecht, Germany

4.1.4 Antibodies

Antibody	Dilutionfactor	Company
Primary		
anti-TGase-2 E-3: sc-48387 (mouse, mAB)	1000	Santa Cruz, Dallas, USA
anti-IDO D5J4E (rabbit, mAB)	1000	Cell Signaling Technology, Inc., Danvers, Germany
anti-GAPDH H12 (mouse, mAB)	1000	Santa Cruz, Dallas, USA
Secondary		
anti-mouse (goat) Alexa 488 conjugate	2000	Thermo Fisher Scientific, Schwerte, Germany
anti-rabbit (goat) Alexa 647 conjugate	2000	Thermo Fisher Scientific, Schwerte, Germany
Directly conjugated		
FITC anti-human CD11b AB	2.5 µL per 5 x 10^5 cells	BioLegend, London, United Kingdom
PE anti-human CD80 AB	2.5 µL per 5 x 10^5 cells	BioLegend, London, United Kingdom
FITC anti-human CD206 AB	2.5 µL per 5 x 10^5 cells	BioLegend, London, United Kingdom
FITC anti-human CD209 AB	2.5 µL per 5 x 10^5 cells	BioLegend, London, United Kingdom

4.1.5 Biomaterials

4.1.5.1 Biomaterials with defined surface topopgraphies

Model surface	Material	Surface Properties
Samples with varying roughness		
P0	Polyurethane	Ra = 0.1 µm
P1	Polyurethane	Ra = 0.25 µm
P2	Polyurethane	Ra = 0.5 µm
P3	Polyurethane	Ra = 1.0 µm

Model surface	Material	Surface Properties
P4	Polyurethane	Ra = 2.2 µm
P5	Polyurethane	Ra = 4.5 µm
P6	Polyurethane	Ra = 9.0 µm
P7	Polyurethane	Ra = 18.0 µm
Samples with varying hydrophobicity		
PEM 1	Anionic Polyethylen multilayer	Contact angle = 17.2°
PEM 2	Anionic Polyethylen multilayer	Contact angle = 40.0°
PEM 3	Anionic Polyethylen multilayer	Contact angle = 46.8°
PEM 4	Anionic Polyethylen multilayer	Contact angle = 54.5°
Samples with varying surface properties		
titanium 1	Titanium	Polished
titanium 2	Titanium	Sandblasted
titanium 3	Titanium	Acid etched
titanium 4	Titanium	Sandblasted and acid etched
titanium 5	Titanium	Hydrophilic sandblasted and acid etched

4.1.5.2 Materials intended for commercial applications

Class	Material
Solid implant materials (materials A)	A_1
	A_2
	A_3
	A_4
	A_5
Polymer-based membranes (materials B)	B_1
	B_2
	B_3
Collagen-based membranes (materials C)	C_1
	C_2
Polymer-based membranes (materials D)	D_1
	D_2
	D_3
	D_4
Gelatin-based gels (materials E)	E_1
	E_2
	E_3
Polymer-based membranes (materials F)	F_1
	F_2
	F_3
	F_4
Collagen-based gels (material G)	G

4.1.6 Expression constructs

Expression construct	Origin
actin-CB	Panza et al., 2015
LifeAct	Riedl et al, 2008

4.1.7 Cell lines

4.1.7.1 Parental cell lines

Cell line	Additional information	Origin
THP-1	TIB-202 human monocyte	ATCC
U937	CRL-1593.2 human monocyte	ATCC

4.1.7.2 Stable cell lines

Cell line	Origin
THP-1_actin-CB	this study
THP_1_Lifeact	this study

4.2 Methods

4.2.1 Biochemical methods

4.2.1.1 Mammalian cell lysis

Monocytic THP-1 cells were seeded at 1.2 x 10^6 cells per well in a 6-well-plate and differentiated as described below (section 4.2.2.2). Subsequently, chemical induction of macrophage polarization was carried out according to section 4.2.2.3. Hereafter, cells were washed and harvested in PBS. Following centrifugation (200 x g, 5 min, 4 °C) cell pellets were snap-frozen in liquid nitrogen and stored at -20 °C until further usage. Cell lysis was performed in 100 µL NP40 lysis buffer (10 mM Tris/HCl pH 7.5, 150 mM NaCl, 0.5 mM EDTA, 0.5% NP-40) by repeated vortexing for 30 min on ice. Lysates were clarified by centrifugation (18,000 x g, 15 min, 4 °C) and protein concentrations of the soluable supernantant were determined by BCA Protein assay (Thermo Fisher) according to manufacturer's protocol. Finally, protein samples were adjusted to equal concentrations.

4.2.1.2 SDS-PAGE and Western Blot

Size dependent separation of proteins was performed using denaturing polyacrylamide gel electrophoresis on a BIO-RAD Mini-PROTEAN® Tetra Cell System. To this end, gels were prepared according to Table 2 and Table 3. Protein samples containing 1x reducing SDS sample

buffer (0.1% 2-Mercaptoethanol, 0.0005% Bromophenol blue, 10% Glycerol, 2% SDS in ddH2O) were denaturated at 95 °C for 10 min, subsequently loaded onto the acrylamide gel and separated at 120 V in running buffer (25 mM Tris/HCl, 192 mM glycine in ddH2O). PageRuler Plus prestained protein ladder was used as a standard.

Table 2: Composition of SDS-running gel

Component	Final concentration
Acrylamide	8-15% (v/v)
Tris/HCl, pH 8.8	375 mM
SDS	0.1% (w/v)
APS	0.05% (w/v)
TEMED	0.1% (v/v)

Table 3: Composition of SDS-stacking gel

Component	Final concentration
Acrylamide	5% (v/v)
Tris/HCl, pH 6.8	60 mM
SDS	0.1% (w/v)
APS	0.05% (w/v)
TEMED	0.1% (v/v)

Transfer of separated proteins from the SDS-gel onto a nitrocellulose membrane (GE Healthcare) by semi-dry Western Blotting (BIO-RAD Trans-Blot Semi-Dry Transfer Cell). Proteins were transferred at 2.5 mA per cm^2 for 90 min using Towbin blotting solution (25 mM Tris/HCl, 192 mM glycine, 20% methanol in ddH2O). Subsequently, membranes were stained with Ponceau S solution (0.5% Ponceau S, 10% acetic acid in ddH2O) for 5 min to reversibly visualize total proteins on membrane. For specific detection of proteins, membranes were incubated with the respective primary antibodies (see section 4.1.4) in M-TBST (5% nonfat dry milk in TBST (0.05% Tween in tris buffered saline)) over night. The following day, membranes were washed three times with TBST for 5 min each and subsequently incubated with fluorescently labeled species-specific secondary antibodies (see section 4.1.4) diluted in M-TBST for 2 h at room temperature. After washing membranes thrice with TBST for 10 min, they were dried at room temperature. A Typhoon-Trio laser scanning system was used to detect fluorescent signals. Quantification of signal intensities was carried out using ImageJ.

4.2.1.3 Cytokine analysis using multiplexed bead-based sandwich immunoassays

All cytokine measurements were performed by Meike Jakobi.

For polyurethane samples, expression levels of IL-1β, IL-1RA, IL-6, IL-8, IL-10, MCP-1, MIP-1 β, and TNF-α were determined using the Magnetic Luminex Performance Assay, Human Cytokine Premixed Kit A (R&D Systems, Wiesbaden, Germany). The reagent volumes were adjusted for a 96 half well plate format. The following volumes were used per well: 25 µL diluted microparticle cocktail, 25 µL standard/sample volume, 30 µL diluted biotin antibody cocktail, and 30 µL streptavidin-phycoerythrin solution. All other steps were performed according to the manufacturer's instructions. Samples were thawed at 4°C and measured undiluted and at a 1:8 dilution. The samples were analyzed as singlets. All measurements were performed on a Luminex FlexMap® 3D analyzer system, using Luminex xPONENT® 4.2 software (Luminex, Austin, TX, USA). For data analysis, MasterPlex QT version 5.0 was employed.

For all other experiments, levels of IL-1β, IL-1Ra, IL-4, IL-6, IL-8, IL-10, IL-12p70, IL-13, GM-CSF, IFNγ, MCP-1, MIP-1 β, TNFα and VEGF were determined using a set of Luminex-based sandwich immunoassays (developed by Meike Jakobi), each consisting of commercially available capture and detection antibodies and calibrator proteins. All assays were thoroughly validated ahead of the study with respect to accuracy, precision, robustness, specificity and sensitivity. Samples were diluted at least 1:4 or even higher. After incubation of the pre-diluted samples or calibrator protein with the capture coated microspheres, beads were washed and incubated with biotinylated detection antibodies. Streptavidin-phycoerythrin was added after an additional washing step for visualization. For control purposes, calibrators and quality control samples were included on each microtiter plate. All measurements were performed on a Luminex FlexMap® 3D analyzer system, using Luminex xPONENT® 4.2 software (Luminex, Austin, TX, USA). For data analysis MasterPlex QT, version 5.0 was employed. Standard curve and quality control samples were evaluated according to internal criteria adapted to the Westgard Rules to ensure proper assay performance.

4.2.2 Cell culture methods

4.2.2.1 Culturing of mammalian cells

All cell culture techniques carried out in this study were performed under sterile conditions in a laminar flow hood. Cell lines used in this study were grown in T25, T75 or T175 culture flasks at 37 °C in a humidified chamber with 5% CO_2. THP-1, THP-1_actin-CB and U937 cells were cultured in suspension in RPMI supplemented with 10% (v/v) Fetal Bovine Serum (FBS) and 1% (v/v) penicillin-streptomycin. Cells were sub-cultured routinely by centrifugation and subsequent resuspension upon reaching 8 x 10^5 cells/mL. Cell number was determined by using the CASY Cell Counter system. All cell lines were tested negative for mycoplasma using the PCR mycoplasma kit Venor GeM Classic (Minerva Biolabs) and the Taq DNA polymerase (Minerva Biolabs). Since this study does not include cell line-specific analysis, all cell lines were used without additional authentication.

4.2.2.2 Differentiation protocol

Differentiation of monocytic cells THP-1 and U937 into macrophage-like cells was carried out by treatment with phorbol-12-myristate-13-acetate (PMA, Sigma-Aldrich). For this purpose, 1.2 x 10^6 cells per well were seeded in 6-well-plates and cultured in the presence of 50 ng/mL PMA for 48 h. Subsequently, PMA-containing medium was removed and cells were rested in PMA-free RPMI medium for further 48 h.

4.2.2.3 Polarization protocol

For chemical induction of macrophage polarization, PMA-treated THP-1 and U937 derived macrophages were plated at a density of 5 x 10^4 cells/cm^2 on tissue culture plate (TCP) and were treated with 50 ng/mL lipopolysaccharide (LPS) derived from *Escherichia coli* O55:B5 (Merck Millipore, USA) and 20 ng/mL IFN-γ (Miltenyi, Germany) to obtain M1 macrophage phenotype or treated with 20 ng/mL IL-4 (Miltenyi, Germany) and 20 ng/mL IL-13 (Miltenyi, Germany) to generate M2 macrophage phenotype.

4.2.2.4 Cell seeding

PMA-treated THP-1 cells were detached using 0.05% Trypsin/EDTA (Gibco, USA), plated at a density of 5 x 10^4 cells/cm^2 on the corresponding substrates, and cultured for 72 h. For biochemical analyses 1.2 x 10^6 cells were seeded into 6-well-plates and subjected to compound treatment.

4.2.2.5 Generation of stable cell lines

Stable cell lines THP-1_actin-CB and THP-1_Lifeact were generated by plasmid transfection of the indicated expression constructs using TransIT-2020 (VWR) according to the manufacturer's protocol. 72 h post transfection cells were subjected to a four week selection period using 1 µg/mL G418 (Carl Roth). Following, GFP-positive cells were sorted using FACS Melody (BD).

4.2.2.6 Flow cytometry analysis

For flow cytometry analysis, cells were harvested using Trypsin/EDTA. Trypsination was stopped using RPMI. Cells were centrifuged at 200 x g for 5 min and washed with 5 mL FACS staining buffer (1% FCS in PBS). Cells were centrifuged again at 200 x g for 5 min and supernatant was discarded. Cells were vortexed and the respective conjugated antibody was added to the cells and incubated on ice for 15 min in the dark. Following staining, cells were washed twice with the FACS staining buffer followed by centrifugation (200 x g for 5 min) and subsequent discarding of the supernatant. Cells were resuspended in 300 µL FACS staining buffer and flow cytometric analysis was performed. Data were analyzed using FlowJo software v10 (FlowJo LLC)

4.2.2.7 Wound healing assay

For wound healing assays, 2 x 10^5 THP-1_wt or THP-1_actin-CB derived macrophages were seeded in 24-well-plates and allowed to adhere for three hours. Scratch wounds were applied with a 100 µl pipette tip and non-adherent and cells were washed twice with PBS. Fresh medium without further stimuli, with 50 ng/mL LPS and 20 ng/mL IFN-γ, or with 20 ng/mL IL-4 and 20 ng/mL IL-13 was added and cells were cultured for 72 h. Phase contrast images were taken immediately (0 h), 24 h and 72 h after wounding with an Axiovert 200M (Zeiss AG) 10 x magnification. Open wound areas were determined with ImageJ software.

4.2.2.8 Immunocytochemistry and fluorescence microscopy

Parental and stable macrophage-like cells were seeded at 20,000 cells per well in µClear 96-well plates (Greiner) and cultivated with the according stimuli for 72 h. Accordingly, cells were seeded at concentrations of 100,000 cells per well in a 24-well-plate. For fixation, cells were twice with PBS and were fixed with 4 % formaldehyde (v/v, PFA, Applichem) in PBS. Subsequently, cells were stained with fluorescently labeled phalloidin and DAPI in PBS for 15 min at room temperature. Images of fixed cells were acquired with an ImageXpress micro XL system and analyzed by the MetaXpress software (64 bit, 6.2.3.733, Molecular Devices).

4.2.2.9 Time-lapse imaging

For time-lapse THP-1_actin-CB derived macrophages were seeded at a concentration of 2 x 10^4 cells per well in µClear 96-well plates (Greiner) and were allowed to adhere for 3 h. Nuclei were stained with 2 µg/mL Hoechst33258. Live-cell imaging was performed by using MetaXpress Micro XL system (Molecular Devices) and 20 X magnification at 37 °C in a humidified atmosphere containing 5 % CO2. Fluorescence images were acquired for up to 72 h, in which the time interval of image acquisition was every 24 h.

4.2.2.10 Image segmentation

Fluorescence images acquired with the ImageXpress Micro XL system were analyzed by the MetaXpress Custom Module editor software (64 bit, 5.1.0.41, Molecular Devices). To allow automated nuclei segmentation, nuclei of live cells were stained with 2 µg/mL Hoechst33258 and nuclei of fixed cells were stained with DAPI.

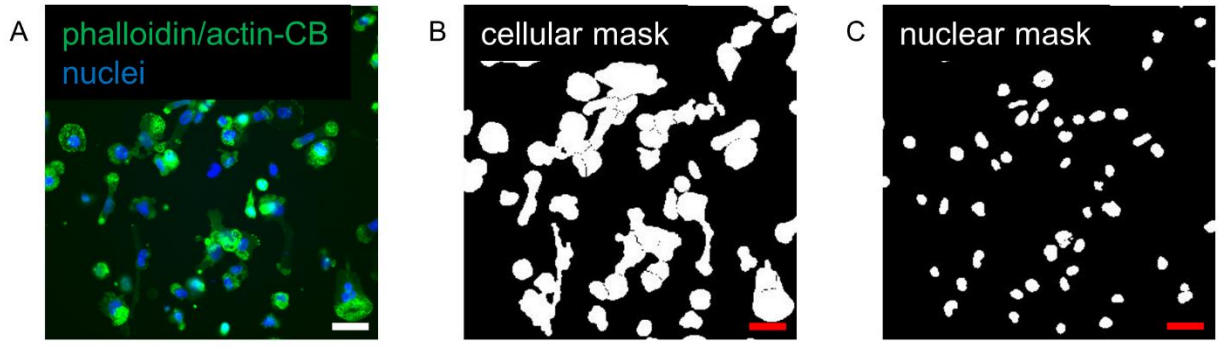

Figure 2: Schematic overview of automated analysis of fluorescence images.

(A) Fluorescence images of THP-1 derived macrophages showing phalloidin signal or actin-CB signal (green) and nuclei stained with DAPI or Hoechst (blue). (B) Representative image segmentation mask based on phalloidin or actin-CB signal using MetaXpress Custom Module editor software (64 bit, 5.1.0.41, Molecular Devices). (C) Automated nuclei segmentation mask of THP-1 derived macrophages based on Hoechst/DAPI staining. Scale bar: 50 µm.

To quantify the cellular morphology of THP-1 derived macrophages an algorithm segmenting the whole cell (nuclear and cytosolic compartment) was applied (**Figure 2**). The settings identifying the phalloidin or actin-CB signal were: (i) an appropriate width between 30 µm and 100 µm and (ii) a minimum intensity of 200 above local background (**Figure 2 B**). Next, nuclei regions were determined based on the DAPI/Hoechst signal utilizing the following settings: (i) an appropriate width between 10 µm and 30 µm and (ii) a minimum intensity of 200 above local background (**Figure 2 C**). An overlay of the cellular and nuclei segmentation mask was then applied to the fluorescence image in order to identify whole cells.

Based on this segmentation, morphological analysis and subsequent image-based quantification was performed using a set of the following predefined morphometric parameters: Cell circularity, cell elongation, and cell area. Cell shape factor and cell elongation factor were used to quantify cell shape. The cell elongation factor was determined as a ratio of the long to the short axis in which a higher value indicates increased elongation. To further distinguish round macrophages from flattened or elongated macrophages, the cell shape factor was applied. This factor describes the cell circularity and takes a value between 0 and 1, whereby a value near 0 indicates a flattened object and a value of 1 indicates a perfect circle. Cell area describes the contiguous area of each cell.

4.2.2.11 Determination of actin structures

Actin structures within THP-1 derived macrophages were determined by manually counting the number of positive cells and the total number of cells employing ImageJ software. Based on these values, the percentage of podosome-positive cells and the percentage of positive cells showing cortical actin was determined. For each condition, at least 100 cells were analyzed of at least two independent experiments. The positive cell average was divided by the total cell number average and multiplied by 100 to obtain the percentage of cells with podosomes or the percentage of cells with cortical actin respectively.

4.2.2.12 SEM imaging

SEM imaging was performed independently by Dr. Antje Biesemeier.

For SEM imaging cells were washed three times with phosphate buffered saline (PBS) and fixed for 2 h on ice using 4% (w/v) paraformaldehyde (PFA) and 2% (w/v) glutaraldehyde in PBS. Samples were subsequently washed thrice in PBS and dehydrated with a graded ethanol series increasing in concentration (30%, 50%, 70%, 80%, 95%, 100%). The samples were then prepared for scanning electron microscopy (SEM) by critical point drying and coated with a 10 nm film of gold-palladium. Surface imaging was performed using a Zeiss Auriga 40 SEM (Zeiss, Oberkochen, Germany) at 3 keV acceleration voltage using the chamber secondary electron detector.

5 RESULTS

5.1 Comparative evaluation of *in vitro* human-based macrophage models for an optical readout of cell morphology

THP-1 and U937 are commonly used human cell lines to study macrophage differentiation (Chanput, Peters, & Wichers, 2015) and subsequent polarization of monocyte derived macrophages into the pro-inflammatory M1 or the anti-inflammatory M2 phenotype *in vitro* (Genin, Clement, Fattaccioli, Raes, & Michiels, 2015; He et al., 2018). Previous studies have shown that these macrophage models resemble the expression profile of polarized primary macrophages (Genin et al., 2015; Taniguchi et al., 2015). Furthermore, upon polarization they adapt different phenotypes in terms of morphology (Taniguchi et al., 2015; Wheeler et al., 2018). However, to date there is no consensual protocol for *in vitro* differentiation and polarization of the monocytic cell lines THP-1 and U937 available. Therefore, a set of protocols for differentiation and polarization of the cell lines were evaluated with the aim to effectively quantify morphological differences between macrophages reflecting their different polarization states.

For this purpose, first, different differentiation protocols were tested (**Figure 3**): THP-1 and U937 cells were treated with PMA in different concentrations and varying treatment durations (24 h, 48 h, and 72 h). To ensure the same overall cultivation time (96 h) for all cells, PMA treatment was followed by a final resting phase in PMA-free medium (72 h, 48 h, 24 h).

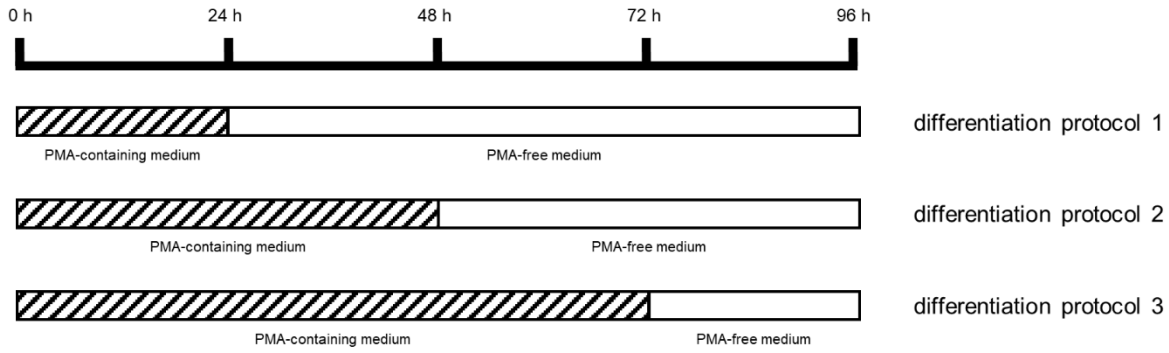

Figure 3: Varying differentiation protocols to induce the macrophage phenotype in monocytic cell lines THP-1 and U937.

Subsequently, cellular morphology was analyzed *in situ* by actin staining using phalloidin Alexa Fluor 555 (phalloidin$_{AF555}$). Actin cytoskeleton staining showed that PMA-treated THP-1 and U937 cells employ different morphologies. Whereas U937 derived macrophages predominantly exhibited a small cellular size and round morphology, THP-1 derived macrophages were larger and more elongated. However, neither PMA-concentrations nor treatment duration affected the morphology of monocyte derived macrophages (**Figure 4 A, C**).

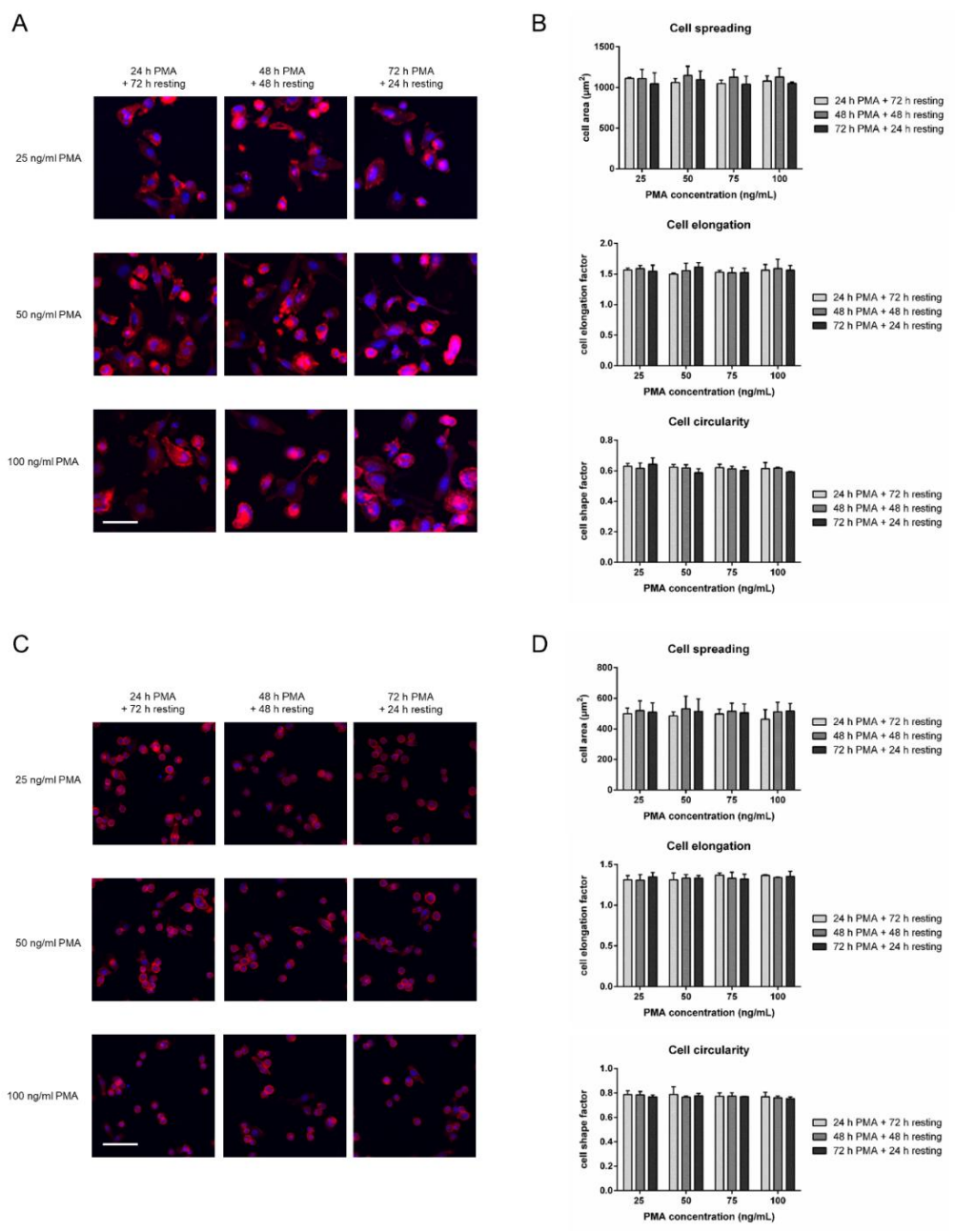

Figure 4: Morphology of THP-1 derived macrophages and U937 derived macrophages following PMA treatment.

(A, C) Fluorescence images of fixed (A) THP-1 derived macrophages or (C) U937 derived macrophages, respectively. Cells were treated with different concentrations of PMA (25 ng/mL, 50 ng/mL, and 100 ng/mL) using varying differentiation protocols (24 h PMA + 72 h resting, 48 h PMA + 48 h resting, 72 h PMA + 24 h resting). For fluorescence imaging cells were PFA-fixed and stained with phalloidin$_{AF555}$ (actin cytoskeleton, red) and DAPI (nucleus, blue). Scale bar: 50 µm. (B, D) Quantified morphological characteristics of (B) THP-1 derived macrophages and (D) U937 derived macrophages. Data are derived from automated image analysis of cells cultured with different concentrations of PMA and different incubation times. Graphs show total cell spreading, cell circularity, and cell elongation. Data are presented as mean ± SD of >200 cells. For statistical analysis student's t-test was performed.

For a representative quantification of the cellular morphology, an automated image segmentation algorithm was employed which allowed the quantitative analysis of populations comprising >200 cells (details of the algorithm are described in section 4.2.2.10). Using this algorithm morphological parameters (cell spreading, cell elongation, and cell circularity) of individual cells were determined (**Figure 4 B, D**). Automated image quantification confirmed morphological differences in size and shape between THP-1 and U937 derived macrophages, as shown by increased cell spreading of THP-1 cells in comparison to U937 cells or a decrease in cell circularity alongside increased cell elongation of THP-1 cells compared to U937 cells, respectively. Furthermore, population-wide analysis revealed that there are no significant effects of PMA concentrations and treatment duration on cellular morphology of THP-1 or U937 derived macrophages. Considering a nearly similar cell spreading and cell shape, the differentiation protocol 2 (48 h treatment with 50 ng/mL PMA; 48 h resting period) was chosen for further experiments to generate U937 or THP-1 derived macrophages in this study.

Next, it was analyzed whether the induction of M1 or M2 phenotypes in THP-1 and U937 derived macrophages correlate with specific morphological changes. To this end, THP-1 and U937 cells were differentiated as described above and subsequently chemically stimulated with LPS and IFN-γ or IL-4 and IL-13 for polarization into the pro-inflammatory M1 phenotype or the anti-inflammatory M2 phenotype respectively (**Figure 5 A**). After chemical stimulation for 72 h, THP-1 derived macrophages displayed distinct morphologies either reflecting the M1 or the M2 phenotype. Whereas morphologies of THP-1 derived M2 macrophages obviously did not differ from M0 macrophages, THP-1 derived M1 macrophages preferably showed a round shape, indicated by an increased cell circularity factor and decreased cell elongation factor compared to M0 macrophages (**Figure 5 B, C**). In contrast, no morphological differences between different polarization states of U937 derived macrophages could be observed (**Figure 5 D, E**).

Considering these findings, THP-1 cells were chosen for all further experiments as morphology was considered an essential readout for this study.

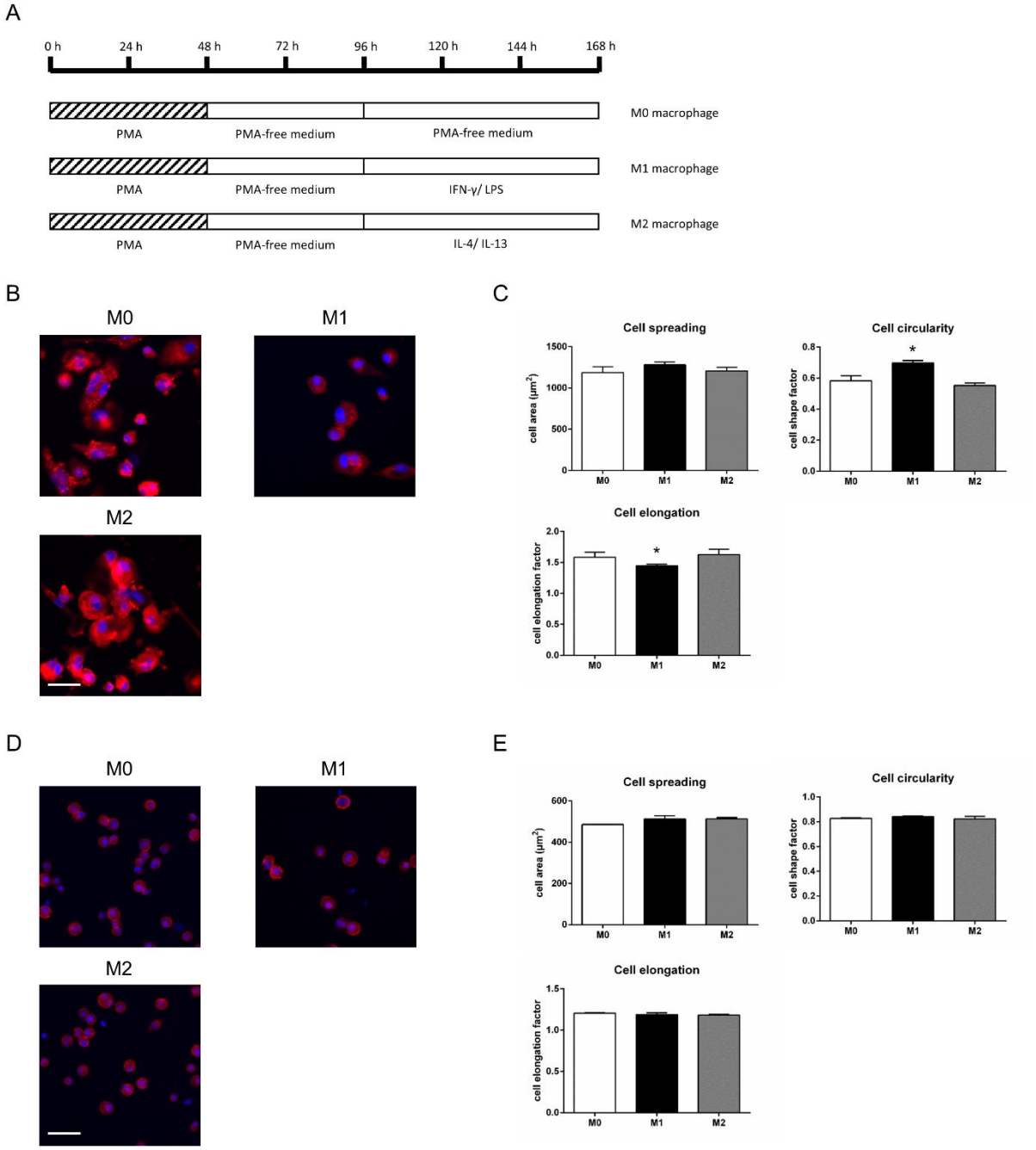

Figure 5: Morphology of THP-1 and U937 derived M0, M1, and M2 macrophages.
(A) Schematic outline of polarization protocols used to induce the macrophage phenotypes M0, M1 and M2 in monocytic cell lines THP-1 and U937. Cells were treated with 50 ng/mL PMA for 48 h, followed by a 48 h resting period in PMA-free medium. Following the differentiation protocol, THP-1 and U937 derived macrophages were cultured in the presence of LPS/IFN-γ to induce the M1 phenotype or IL-4/IL-13 to induce the M2 phenotype for 72 h. Macrophages without further chemical stimulation were defined as M0 macrophages. Subsequently, cells were PFA-fixed and stained with phallodin$_{AF555}$ (actin cytoskeleton, red) and DAPI (nucleus, blue). Scale bar: 50 µm. (B,

*D) Representative fluorescence images of fixed (B) THP-1 and (D) U937 derived M0, M1, and M2 macrophages. (C, E) Quantification of morphological characteristics (total cell spreading, cell circularity, and cell elongation) of (C) THP-1 and (E) U937 derived macrophages polarized into the M0, M1, or M2 phenotype. Data are presented as mean ± SD of >200 cells. For statistical analysis student's t-test was performed. * $p < 0.05$ vs M0.*

Taken together, the results of this section support the idea that THP-1 derived macrophages undergo morphological changes towards a more circular shape upon polarization into the pro-inflammatory M1 phenotype as previously stated for macrophages in different studies (Jain & Vogel, 2018; McWhorter et al., 2013).

5.2 Characterization of polarization in THP-1 derived macrophages

After demonstrating morphological changes for THP-1 derived macrophages upon chemical stimulation, the next question was how to confirm the desired macrophage polarization states. As described afore in section 3.2.2, the polarization phenotype can be characterized by a wide set of different readout parameters, including cytokine secretion, expression of surface marker proteins (e.g. CD molecules) and intracellular expressed factors or proteins. Accordingly, the activation of THP-1 derived macrophages in response to the chemical polarization signal was validated using biochemical and cell biological assays, such as bead-based sandwich immunoassays, flow cytometry and Western Blot.

5.2.1 Quantitative analysis of secreted cytokines

The gold standard for the quantitative measurement of cytokines and other biomarkers have long been enzyme linked immunosorbent assays (ELISAs). However, ELISAs are limited in the number of samples and analytes that can be measured. For the measurement of a high number of analytes multiplex bead array assays are nowadays applied, using an automated 96-well format (Elshal & McCoy, 2006). For the research campus "system immunology at biological-technical interfaces", in which the present study was also carried out, cytokine secretion was defined as an essential readout and a large number of different samples were generated. Thus, a bead-based sandwich immunoassay was developed for the cytokine expression analyses. The development and validation of this assay was performed independently by Meike Jakobi. Utilizing this cytokine detection panel 14 different pro-inflammatory (IL-1β, IL-6, IL-8, IL-12p70, GM-CSF, IFN-γ, MCP-1, MIP-1 β, and TNF-α) and anti-inflammatory cytokines (IL-1Ra, IL-4, IL-10, IL-13, and VEGF) could be quantified. Measurements of cytokines in the supernatant were also performed by Meike Jakobi.

Secretion of pro- and anti-inflammatory cytokines and chemokines were utilized to assess polarization states of THP-1 derived macrophages. Herein, the expression of pro-inflammatory cytokines is particularly associated with the M1 phenotype whereas upregulated levels of anti-inflammatory cytokines are characteristic for the M2 phenotype.

For the quantification of the cytokine response, THP-1 derived macrophages were either stimulated with LPS/IFN-γ into the pro-inflammatory M1 phenotype or with IL-4/IL-13 to induce the anti-inflammatory M2 phenotype for 72 h. Macrophages left untreated were considered as M0 macrophages. As expected, levels of pro- and anti-inflammatory cytokines were low for naïve THP-1 derived M0 macrophages (**Figure 6**). Instead, after LPS/IFN-γ stimulation THP-1 derived macrophages showed an increased expression of pro-inflammatory cytokines concomitantly with a decreased expression of the anti-inflammatory marker IL-10. Moreover, expression of the wound healing factor VEGF was significantly upregulated. Contrary to M1 activation, induction of the M2 phenotype was not associated with highly up-regulated pro-inflammatory cytokines but a significant increase of the anti-inflammatory cytokine IL-1Ra and decreased VEGF expression.

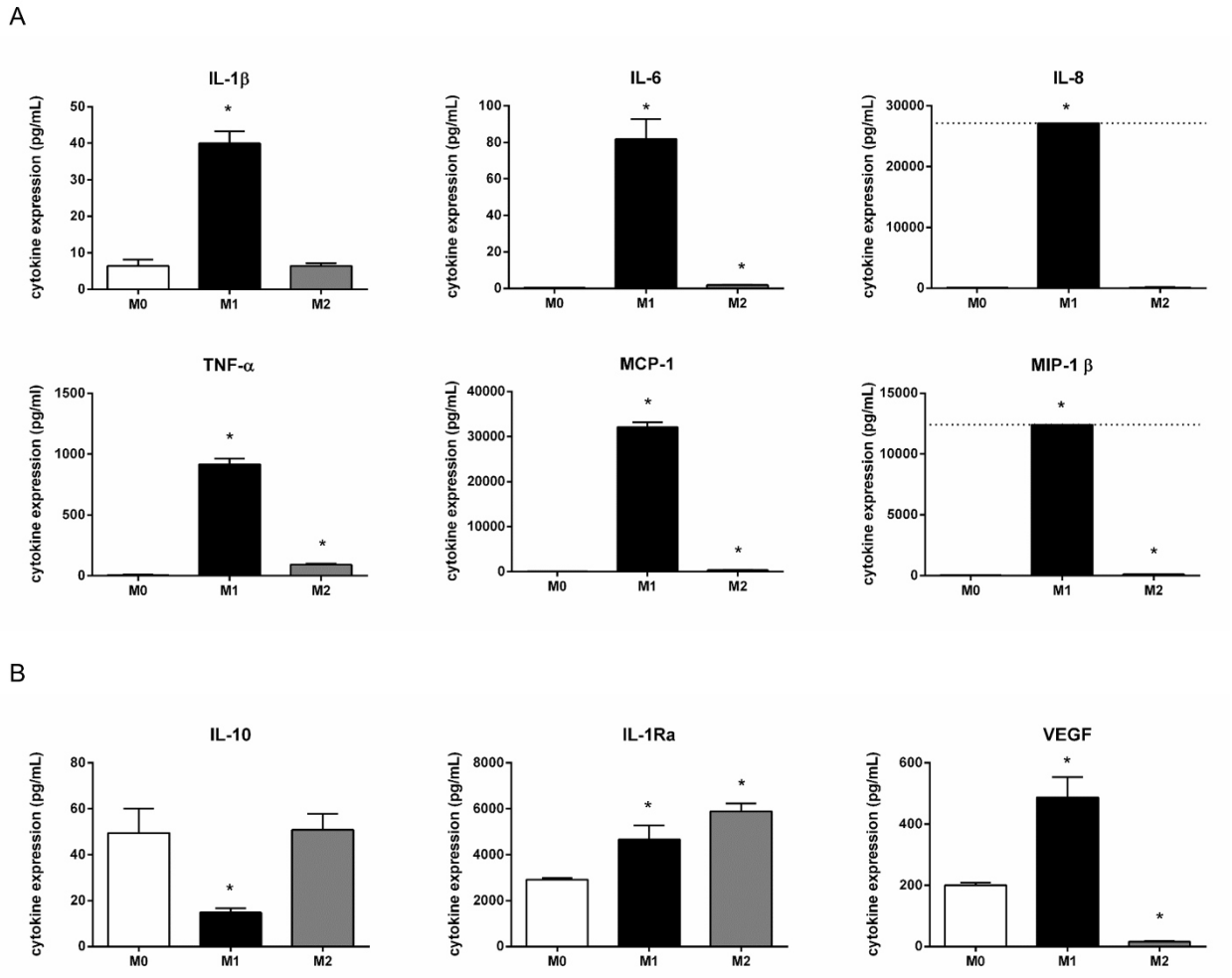

Figure 6: Pro- and anti-inflammatory cytokine production from THP-1 derived M0, M1, and M2 macrophages. *THP-1 derived macrophages were cultured without further chemical stimuli (M0), in the presence of LPS and IFN-γ (M1), or in the presence of IL-4 and IL-13 for 72 h. Expression of (A) pro-inflammatory or (B) anti-inflammatory cytokines was assessed in the supernatant using the cytokine detection panel developed by Meike Jakobi. The dotted line represents the Upper Limit of Quantification (ULoQ). Results are presented as mean cytokine concentration (pg/mL) ± S.D. of three biological replicates. For statistical analysis student's t-test was performed. * $p < 0.05$ vs M0. Cytokines were measured independently by Meike Jakobi.*

In summary, the M0, M1, and M2 phenotype of THP-1 derived macrophages could be confirmed by secretion levels of cytokines.

5.2.2 FACS analysis of expressed surface markers

The next marker analyzed within chemically induced macrophage polarization was abundance of several surface marker proteins: CD11b, CD80, CD206, and CD209. Expression of the macrophage marker CD11b (Chanput, Mes, & Wichers, 2014) was used to further confirm successful differentiation of THP-1 cells. Additionally, while high expression of CD80 is observed in M1

macrophages, CD206 and CD209 are typically associated with M2 macrophages (Y. H. Zhang, He, Wang, & Liao, 2017). Using flow cytometry, the expression of these surface markers was analyzed according to the gating strategy in **Figure 7 A**.

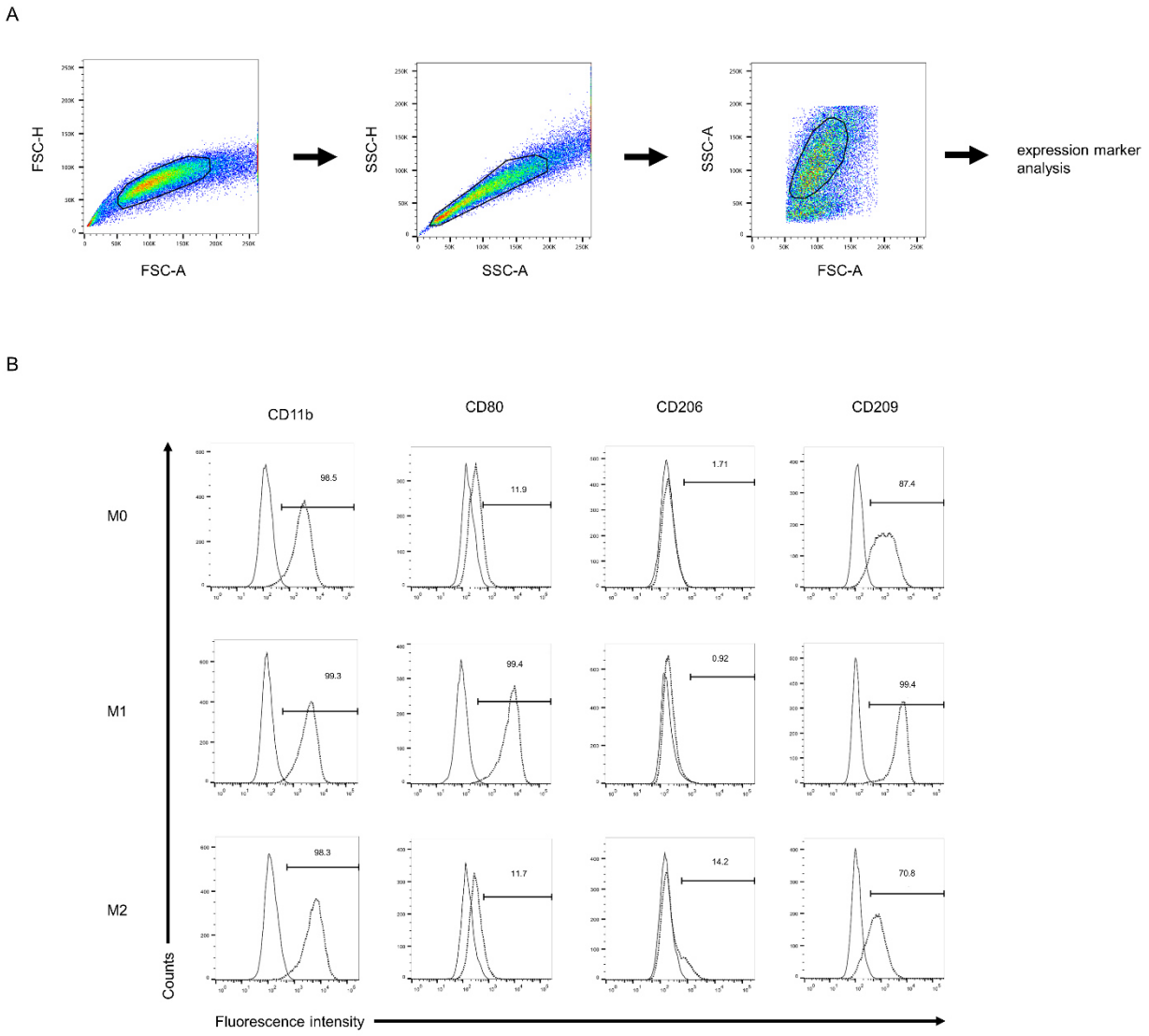

Figure 7: Cell surface marker expression from THP-1 derived macrophages upon polarization into the M0, M1, and M2 phenotype.
THP-1 derived macrophages were left non-treated (M0) or were treated with LPS/IFN-γ (M1) or IL-4/IL-13 (M2) for 72 h. The expression of cell surface markers CD80, CD206, and CD209 was assessed using flow cytometry. (A) Gating strategy used to identify populations of single cell THP-1 derived macrophages. (B) Shown are the results for unstained cells (solid line) or cells stained with specific fluorescence-coupled antibodies (dotted line). Values given in the histogram represent the percentage of corresponding surface marker-positive cells. The results are representative of three independent experiments showing similar results.

Surface marker expression in THP-1 derived macrophages was analyzed following treatment with LPS/IFN-γ (M1-activation) or IL-4/IL-13 (M2 activation) for 72 h. As shown in **Figure 7 B**, CD11b expression was highly upregulated in all THP-1 derived macrophage subsets, suggesting the macrophage character following PMA treatment. Upon subjection to M1 chemical polarization, a marked up-regulation of the pro-inflammatory marker CD80 and anti-inflammatory marker CD209 was observed. However, no expression of CD 206 was observed in THP-1 derived M1 macrophages. In contrast, following M2 chemical stimulation CD206 expression was partially increased along with upregulated CD209 expression, whereas abundance of CD80 was not affected. M0 macrophages cultured without further treatment only showed an upregulation of the marker CD209.

In summary, flow cytometry results using CD80 and CD206 verified M1 and M2 phenotypes upon chemical induction. Expression of the marker CD209 was deemed insufficient to distinguish THP-1 derived macrophage polarization as it was expressed in all conditions examined.

5.2.3 Quantitative analysis of immune-associated protein expression

To further confirm successful polarization of THP-1 derived macrophages into the pro-inflammatory M1 phenotype or the anti-inflammatory M2 phenotype, the expression of IDO and transglutaminase 2 (TG2), markers particularly expressed by M1 macrophages or M2 macrophages respectively. While IDO is an IFN-γ-inducible enzyme which limits the intensity of inflammation (Rani, Jordan, Divanovic, & Herbert, 2012), TG2 is upregulated by IL-4 and is involved in cross-linking of cellular proteins, phagocytosis of apoptotic cells, and extracellular matrix generation among others (Martinez et al., 2013).

To analyze the expression of IDO and TG2, quantitative Western blot analysis was performed (**Figure 8**). Following stimulation with LPS/IFN-γ or IL-4/IL-13 for 72 h, cells were lysed and equal amounts of soluble protein lysates were subjected to SDS-PAGE and subsequent Western blot analysis. As shown in **Figure 8 A**, only polarization into M1 phenotype induced an increased expression of IDO. On the other hand, an increased expression of TG2 could be observed for THP-1 derived M2 macrophages compared to M0 and M1 (**Figure 8 B**) which was further confirmed by densitometric analysis of three biological replicates.

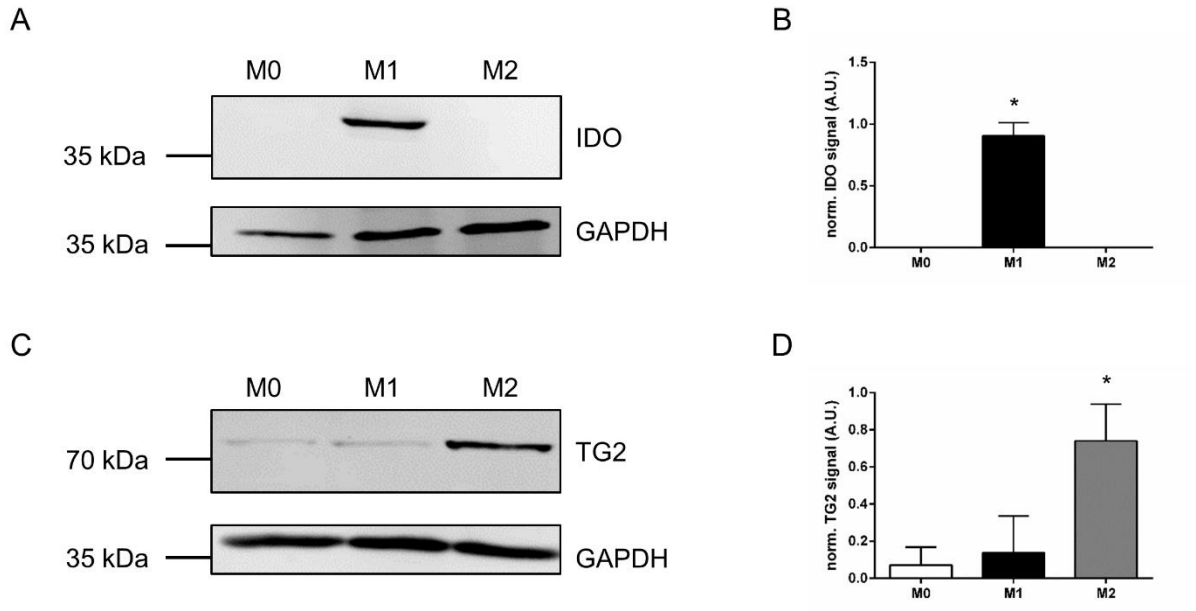

Figure 8: Effects of M1 and M2 polarization on protein expression in THP-1 derived macrophages.
*THP-1 derived macrophages were left untreated (M0) or incubated with LPS/IFN-γ to induce the M1 phenotype or IL-4/IL-13 for the induction of the M2 phenotype for 72 h. Following cultivation cells were lysed using 0.5% NP-40 lysis buffer and equal protein amounts of the soluble fraction were subjected to SDS-PAGE followed by Western Blot analysis. (A, C) Assessment of the proteins (A) IDO and (C) TG2 in THP-1 derived M0, M1 and M2 macrophages by western blotting. (B, D) Quantitative analysis of (B) IDO level and (D) TG2 level in differently polarized macrophages (M0, M1, and M2) normalized to GAPDH. Signal intensities were quantified from three biological replicates. Data are presented as norm. signal intensity ± S.D. For statistical analysis student's t-test was performed. * $p < 0.05$ vs. M0.*

5.2.4 THP-1 derived macrophage polarization states

Taken together, the results from the experiments of this section clearly support the suitability of the THP-1 cell line model for macrophage polarization into M0, M1 and M2 states. Notably, these finding further suggest that monitoring morphological changes upon chemical stimulation previously described in section 5.1 might be useful to determine distinct polarization states.

5.3 Assessment of biomaterial-induced immune response using THP-1 derived macrophages

The impact of biomaterials and their surface properties on cellular and especially immune responses has been previously demonstrated in a number of *in vitro* and *in vivo* studies. In this context, alterations in immune responses to biomaterials have been linked to specific surface properties such as surface chemistry, wettability, and topography or by incorporating bioactive molecules (reviewed in Mariani et al. (2019)). For example, degree of surface roughness and surface wettability properties were associated with differential immune responses (Brodbeck et al., 2002; Li et al., 2018; Lv et al., 2018; Shayan et al., 2018). Besides primary cells, cell lines are often used to study biomaterial-induced responses *in vitro*, as they present a reproducible model. Studies based on THP-1 derived macrophages are regularly employed, especially due to their proven correlation to *in vivo* effects (Alfarsi, Hamlet, & Ivanovski, 2014; Buser et al., 1991; Fernandes, Zhang, Magri, Renno, & van den Beucken, 2017). Hence, the model developed in this study was considered suitable to assess the effect of biomaterials on inflammatory reactions. Although, as mentioned above, various studies have shown that surface properties trigger distinct responses, a thorough understanding of the relationship between immune response and material properties is still lacking. Therefore, it was first examined whether systematic changes of defined surface properties on polyurethane and titanium also result in changes of the elicited immune response. In the next step, different classes of materials intended for commercial applications were analyzed. The investigation of these materials was conducted within the research campus "system immunology at biological-technical interfaces". Since materials were provided voluntarily by companies, exact composition and designations cannot be disclosed. However, these analyses allowed a narrower look on the effect of physical properties on the elicited immune response.

5.3.1 Polyurethane samples with varying surface roughness

The first biomaterials tested regarding their impact on the inflammatory and morphological response were polyurethane samples with defined surface roughness values ranging from 0.1 µm to 18 µm in average roughness in accordance to the VDI 3400 industrial standard (Segan et al., 2020). Degree of roughness increased from the flat surface PU 0 with no intentional roughness to PU 7, the roughest surface investigated in this study (**Table 4**). Polyurethane specimens were

fabricated independently by injection molding and provided for this study by the group of Prof. Dr. Günter Lorenz (Reutlingen University).

Table 4: Average roughness values of polyurethane specimens.
Samples increased in degree of roughness from PU 0 (no intentional roughness) to PU 7 (roughest surface).

Sample lable	PU 0	PU 1	PU 2	PU 3	PU 4	PU 5	PU 6	PU 7
Roughnes value (µm)	0.1	0.25	0.5	1.0	2.2	4.5	9.0	18.0

Immune cell activation on biomaterials occurs through adhesion and subsequent sensing of the underlying surface. Thus, at first, adhesion and interaction with topographical features of THP-1 derived macrophages cultured on polyurethane substrate (PU 6) was qualitatively evaluated through SEM imaging. Following three days of culture, macrophages were found to adhere in a heterogeneous fashion of isolated single cells and clusters of cells (**Figure 9**). Furthermore, SEM images showed in detail how THP-1 derived macrophages interact with the underlying topographical features such as elevations, dips, or protrusions.

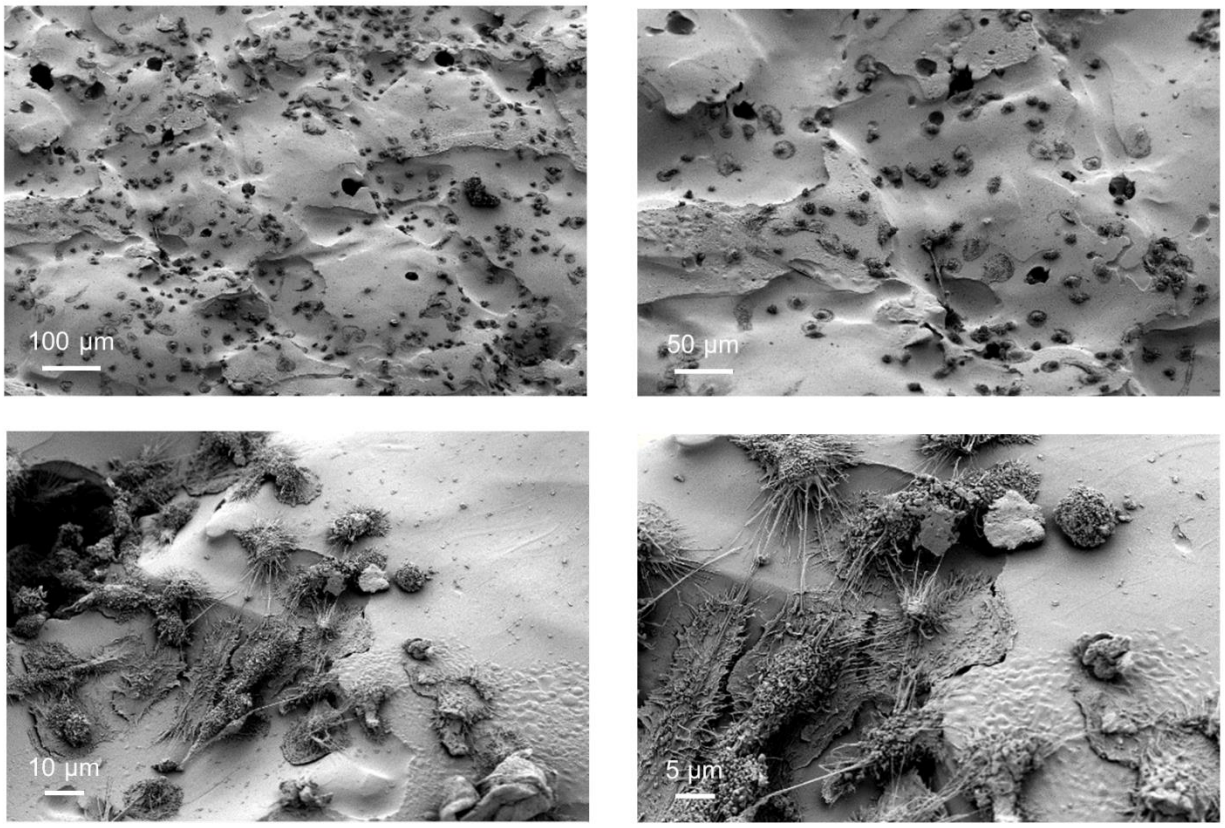

Figure 9: Representative scanning electron microscopy (SEM) images of THP-1 derived macrophages cultured on the polyurethane specimen PU 6.

SEM images show adherent THP-1 derived macrophages on polyurethane specimen PU 6 following three days of culture. Subsequently, cells were fixed in PFA and glutaraldhehyde, dehydrated in a graded series of ethanol and then prepared for SEM by critical point drying and coating with a 10 nm film of gold. Images were acquired at 3 keV acceleration voltage in collaboration with Dr. Antje Biesemeier.

After demonstrating that THP-1 derived macrophages adhere to the polyurethane surface in principle, next the morphology of macrophages cultured on polyurethane samples without intentional roughness (PU 0) and polyurethane samples with increasing degrees of surface roughness (PU 1 – PU 7) was investigated. To this end, THP-1 derived macrophages were cultured on polyurethane specimens for 72 h. As controls, cells were cultured on tissue culture plate (TCP) without further stimulation (M0) or were further polarized into the M1 phenotype (LPS/IFN-γ) or M2 phenotype (IL-4/IL-13). Subsequently, cells were fixed and stained with phalloidin$_{AF555}$ (green) as well as SYBR-Green for visualization of nuclei (blue). For quantitative description of the cellular morphology the morphometric parameters cell area, cell shape factor, and cell elongation factor were considered. Microscopic analysis showed distinct morphologies for macrophages under control conditions: M1 macrophages showed a more rounded shape as indicated by decreased cell elongation factor and increased cell shape factor compared to M0 and M2 macrophages (**Figure 10**).

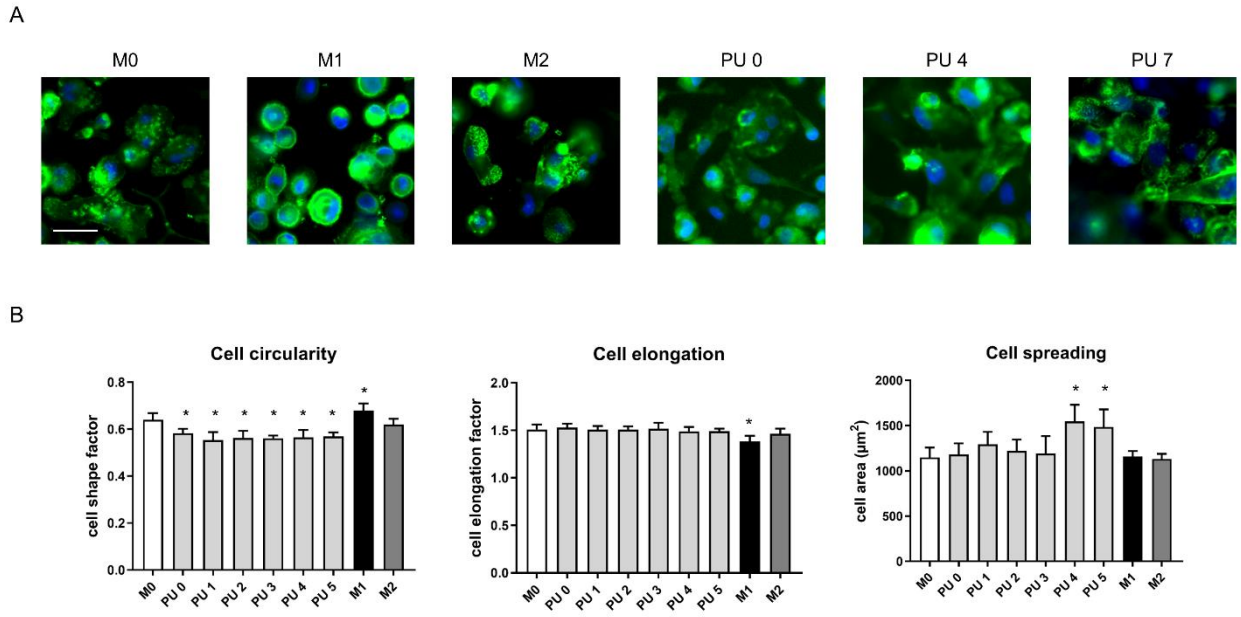

Figure 10: Morphology of THP-1 derived macrophages cultured on polyurethane specimens with different surface roughness and tissue culture plates (TCP) for controls.
(A) Representative fluorescence images of THP-1 derived macrophages cultured on different surfaces for 72 h. Cells grown on TCP were left untreated (M0) or were cultured in the presence of LPS/IFN-γ to induce the M1 phenotype or IL-4/IL-13 to induce the M2 phenotype. Moreover, cells were cultured on polyurethane specimens with different

*degrees of surface roughness (PU 0, PU 4, PU 7). For fluorescence imaging, cells were PFA-fixed and stained with phalloidin$_{AF555}$ (actin cytoskeleton, red) and SYBR Green (nucleus, blue). Scale bar: 50 µm. (B) Quantitative analysis of morphological characteristics (cell circularity, cell elongation, and total cell spreading) of THP-1 derived macrophages cultured on TCP (M0, M1, M2) and polyurethane specimens with varying surface roughness (PU 0 – PU 7). Data are presented as mean ± SD of >200 cells. For statistical analysis ordinary one-way ANOVA followed by a post hoc Tukey's test was performed. * $p < 0.05$ vs. M0.*

Upon cultivation on polyurethane specimens, THP-1 derived macrophages exhibited a less rounded morphology compared to M0 macrophages (**Figure 10**). However, the degree of surface roughness on the polyurethane samples did not seem to affect cell circularity and cell elongation. Cell area was merely increased on samples PU 4 and PU 5. The high degree of surface roughness prevented a morphometric image analysis of cells cultivated on samples PU 6 and PU 7

To further characterize the macrophage response, the secretion of pro-and anti-inflammatory cytokines was analyzed. As expected, M0 macrophages cultured on TCP expressed low levels of pro- and anti-inflammatory cytokines. Stimulation with LPS/IFN-γ (M1 activation) resulted in an up-regulation of pro-inflammatory markers, while following stimulation with IL-4/IL-13 (M2 activation) downregulated production of the pro-inflammatory cytokine IL-8 was observed. Macrophages cultured on polyurethane specimens responded with marginally elevated levels of pro-inflammatory cytokines, clearly below the level of M1 macrophages. Nevertheless, surface roughness degrees did not seem to exert a relevant effect on cytokine expression and release (Figure 12).

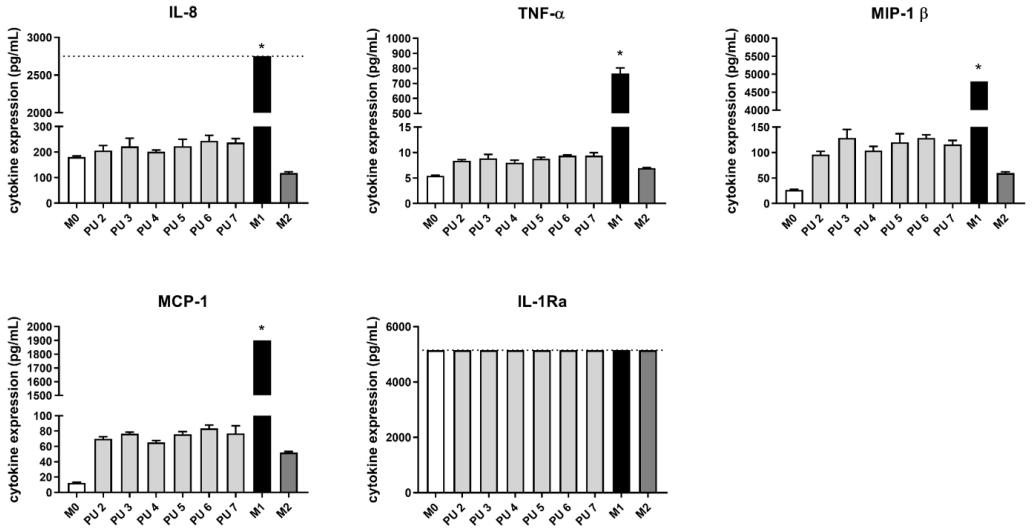

Figure 11: Pro- and anti-inflammatory cytokine production from THP-1 derived macrophages cultured on polyurethane specimens with different surface roughness and tissue culture plates (TCP) for controls.

*Expression of (A) pro-inflammatory or (B) anti-inflammatory cytokines was assessed in the supernatant from THP-1 derived macrophages cultured on polyurethane samples with increasing surface roughness ranging from PU 0 to PU 7 for 72 h or control cells cultured on TCP (M0, M1 (LPS/IFN-γ), M2 (IL-4/IL-13)) using the developed cytokine detection panel. The dotted line represents the Upper Limit of Quantification (ULoQ). Results are presented as mean cytokine concentration (pg/mL) ± S.D. of three biological replicates. For statistical analysis Kruskal-Wallis ANOVA followed by a post hoc Dunn's test was performed. * $p < 0.05$ vs. M0. Cytokines were measured independently by Meike Jakobi.*

In summary, the results obtained in this section indicated that surface roughness in the micrometer range on polyurethane have no impact on the inflammatory immune response. Furthermore, upon determining the cellular morphology of macrophages cultured on polyurethane samples this could be associated with the observed immune response: A lower expression of pro-inflammatory cytokines seems to correlate with a slightly elongated morphology.

5.3.2 Titanium samples with different surface topographies

Titanium and its alloys belong to the most prominent biomaterials used for implants due to their high biocompatibility (L. C. Zhang & Chen, 2019). However, recent studies demonstrated that changes in titanium surface properties result in specific cellular responses, thus altering the healing process following implantation (Alfarsi et al., 2014; Hotchkiss et al., 2016). Among these modifications are sandblasting, acid etching and surface coatings (Hotchkiss et al., 2016). To test whether titanium surface modifications might change immunological responses, a set of five titanium samples differing in their surface properties were provided by the research campus "system immunology at biological-technical interfaces" (**Table 5**) and analyzed with the THP-1 derived macrophage cell model.

Table 5: Average roughness values of polyurethane specimens.

Sample lable	Surface properties
titanium 1	polished
titanium 2	sandblasted
titanium 3	acid etched
titanium 4	sandblasted and acid etched
titanium 5	hydrophilized sandblasted and acid etched

In a first step, principal cell attachment on titanium 4 was qualitatively evaluated by SEM imaging. Following three days of culture, THP-1 derived macrophages were found to adhere on the rough titanium specimen. Most of the cells were elongated in shape with a flattened cell body(**Figure 12**).

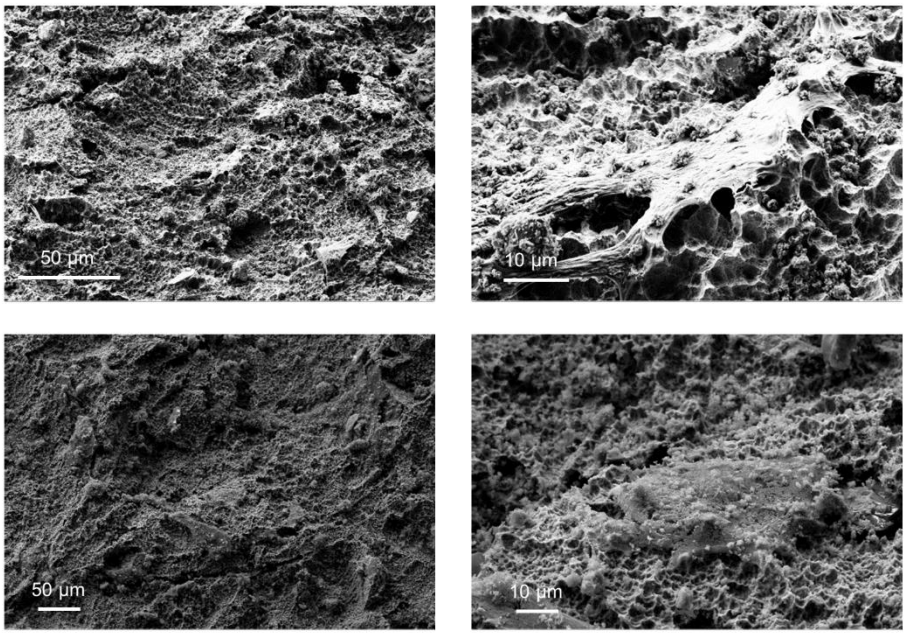

Figure 12: Representative scanning electron microscopy images of THP-1 derived macrophages grown on the sandblasted and acid-etched titanium (titanium 4).
SEM images show cells after 72 h of culture on titanium 4. Subsequently, cells were fixed in PFA and glutaraldhehyde, dehydrated in a graded series of ethanol and then prepared for SEM by critical point drying and coating with a 10 nm film of gold. Images in the right column were obtained under higher magnification of the same image section as the left column. At 3 keV acceleration voltage images were taken in collaboration with Dr. Antje Biesemeier.

Subsequently, the morphology of THP-1 derived macrophages cultured on titanium 1 – titanium 5 for 72 h was assessed by wide field fluorescence microscopy. As controls, macrophages were cultured on TCP without further stimulation or were either stimulated with LPS/IFN-γ into the pro-inflammatory M1 phenotype or with IL-4/IL-13 into the anti-inflammatory M2 phenotype for 72 h respectively. Immunofluorescence imaging upon staining with phallodin$_{AF555}$ (actin cytoskeleton, green) and DAPI (nuclei, blue) of fixed cells revealed distinct predominant morphologies in THP-1 derived macrophages cultured on different surfaces (**Figure 13**). Briefly, as observed before M1 macrophages display a more circular morphology compared to M0 and M2 macrophages, which was further quantified by automated image analysis (**Figure 13 B**). In general, cultivation of THP-1 derived macrophages on the surfaces titanium 1, titanium 2, and titanium 4 resulted in a predominant elongated morphology, while cells on the surfaces titanium 3 and titanium 5 showed a more rounded cell shape.

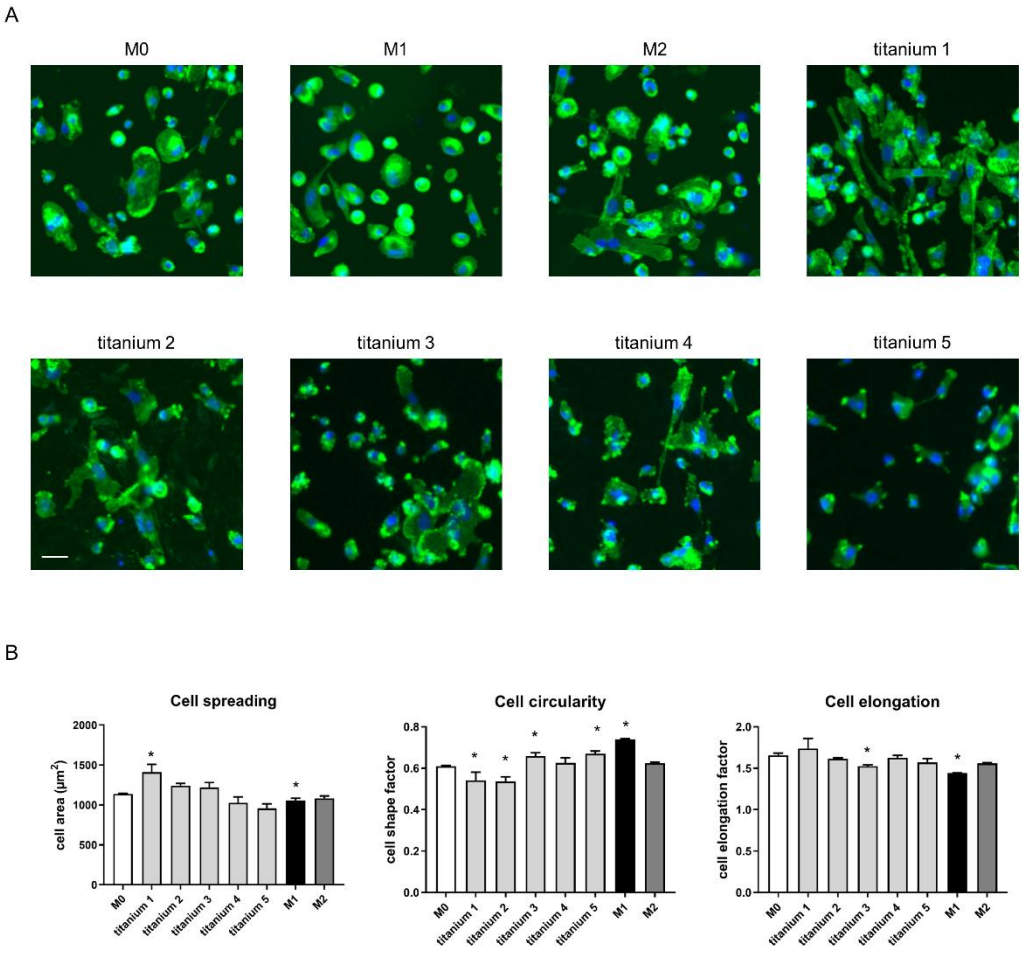

Figure 13: Morphological changes of THP-1 derived macrophages upon cultivation on tissue culture plates (TCP) and on titanium samples with varying surface properties.
*(A) Representative images of fixed THP-1 derived macrophages stained with phalloidin$_{AF555}$ (green) and DAPI (blue) after 72 h of culture on the corresponding titanium surfaces or TCP. For controls on TCP, cells were polarized into M0 macrophages (no stimulation), M1 macrophages (LPS/IFN-γ), or M2 macrophages (IL-4/IL-13). Scale bar: 50 µm. (B) Quantification of morphological parameters cell spreading, cell circularity and cell elongation in >200 THP-1 derived macrophages on the corresponding surfaces. Data are presented as mean ± S.D. of three biological replicates. For statistical analysis ordinary one-way ANOVA followed by a post hoc Dunnett's test was performed. * $p < 0.05$ vs. M0.*

To determine whether the observed differences in macrophage morphology between titanium samples correlate with a changed macrophage polarization phenotype, the secretion of pro- and anti-inflammatory cytokines was analyzed (**Figure 14**).

Controls behaved as in previous experiments (details are described in section 5.3.1). The results for the titanium samples showed that macrophages responded with distinct inflammatory cytokine profiles. The sand blasted titanium 2 resulted in the highest pro-inflammatory cytokine response with significantly increased expression of the cytokines IL-8, TNF-α, and MIP-1 β compared to

M0 macrophages. In contrast, cultivation of THP-1 derived macrophages on the acid etched titanium 3 had no effects on cytokine expression. Moreover, titanium 4 and titanium 5 induced a slightly increased pro-inflammatory response as reflected by IL-8, TNF-α, and MIP-1 β expression. In addition to slightly elevated pro-inflammatory cytokine expression, macrophages cultured on titanium 1 responded with a significantly increased expression of the anti-inflammatory cytokine IL-10. These cytokine results indicated that surface property changes alter the biomaterial-induced immune responses of titanium.

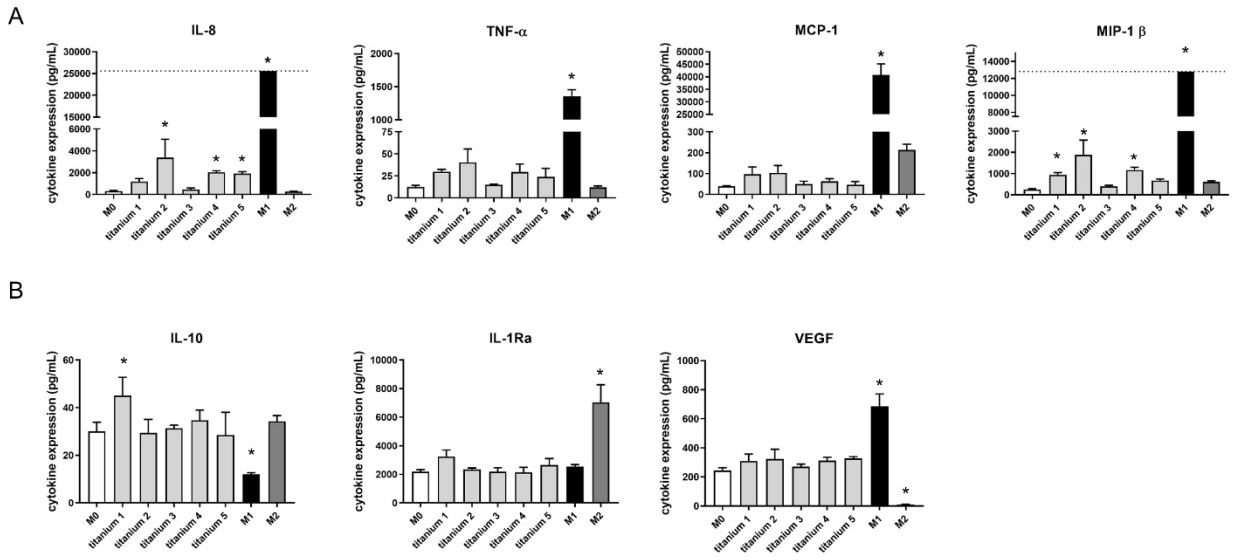

Figure 14: Pro- and anti-inflammatory cytokine response from THP-1 derived macrophages cultured on titanium samples with varying surface properties and tissue culture plates (TCP) for controls.
*Cytokine expression of macrophages grown on titanium specimens with different surface properties (titanium 1 – titanium 5) and control macrophages on TCP (M0 (no stimulation), M1 (LPS/IFN-γ stimulation), M2 (IL-4/IL-13 stimulation)) was analyzed after three days of culture. (A) Pro- and (B) anti-inflammatory cytokines were analyzed by the multiplexed cytokine detection panel. The dotted line represents the Upper Limit of Quantification (ULoQ). Shown are the expression levels (pg/mL) of three biological replicates. Data are presented as mean ± S.D. For statistical analysis ordinary one-way ANOVA followed by a post hoc Dunnett's test was performed. * $p < 0.05$ vs. M0. Cytokines were measured independently by Meike Jakobi.*

Based on these findings, it has been sought to correlate the observed morphologies and the corresponding inflammatory response following cultivation on the different titanium samples. However, no direct relationship between the two readout parameters could be found. While M1 activation on TCP led to a round cellular shape accompanied by significantly increased pro-inflammatory cytokine secretion, a more circular morphology of cells on titanium 3 and 5 was not associated with elevated pro-inflammatory responses.

Therefore, in the next step, more distinct actin arrangements within THP-1 derived macrophages were examined as a potential further readout. Previous studies have observed that the polarization of M1 and M2 macrophages was associated with differences in formation of podosomes (conical, actin-rich structures). In this context previous studies showed that M1 macrophages yielded less podosomes compared to M2 polarized macrophages (Cougoule et al., 2012). To test whether presence of podosomes might reflect the polarization state of THP-1 derived macrophages, podosome formation was manually evaluated on the basis of fluorescence images as previously shown in **Figure 13**. This quantification showed that the addition of LPS/IFN-γ (M1 activation) reduced the number of cells with podosomes significantly compared to M0 macrophages, whereas THP-1 derived M2 macrophages exhibited numbers of podosomes in comparison to naïve M0 ones (**Figure 15**). More importantly, an increased mean percentage of podosome-positive cells was observed on titanium 1 and a reduction on titanium 2 – titanium 5, with titanium 5 showing the lowest number of podosome-positive cells.

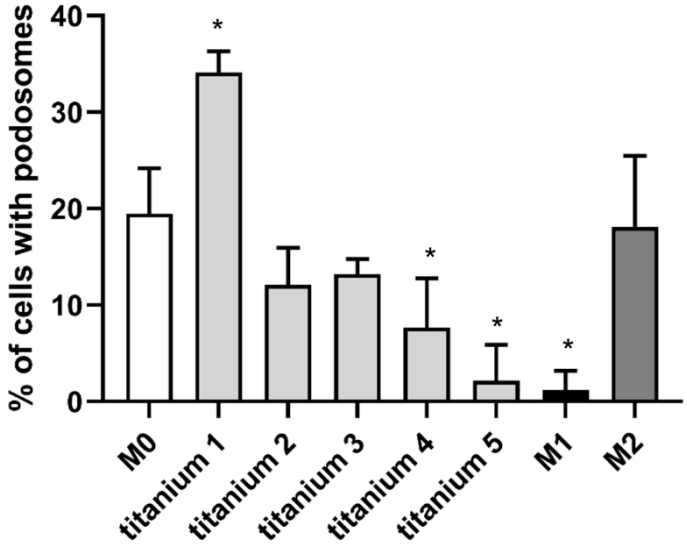

Figure 15:Percentage of cells with podosomes in THP-1 derived macrophages cultured on tissue culture plates (TCP) and on titanium samples with varying surface properties.
*After 72 h of culture podosomes in THP-1 derived macrophages on the corresponding titanium surfaces or TCP were analyzed. For controls on TCP, cells were polarized into M0 macrophages (no stimulation), M1 macrophages (LPS/IFN-γ), or M2 macrophages (IL-4/IL-13). >100 THP-1 derived macrophages were analyzed for each condition. Data are presented as mean ± S.D. of three biological replicates. For statistical analysis ordinary one-way ANOVA followed by a post hoc Dunnett's test was performed. * $p < 0.05$ vs. M0.*

Admittedly, the evaluation of cells with podosomes did also not directly correlate the cytokine responses to the investigated titanium samples, but an overall tendency of pro-inflammatory responses to cause a decrease in percentage of podosome-positive cells was evident. Nevertheless, the lowest number of cells observed on titanium 5 was not reflected by the highest pro-inflammatory cytokine response.

5.3.3 Biomaterials intended for commercial applications

Following the investigation of elicited inflammatory reactions to defined changes in surface topography on polyurethane and titanium, the next question was how biomaterials intended for commercial applications affect the inflammatory response. For this purpose, different types of biomaterials were provided voluntarily by industrial cooperation partners for the research campus "system immunology at biological-technical interfaces" and were analyzed regarding the induced cytokine responses. In order to exclude tracing the biomaterials back to the manufacturer, exact composition and designations cannot be disclosed. Apart from material classes, the different biomaterials from industrial cooperation partners also differed in their field of application ranging from joint components to biosensors and wound dressings. Based on the manufacturer, material class and intended field of application, materials were then classified into materials A-G (as listed in section 4.1.5.2).

As in afore mentioned experiments regarding the investigation of biomaterial-induced immunoresponses, the following control conditions were applied: THP-1 derived macrophages without further chemical stimulation (M0 macrophages), M1 macrophages (LPS/IFN-γ) and M2 macrophages (IL-4/IL-13). In general, levels of pro- and anti-inflammatory cytokines were comparable to previous experiments (details are described in section 5.3.1). The immune responses from control cells were used to classify the extend of cytokine responses on biomaterials in the following experiments.

5.3.3.1 Solid implant materials (materials A)

The first set of biomaterials tested in this context were solid implant materials intended for joint components (materials A). Following 72 h cultivation of THP-1 derived macrophages on these materials, the pro-and anti-inflammatory cytokine response was analyzed (**Figure 16**). While materials A_1, A_2 and A_3 induced immune responses comparable to the one of M0 THP-1

derived macrophages, cultivation on materials A_4 and A_5 led to an increased expression of pro-inflammatory cytokines (IL-8, MIP-1 β) (**Figure 16 A**). Furthermore, material A_4 and A_5 induced a significant increase of the marker IL-1Ra (**Figure 16 B**). Expression of the anti-inflammatory markers VEGF and IL-10 was not affected by the investigated materials A.

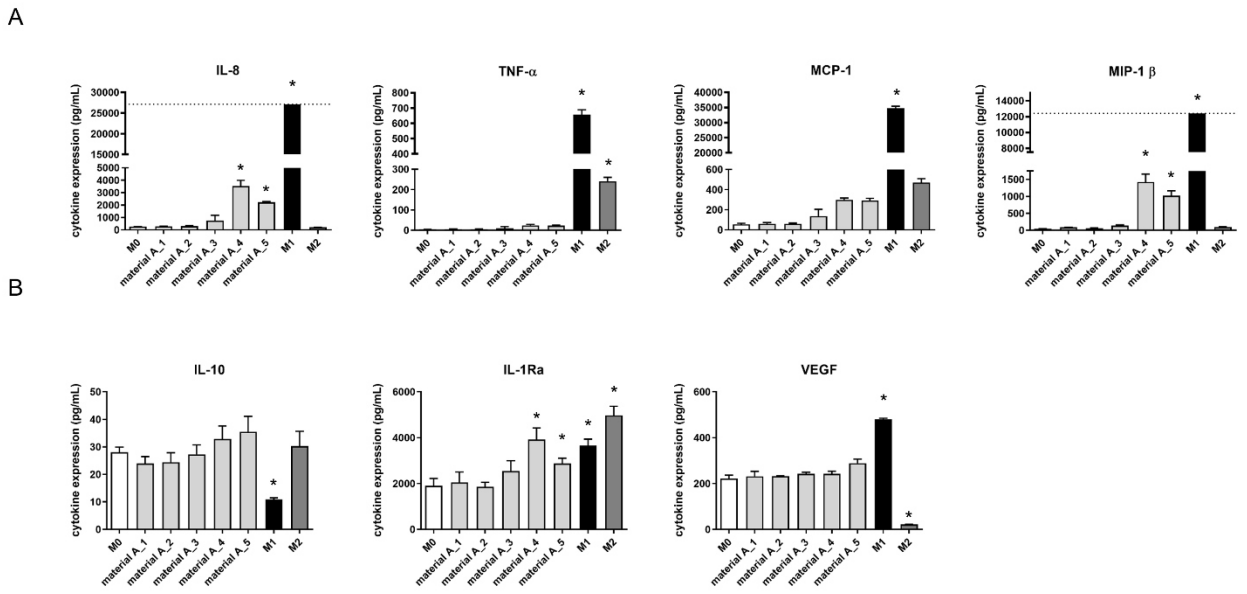

Figure 16: Pro- and anti-inflammatory cytokine responses of THP-1 derived macrophages following cultivation on solid implant materials (materials A) for 72 h.
THP-1 derived macrophages were cultured on materials A_1 – A_5 for 72 h. As controls, macrophages were grown on tissue culture plate without stimulation (M0) or were incubated with LPS/IFN-γ (M1) or IL-4/IL-13 (M2). (A*) Pro-inflammatory and (B) anti-inflammatory cytokine expression was studied utilizing the cytokine detection panel. Results are presented as expression levels (pg/mL) of three biological replicates. The dotted line represents the Upper Limit of Quantification (ULoQ). Data are presented as mean ± S.D. For statistical analysis ordinary one-way ANOVA followed by a post hoc Dunnett's test was performed. * $p < 0.05$ vs. M0. Cytokines were measured independently by Meike Jakobi.*

5.3.3.2 Polymer-based membranes (materials B)

The next biomaterials analyzed were polymer-based membranes (materials B). Quantification of secreted cytokines revealed that cultivation of THP-1 derived macrophages on biomaterials B did not affect the expression of pro-inflammatory cytokines significantly (IL-8, TNF-α, MIP-1 β, and VEGF) (**Figure 17 A**). Likewise, no changes in the expression of anti-inflammatory cytokines (IL-10, IL1-Ra and VEGF) were observed (**Figure 17 B**). These results indicated an overall immune inertness of material B.

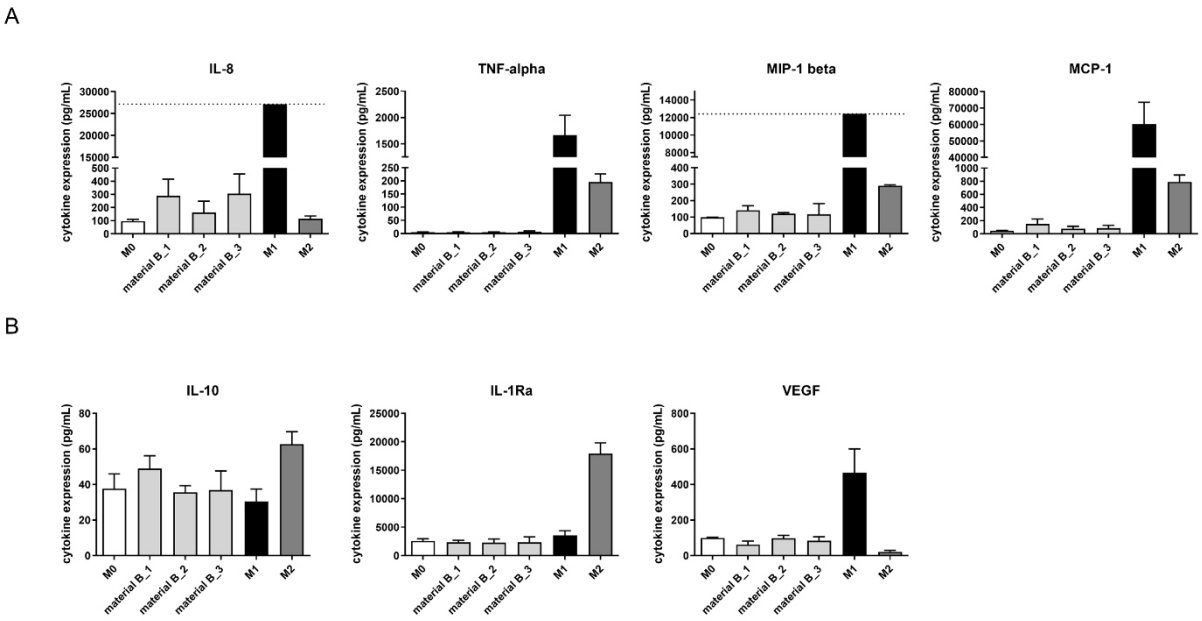

Figure 17: Pro- and anti-inflammatory cytokine responses following cultivation of THP-1 derived macrophages on polymer-based membranes (materials B) for 72 h.
*Secretion of (A) pro-inflammatory and (B) anti-inflammatory cytokines following three-day culture on materials B_1 – B_3 or controls grown on tissue culture plate (M0 (no stimulation), M1 (LPS/IFN-γ stimulation), M2(IL-4/IL-13 stimulation)) were assessed by multiplexed sandwich immunoassays. Results are presented as expression levels (pg/mL) of three biological replicates. The dotted line represents the Upper Limit of Quantification (ULoQ). Data are presented as mean ± S.D. For statistical analysis ordinary one-way ANOVA followed by a post hoc Dunnett's test was performed. * $p < 0.05$ vs. M0. Cytokines were measured independently by Meike Jakobi.*

5.3.3.3 Collagen-based membranes (materials C)

To analyze the biomaterial-induced immune response of collagen-based membranes (materials C), THP-1 derived macrophages were grown on the corresponding surfaces for 72 h. Subsequently, cytokine production from macrophages after contact with materials C was assessed by multiplexed bead-based immunoassays. Quantification of the levels of pro-inflammatory cytokines IL-8, TNF-α, MCP-1, and MIP-1 β (**Figure 18 A**) along with the levels of anti-inflammatory cytokines IL-10, IL-1Ra, and VEGF (**Figure 18 B**) showed an increased pro-inflammatory immune response together with a decreased anti-inflammatory response. Expression of the pro-inflammatory cytokines IL-8 and TNF-alpha was significantly increased compared to M0 macrophages cultured on TCP, while the levels of the wound healing factor VEGF, the anti-inflammatory cytokine IL-10 and the pro-inflammatory cytokine MCP-1 were secreted at lower levels for materials C. No differences between cytokine expression of material C_1 and material C_2 were observed.

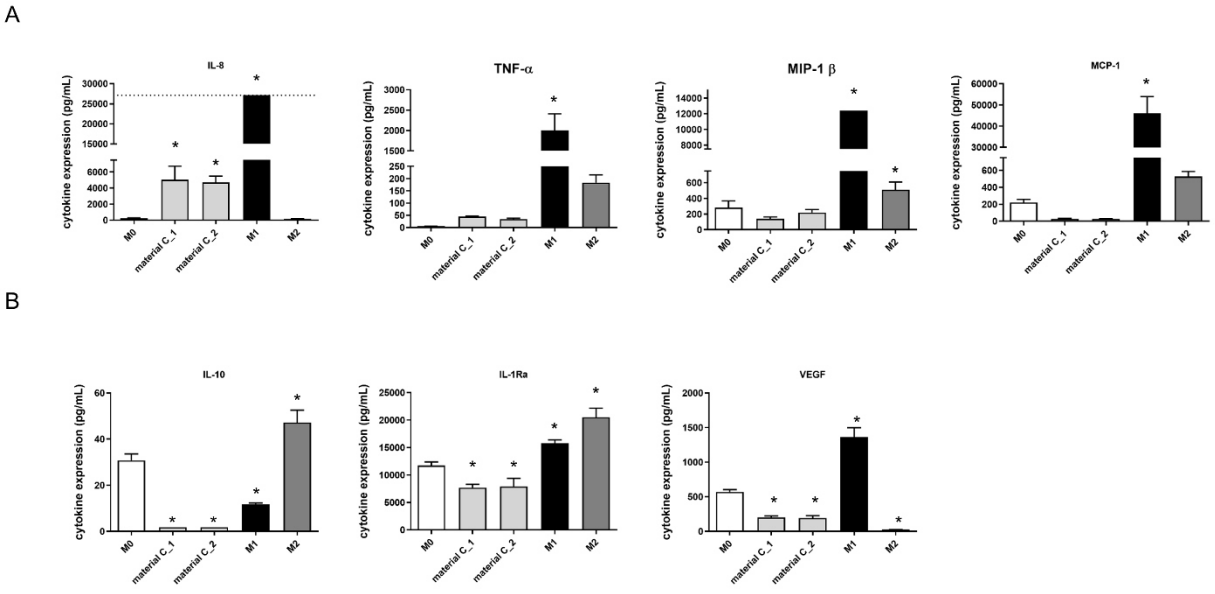

Figure 18: Secretion of pro-and anti-inflammatory cytokines upon cultivation of THP-1 derived macrophages on collagen-based membranes (materials C) for 72 h.
*Cytokine release from control THP-1 derived macrophages cultured on tissue culture plate (M0, M1 (LPS/IFN-γ), M2 (IL-4/IL-13)) or on materials C. (A) Pro- and (B) anti-inflammatory cytokines were assessed using the in house developed cytokine detection panel. Shown are expression levels (pg/mL) of three biological replicates. The dotted line represents the Upper Limit of Quantification (ULoQ). Data are presented as mean ± S.D. For statistical analysis ordinary one-way ANOVA followed by a post hoc Dunnett's test was performed. * $p < 0.05$ vs. M0. Cytokines were measured independently by Meike Jakobi.*

5.3.3.4 Polymer-based membranes (materials D)

In the next step, the spectrum of pro- and anti-inflammatory cytokines from THP-1 derived macrophages cultured on polymer-based membranes (materials D) was assessed following three days of culture on the biomaterials (**Figure 19**). Compared to cells cultured on TCP without further stimulation (M0 macrophages) no significant differences for the pro-inflammatory markers IL-8, TNF-α, MCP-1, and MIP-1 β as well as anti-inflammatory markers IL-10, IL-1Ra, and VEGF were detected. However, cultivation on the material D_4 resulted in a significantly upregulated MIP-1 β expression. Moreover, expression levels of the wound healing factor VEGF were significantly decreased on material D_2, D_3, and D_4.

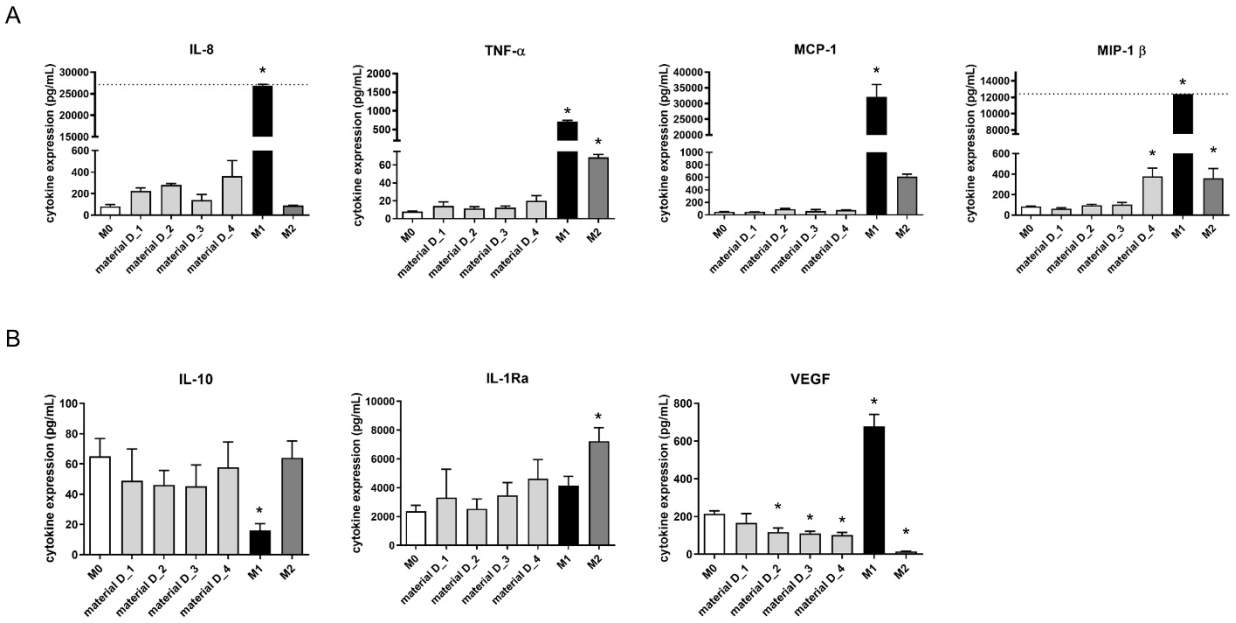

Figure 19:Pro- and anti-inflammatory cytokine secretion of THP-1 derived macrophages grown on polymer-based membranes (materials D) for 72 h.
*THP-1 derived macrophages were cultured for three days on materials D or on tissue culture plate (M0, M1 (LPS/IFN-γ), M2 (IL-4/IL-13)), after which the concentrations of pro-inflammatory (A) and anti-inflammatory (B) cytokines were assessed using the cytokine detection panel developed by Meike Jakobi. Shown are expression levels (pg/mL) of three biological replicates. The dotted line represents the Upper Limit of Quantification (ULoQ). Data are presented as mean ± S.D. For statistical analysis ordinary one-way ANOVA followed by a post hoc Dunnett's test was performed. * $p < 0.05$ vs. M0. Cytokines were measured independently by Meike Jakobi.*

5.3.3.5 Gelatin-based gels (materials E)

To investigate the immune responses to the different gelatin-based gels (materials E), quantification of secreted cytokines was performed after 72 h of culture. As shown in **Figure 20,** pro-inflammatory markers were highly elevated in response to material E_1, material E_2, and material E_3, as indicated by high levels of the pro-inflammatory cytokines IL-8, MCP-1, and MIP-1 β. Noteworthy, these levels were accompanied by a decreased expression of the anti-inflammatory cytokine IL-10. Furthermore, VEGF expression was significantly elevated on material E_1. Taken together, these results demonstrated that the manufacturing material used for materials E elicits high pro-inflammatory responses.

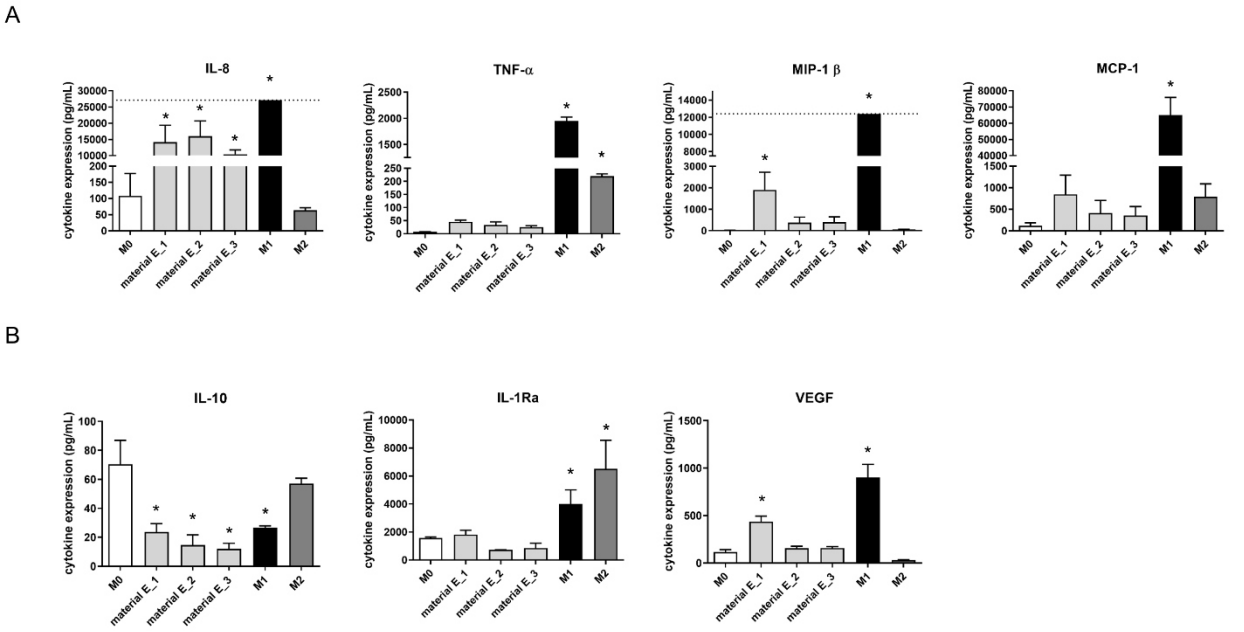

Figure 20: Quantitative analysis of secreted pro- and anti-inflammatory cytokines upon cultivation of THP-1 derived macrophages on gelatin-based geld (materials E) for three days.
*The (A) pro- and (B) anti-inflammatory cytokine secretion in culture medium following three-day cultivation of THP-1 derived macrophages on materials E and tissue culture plate without further stimulation (M0), LPS/IFN-γ stimulation (M1), and IL-4/IL-13 stimulation (M2) was measured by the in house developed multiplexed immunoassay. Shown are expression levels (pg/mL) of three biological replicates. The dotted line represents the Upper Limit of Quantification (ULoQ). Data are presented as mean ± S.D. For statistical analysis ordinary one-way ANOVA followed by a post hoc Dunnett's test was performed. * $p < 0.05$ vs. M0. Cytokines were measured independently by Meike Jakobi.*

5.3.3.6 Polymer-based membranes (materials F)

Next, immune responses to polymer-based membranes (materials F) were analyzed by multiplexed bead-based immunoassays. Analysis of pro- and anti-inflammatory cytokines showed that the cultivation of THP-1 derived macrophages on materials F_1 – F_4 resulted in distinct inflammatory responses (**Figure 21**). The highest pro-inflammatory response was observed for the material F_1 (**Figure 21 A**). Compared to M0 macrophages cultured on TCP, cultivation on material F_1 led to a significantly increased expression in cytokine levels for IL-8, MCP-1, and MIP-1 β. While materials F_2 and F_4 showed weak to no changes of pro-inflammatory cytokines, material F_3 led to almost no changes of these markers. Furthermore, elevated expression of the anti-inflammatory markers IL-10 and IL-1Ra were observed following macrophage cultivation on materials F_1 and F_2 (**Figure 21 B**). Expression of the wound healing factor VEGF on the other hand was significantly elevated on material F_2 and material F_3.

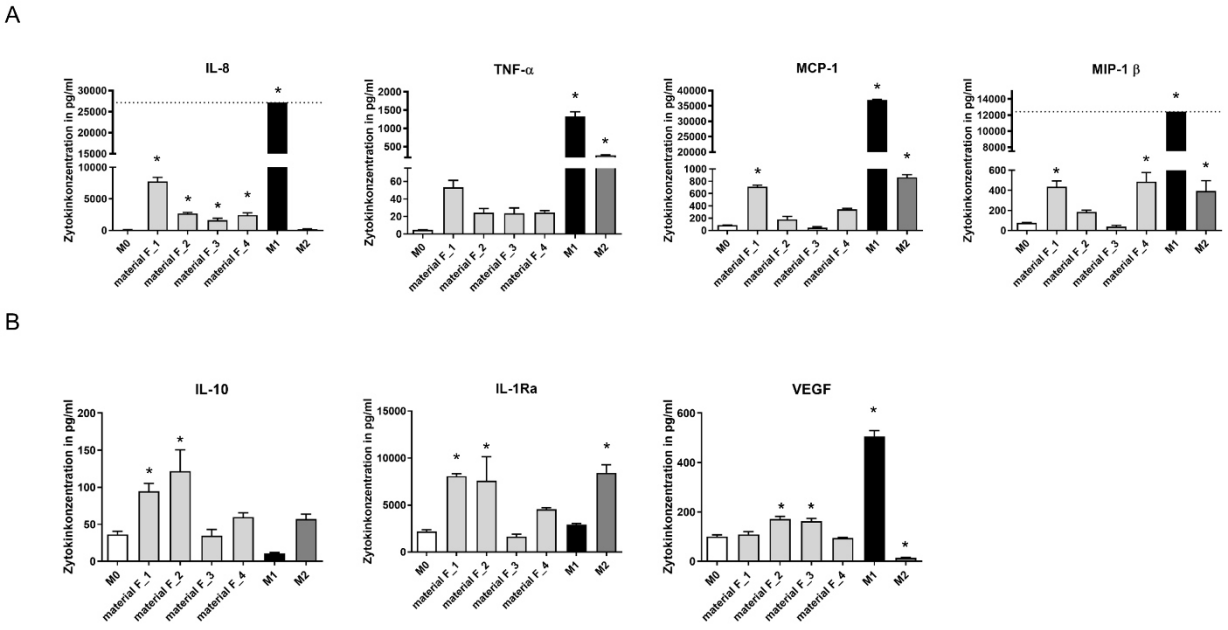

Figure 21:Study of Pro- and anti-inflammatory cytokine expression from THP-1 derived macrophages cultured on collagen-based membranes (materials F) for 72 h.*THP-1 macrophages were grown on materials E or cultured on tissue culture plate and left unstimulate (M0) or were polarized in M1 and M2 macrophages by respectively LPS/IFN-γ stimulation or IL-4/IL-13 stimulation, respectively. (A) Pro- and (B) anti-inflammatory cytokine secretion levels were measured utilizing the developed cytokine detection panel. Shown are expression levels (pg/mL) of three biological replicates. The dotted line represents the Upper Limit of Quantification (ULoQ). Data are presented as mean ± S.D. For statistical analysis ordinary one-way ANOVA followed by a post hoc Dunnett's test was performed. * $p < 0.05$ vs. M0. Cytokines were measured independently by Meike Jakobi.*

5.3.3.7 Collagen-based gels (material G)

A set of collagen-based gels (material G) was the last biomaterial intended for commercial applications analyzed regarding its elicited inflammatory responses. Upon 72 h of culture on material G, THP-1 derived macrophages responded with an upregulated pro-inflammatory response as indicated by significantly elevated expression levels of IL-8 and MIP-1 β (**Figure 22 A**). This observation was accompanied by a decreased expression of the anti-inflammatory cytokine IL-10 (**Figure 22 B**).

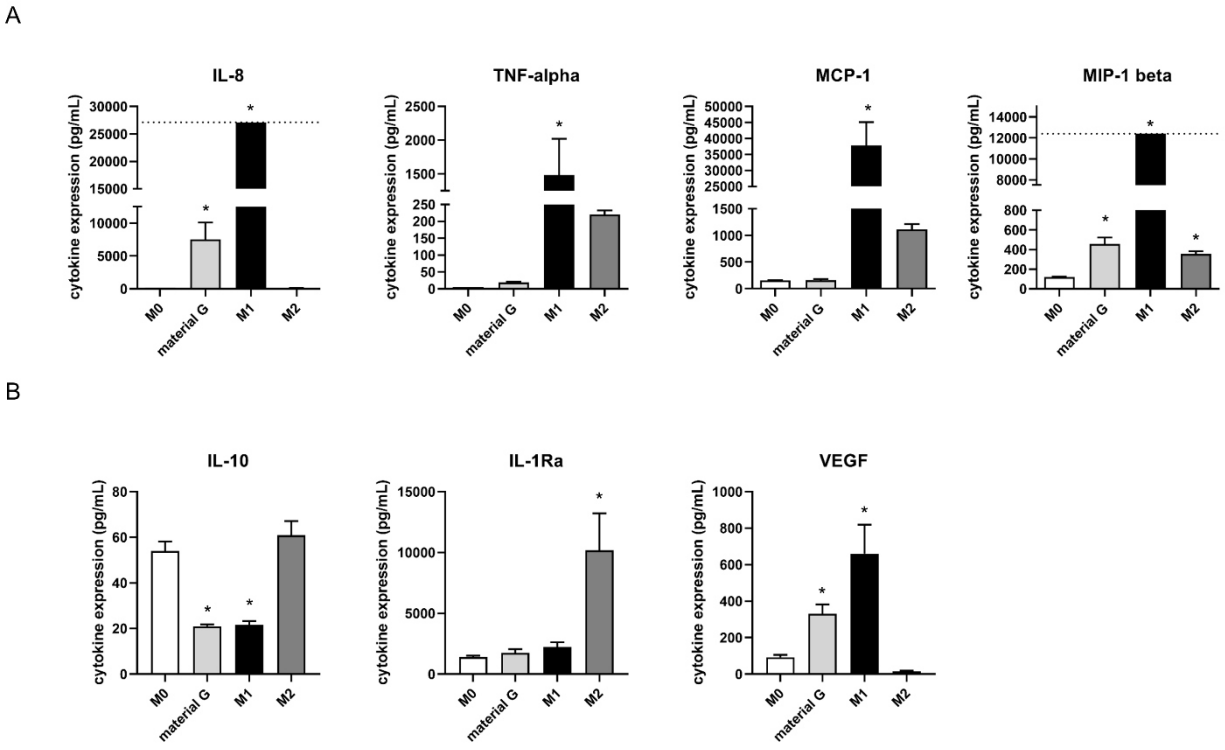

Figure 22: Expression of pro- and anti-inflammatory cytokines from THP-1 derived macrophages cultured on collagen-based gels (material G).
*THP-1 derived macrophages were cultured for 72 h on material G or on tissue culture plate (M0, M1 (LPS/IFN-γ), M2 (IL-4/IL-13)). The concentration of cytokines was assessed using the in house developed cytokine detection panel. Shown are expression levels (pg/mL) of three biological replicates. The dotted line represents the Upper Limit of Quantification (ULoQ). Data are presented as mean ± S.D. For statistical analysis ordinary one-way ANOVA followed by a post hoc Dunnett's test was performed. * $p < 0.05$ vs. M0. Cytokines were measured independently by Meike Jakobi.*

5.3.3.8 Summary of inflammatory responses of biomaterials for commercial applications

Taken together, the different biomaterials intended for commercial applications induced varying immune responses in THP-1 derived macrophages (**Table 6**). For some classes of materials, including materials B (polymer-based membranes) and materials E (gelatin-based gels), cytokine responses were comparable within the classes. For others, such as materials A (solid implant materials), vast differences were observed. Thus, these findings strongly support the hypothesis that not only surface chemistry but also all other surface properties (such as stiffness, pore size, and topography) of biomaterials induce different macrophage polarization. To further confirm this and to possibly link the observed immune responses to specific biomaterial surface characteristics, extensive material analyses are necessary. Nevertheless, these observations demonstrated that the

THP-1 based macrophage model is a suited and sensitive system for testing biomaterial-induced immune responses.

Table 6: Investigated biomaterials and their predominant reaction

Class	Biomaterial	Predominant reaction	Classification of immune reaction
Solid implant materials	material A_1	Immune-inert	/
Solid implant materials	material A_2	Immune-inert	/
Solid implant materials	material A_3	Immune-inert	/
Solid implant materials	material A_4	Pro-inflammatory	High
Solid implant materials	material A_5	Pro-inflammatory	High
Polymer-based membranes	material B_1	Immune-inert	/
Polymer-based membranes	material B_2	Immune-inert	/
Polymer-based membranes	material B_3	Immune-inert	/
Collagen-based membranes	material C_1	Pro-inflammatory	High
Collagen-based membranes	material C_2	Pro-inflammatory	High
Collagen-based membranes	material D_1	Immune-inert	/
Collagen-based membranes	material D_2	Immune-inert	/
Collagen-based membranes	material D_3	Immune-inert	/
Collagen-based membranes	material D_4	Pro-inflammatory	Low
Gelatin-based gels	material E_1	Pro-inflammatory	High
Gelatin-based gels	material E_2	Pro-inflammatory	High
Gelatin-based gels	material E_3	Pro-inflammatory	High
Polymer-based membranes	material F_1	Pro-inflammatory	High
Polymer-based membranes	material F_2	Anti-inflammatory	High
Polymer-based membranes	material F_3	Immune-inert	/
Polymer-based membranes	material F_4	Pro-inflammatory	Low
Collagen-based gels	material G	Pro-inflammatory	High

5.4 Generation of stable THP-1 cell lines expressing actin biomarkers

As described previously in this study, actin-cytoskeleton is a suitable marker to trace morphological changes which are known to correlate with chemically induced macrophage polarization. The following section describes the application of two previously established intracellularly functional actin-biosensors, namely LifeAct and actin-chromobody (actin-CB), to generate a THP-1 derived macrophage model to monitor dynamic changes of cytoskeleton and the overall morphology in living cells.

To study dynamic actin cytoskeleton rearrangements and morphological changes during cultivation on biomaterials, the genetically encoded biosensors LifeAct or actin-CB were introduced into THP-1 cells. Since transient transfection results in large intercellular heterogeneity of the expression levels, both biosensors were stably introduced into THP-1 cells using plasmid transfection followed by selective pressure as outlined in **Figure 23**. Polyclonal pools displaying homogenous intracellular expression levels were obtained by utilizing Fluorescence-activated cell sorting (FACSorting).

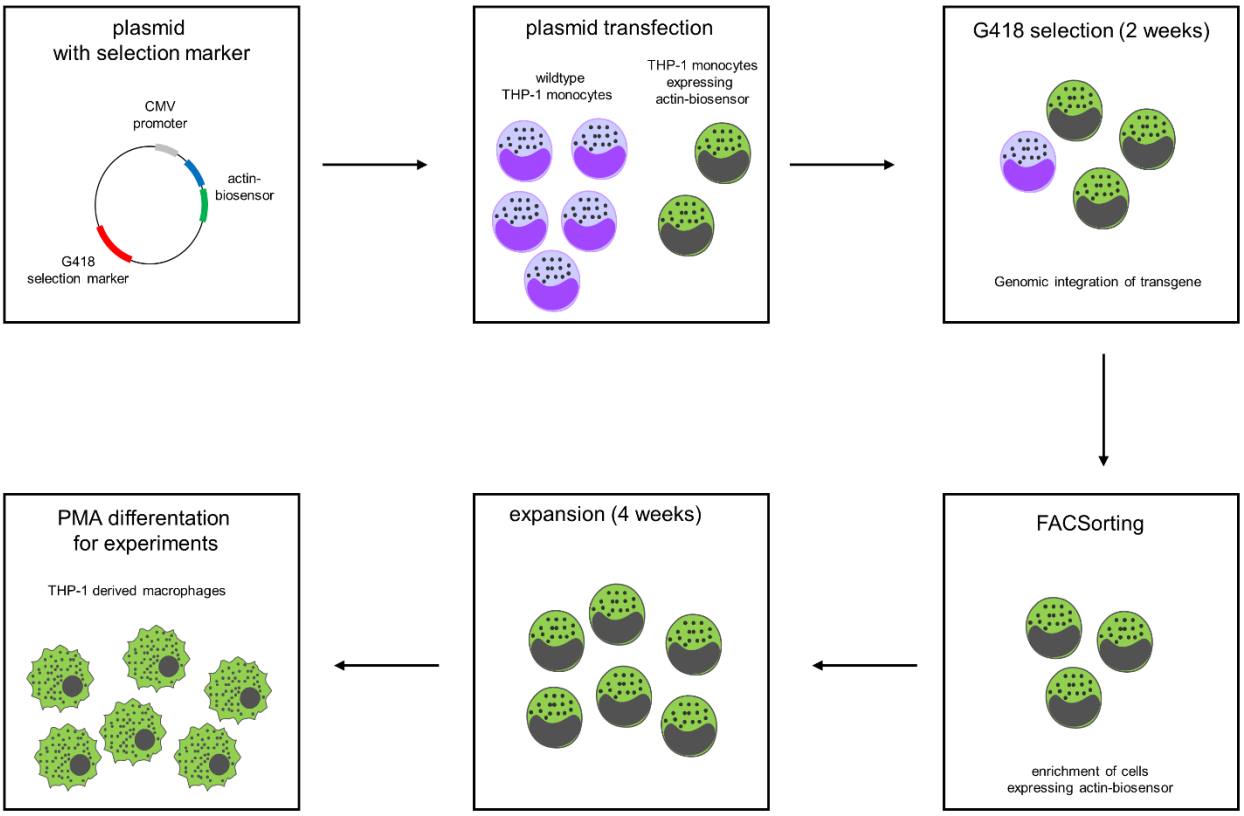

Figure 23: Schematic overview of stable THP-1 cell line generation.
Shown is the workflow for stable THP-1 cell generation achieved by random genomic integration of the transgene. FACSorting of GFP-positive events resulted in an enrichment of cells expressing the actin-biosensors.

5.4.1 Comparison of stable cell lines to THP-1 wildtype

To test whether integration of actin-CB or LifeAct impacts the cellular response to chemically induced macrophage polarization (LPS/IFN-γ or IL-4/IL-13), a set of experiments was performed to analyze cell morphology, cytokine and chemokine secretion and migration of THP-1 derived macrophages. Therefore, generated stable cell lines THP-1_actin-CB and THP-1_LifeAct were compared to the parental THP-1_wt.

5.4.1.1 Quantitative image analysis

Actin-CB and LifeAct are well established genetically encoded biosensors to visualize actin structures and dynamics in living cells (Panza et al., 2015; Riedl et al., 2008). To validate effects of both biosensors on cellular morphology and actin structures in macrophages, first, THP-1_wt,

THP-1_actin-CB and THP-1_LifeAct were differentiated into THP-1 derived macrophages as previously described in section 5.1, followed by LPS/IFN-γ treatment for 72 h to induce M1 polarization and IL-4/IL-13 treatment for 72 h to induce M2 polarization. Briefly, phalloidin staining was performed to ensure that actin-biosensors visualize endogenous actin while not interfering with its localization. THP-1_actin-CB (green), THP-1_LifeAct (green), and THP-1_wt were PFA-fixed and stained with phalloidin$_{AF555}$ (red) and DAPI for nuclei (blue) (**Figure 24 A, B, C**). Images showed that actin-CB as well as LifeAct co-localized with phalloidin signal in M0, M1 and M2 macrophages: Whereas cortical actin structures were predominantly observed in THP-1 derived M1 macrophages, conical, podosomal structures were the most common features in M0 and M2 macrophages. Nevertheless, high levels of background fluorescence were noticeable for THP-1_LifeAct, thus obscuring endogenous actin structures. Additionally, morphological changes were assessed. Following LPS/IFN-γ treatment (M1 activation), all three macrophages, derived from THP-1_wt, THP-1_actin-CB and THP-1_LifeAct, underwent a change from an elongated shape, as seen in THP-1 derived M0 and M2 macrophages, to a round phenotype. To further confirm these observations, morphological parameters cell circularity and cell elongation of individual cells were quantified (**Figure 24 D**). As shown by increased cell shape factor and decreased cell elongation factor of M1 macrophages compared to M0 and M2 macrophages in all three cell lines, morphology of THP-1_actin-CB and THP-1_LifeAct did not differ from THP-1_wt in the analyzed conditions.

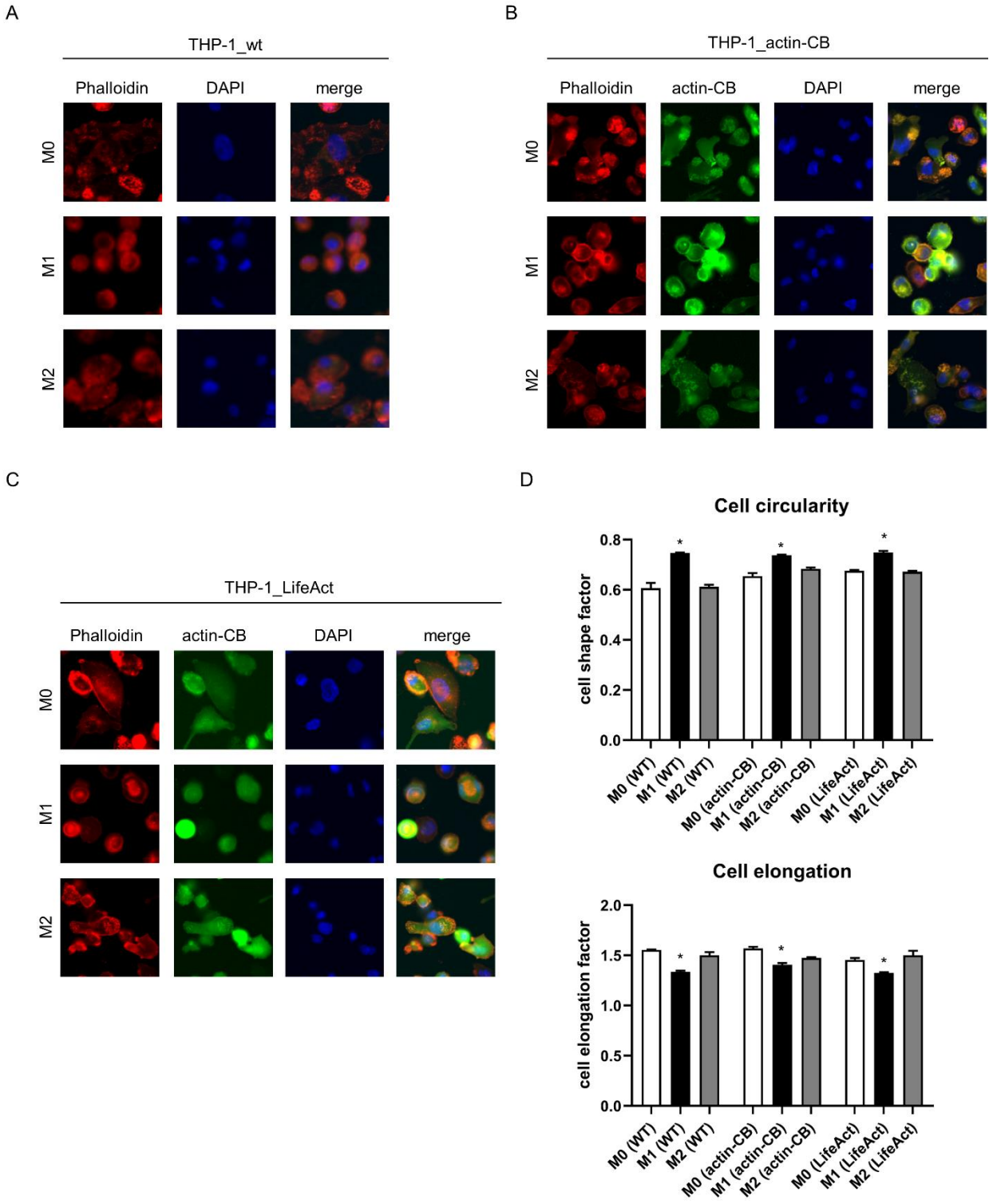

Figure 24: THP-1_wt, THP-1_actin-CB, and THP-1_LifeAct show similar cellular morphologies in response to M0, M1 and M2 polarization

THP-1_wt, THP-1_actin-CB and THP-1_LifeAct derived macrophages were left non-treated (M0) or were treated with LPS/IFN-γ or IL-4/IL-13 to induce the M1 or M2 phenotype, respectively. After 72 h cultivation period, cells were PFA-fixed and stained with phalloidin$_{AF555}$ (red) and DAPI (blue). Actin-binder signal is presented in green. (A, B, C) Representative fluorescence images of (A) THP-1_wt, (B) THP-1_actin-CB and (C) THP-1_LifeAct derived

*M0, M1, and M2 macrophages. THP-1_actin-CB and THP-1_LifeAct are stably expressing intracellular actin-biomarkers. Scale bar: 50 µm. (D) Bar charts of quantified cell circularity and cell elongation of THP-1 derived macrophages polarized into the M0, M1, or M2 phenotype using phalloidin signal. Morphological characteristics were calculated from two samples (n=2), comprising >200 cells. Error bars: S.D. For statistical analysis ordinary student's t-test was performed. * p < 0.05 vs M0 (WT), M0 (actin-CB), or M0 (LifeAct) respectively.*

Taken together, the comparative study of THP-1_wt, THP-1_actin-CB and THP-1_LifeAct cells regarding cell morphology showed that stable integration of neither actin-CB nor LifeAct has a substantial impact on morphological changes following chemically induced macrophage polarization. However, since THP-1_LifeAct cells showed higher levels of background fluorescence, THP-1_actin-CB cells were chosen for all further experiments.

5.4.1.2 Quantitative analysis of secreted cytokines

Using the newly generated THP-1_actin-CB cell line, the next question was whether these cells still respond with a comparable cytokine secretion profile of pro- and anti-inflammatory cytokines and chemokines following induction of the pro-inflammatory M1 phenotype or the anti-inflammatory M2 phenotype. To address this question cytokine levels in the supernatant were determined utilizing the developed cytokine detection panel.

For this purpose, THP-1_actin-CB cells were differentiated into macrophages and subsequently polarized into the M1 or M2 phenotype or M0 as control. Quantification of cytokine secretion revealed low levels of pro- and anti-inflammatory cytokines for THP-1_actin-CB derived M0 macrophages (**Figure 25**). Upon subjection to LPS/IFN-γ stimuli, an up-regulation of pro-inflammatory cytokines, markers for the M1 phenotype, was observed. This was accompanied by a decreased expression of the anti-inflammatory marker IL-10. M2 chemical polarization of THP-1_actin-CB macrophages resulted in an upregulated secretion of the anti-inflammatory cytokine IL-1Ra. The M2 phenotype was not associated with up-regulation of pro-inflammatory cytokines. Results obtained for the cytokines IL-4, IL-13, IL-12p70, IFN-γ, and GM-CSF were not affected of the treatments and are therefore not shown. Admittedly differences in absolute levels of cytokine expression can be seen in comparison to the parental wildtype cells (see section 5.2.1). However, the overall response is highly similar.

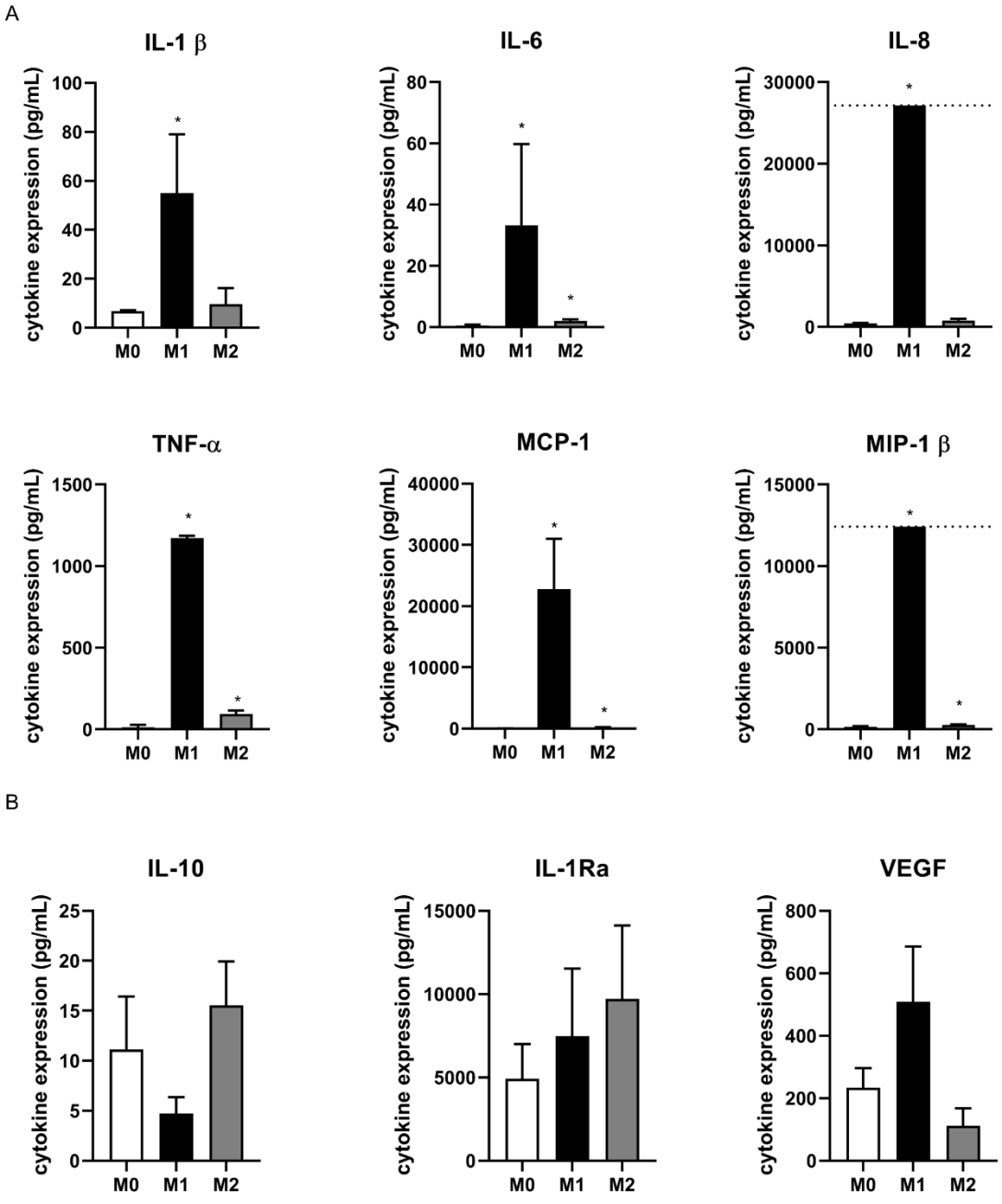

Figure 25: Pro- and anti-inflammatory cytokine production from THP-1_actin-CB derived M0, M1, and M2 macrophages.

*THP-1_actin-CB derived macrophages were cultured without further chemical stimuli (M0), in the presence of LPS and IFN-γ (M1), or in the presence of IL-4 and IL-13 for 72 h. Expression of (A) pro-inflammatory or (B) anti-inflammatory cytokines was assessed in the supernatant using the cytokine detection panel developed by Meike Jakobi. The dotted line represents the Upper Limit of Quantification (ULoQ). Results are presented as mean cytokine concentration (pg/mL) ± S.D. of three biological replicates. For statistical analysis student's t-test was performed. * $p < 0.05$ vs. M0. Cytokines were measured independently by Meike Jakobi.*

5.4.1.3 Scratch-Assay

As previously mentioned, macrophages play a central role in inflammatory reactions and wound healing. Therefore, high motility is an essential aspect of macrophage function, allowing them to rapidly respond to attracting signals. Within this scope, it was observed that M1-macrophages show weak migration due to strong adhesion in comparison to moderate adhered M2-macrophages with dynamic motility (Cui, Ardell, Podolnikova, & Yakubenko, 2018). Among others, actin is majorly involved in cellular processes like adhesion and migration (Parsons, Horwitz, & Schwartz, 2010; Yamaguchi & Condeelis, 2007).

Thus, to investigate whether the actin-CB binding to actin cytoskeleton influences the motility of macrophages, wound healing assay was performed. For this purpose, THP-1_wt and THP-1_actin-CB derived macrophages were seeded at high densities and cultured in the absence of further stimuli or the presence of LPS/IFN-γ or IL-4/IL-13. Open wound areas were assessed 72 h post wounding (**Figure 26**). Determination of open wound areas showed that THP-1 derived M0, M1, and M2 macrophages showed differences between the two cell lines regarding cell migration. For THP-1_wt derived M0 and M2 macrophages the open wound area was clearly lower than for M1 macrophages. While THP-1_actin-CB derived M0 and M2 macrophages also showed less open wound areas compared to M1 macrophages, the differences were not as clear as in THP-1_wt derived macrophages. Nevertheless, the tendency of cell migration of stimulation was still the same.

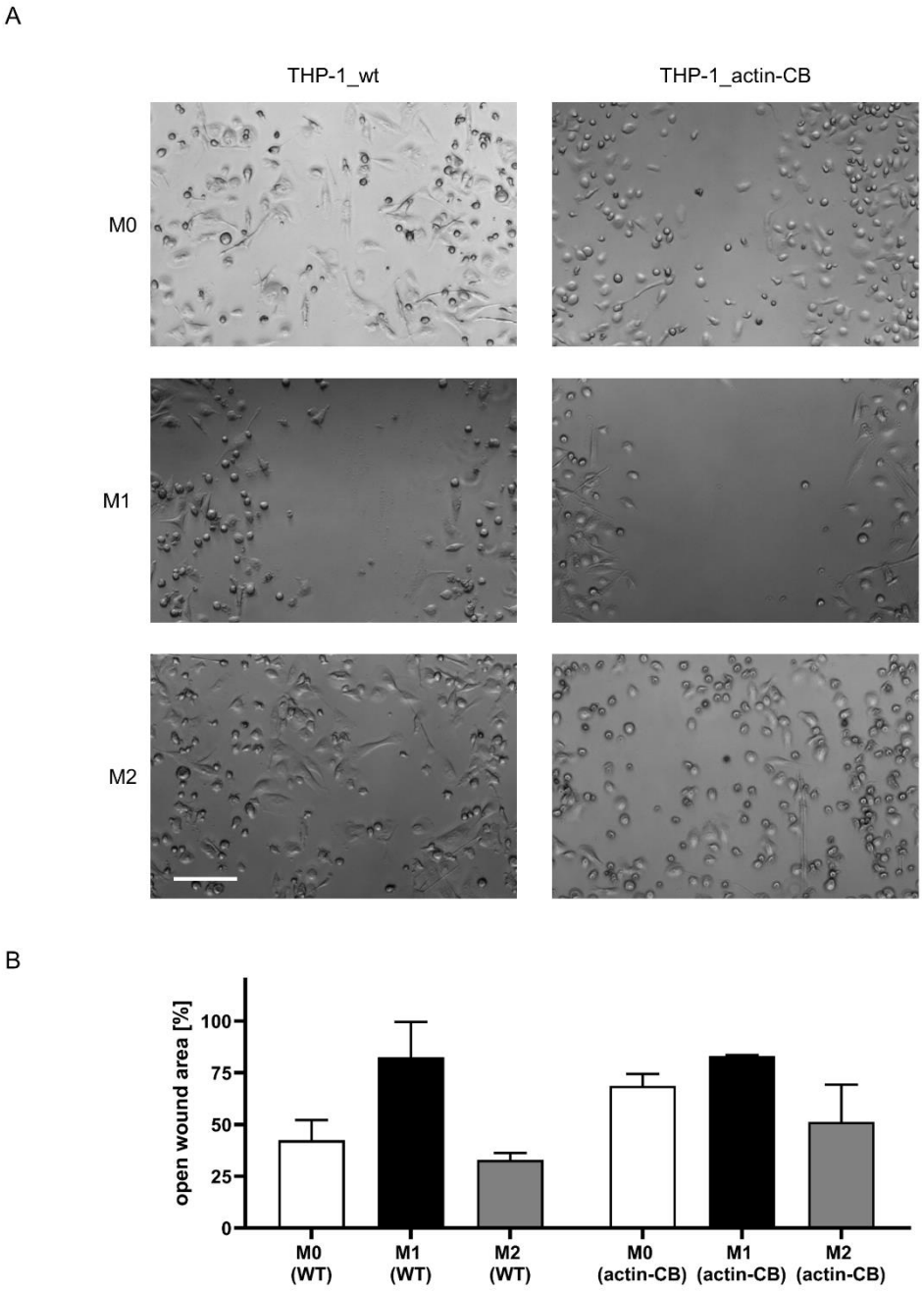

Figure 26: THP-1_wt and THP-1_actin-CB show comparable migration following chemical M1 and M2 polarization.

*Cell migration was assessed utilizing wound healing assay. THP-1_wt and THP-1_actin-CB derived macrophages were seeded at 2 x 10^5 cells/mL. 3 h post seeding, scratch wounds were applied and macrophages were cultured without further chemical stimuli (M0), in the presence of LPS and IFN-γ (M1), or in the presence of IL-4 and IL-13 for 72 h. Phase contrast images were taken immediately after wounding and 72 h after wounding. (A) Shown are representative wound areas of THP-1_wt and THP-1_actin-CB derived M0, M1, and M2 macrophages 72 h after wounding. Scale bar: 200 µm. (B) Bar graphs showing the mean percentages of the remaining open wound area after 72 h relative to the 0 h values ± S.D. of three biological replicates. For statistical analysis student's t-test was performed. * $p < 0.05$ vs. M0 (WT) or M0 (actin-CB) respectively.*

5.4.2 Monitoring dynamic changes of actin-cytoskeleton in THP-1_actin-CB

The approaches used so far in this thesis to study biomaterial induced cellular responses are exclusively based on endpoint assays (such as immunoassays or stainings of fixed cells) which are limited in that they only allow a determination of responses at a specific time point. Hence, to trace temporal dynamics of actin cytoskeleton and morphology in real-time, THP-1_actin-CB derived macrophages were applied. In this regard, responses of THP-1 derived macrophages stably expressing the actin-CB to anionic polyelectrolyte multilayers (PEMs) as possible coatings of biomaterial interfaces were investigated. PEMs are nanoscale, bilayer coatings that are created by a procedure called Layer-by-Layer: the buildup is based on alternative deposition of oppositely charged polyelectrolyte monolayers (polycations and polyanions) on surfaces (Krastev, Rudt, Xiong, & Hartmann, 2018). PEM coatings investigated in this thesis were generated, characterized and kindly provided by the research group of Dr. Hanna Hartmann.

For live-imaging of actin cytoskeleton and morphology, four different PEM coatings (PEM 1 – PEM 4) with differing surface wettability on TCP were analyzed. By applying drop shape analysis, the static contact angle was determined which hereby provides information about the wettability of the biomaterial: Higher contact angle values indicate increased surface hydrophobicity. The results revealed an increase of surface hydrophobicity from PEM 1 to PEM 4 (**Table 7**).

Table 7: Wettability of polyelectrolyte multilayer coatings with differing contact angles.
Contact angles were determined by drop shape analysis.

Sample	Contact angle
PEM 1	18°
PEM 2	40°
PEM 3	48°
PEM 4	55°

As afore mentioned, immunological reactions to implant materials occur following cell adhesion and subsequent interaction with biomaterial surfaces. Accordingly, the first step was to examine whether THP-1_actin-CB derived macrophages would adhere and spread on the PEM coatings with varying surface wettability. To this end, SEM was applied to visualize immune cell interactions with PEM-coated surfaces. SEM imaging revealed cell adhesion on all PEM coatings following three days of culture regardless the surface wettability (**Figure 27**). Although macrophages constituted a heterogeneous population exhibiting various morphologies, certain cellular shapes were predominant for specific PEM surfaces as shown by the SEM images. As shown in **Figure 27 A**, THP-1_actin-CB derived macrophages cultured on PEM 1 had a tendency

to show low cell spreading. In general, large cell bodies accompanied by round shape was observed for macrophages grown on PEM 2 and 3 (**Figure 27 B, C**). In contrast, cells cultured on PEM 4 typically acquired an elongated morphology (**Figure 27 D**). Taken together, SEM observations suggested the potential for THP-1_actin-CB derived macrophages to interact with the PEM coatings and first indications of potential difference in their cellular morphology.

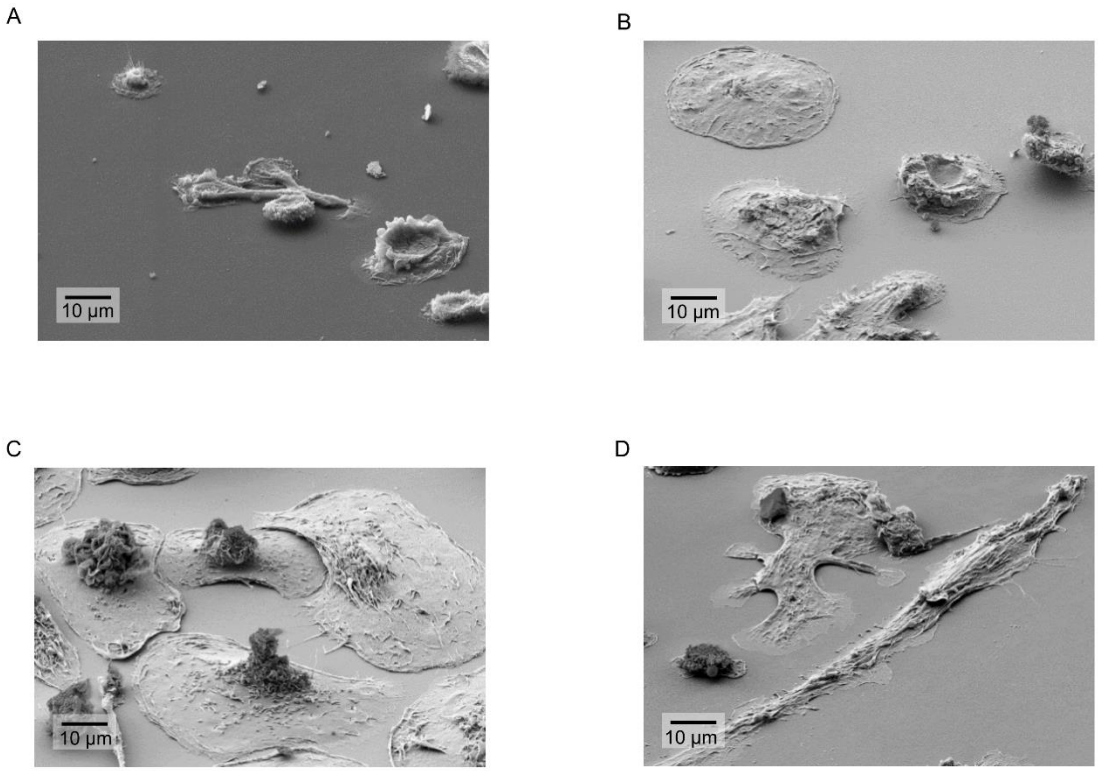

Figure 27: Representative scanning electron microscopy (SEM) images of THP-1_actin-CB derived macrophages cultured on polyelectrolyte multilayers (PEMs) with varying surface hydrophobicity for three days.
Macrophages were cultured on PEMs with increasing hydrophobicity from left to right: (A) PEM 1, (B) PEM 2, (C) PEM 3 and (D) PEM 4. After 72 h of culture, cells were fixed in PFA and glutaraldhehyde, dehydrated in a graded series of ethanol and then prepared for SEM by critical point drying and coating with a 10 nm film of gold. Images were acquired at 3 keV acceleration voltage in collaboration with Dr. Antje Biesemeier.

To complement the qualitative assessment of macrophage morphology on PEM surfaces, fluorescence imaging microscopy was applied (**Figure 28 A**). Quantification of cellular morphology was examined by determining the cell shape factor in a time-lapse experiment using THP-1_actin-CB derived macrophages. To this end, fluorescence images were continuously recorded at 24 h, 48 h, and 72 h. Fluorescence images recorded after 24 h already showed distinct cellular morphologies of THP-1 derived macrophages, dependent on culture surface and stimulation. While cells following LPS/IFN-γ stimulation (M1 activation) predominantly exhibited

a round shape, macrophages cultured under other conditions showed a more elongated morphology. After 48 h and 72 h of culture, these differences became even more pronounced, with THP-1 derived macrophages on PEM 4 representing the most elongated phenotype. These differences could also be confirmed by quantitative analysis (**Figure 28 B**).

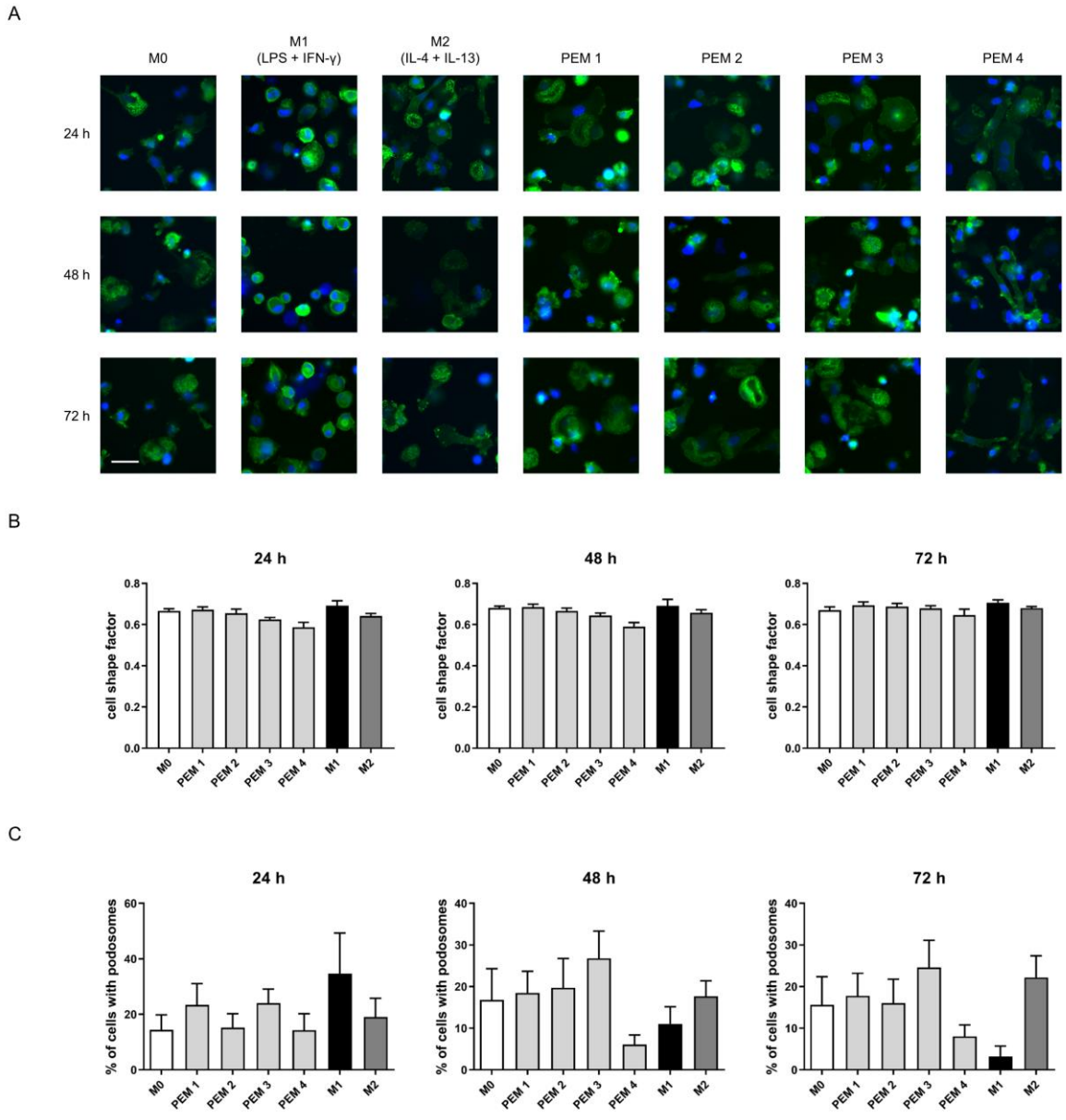

Figure 28: Monitoring dynamic changes of cell morphology and actin structures THP-1_actin-CB derived macrophages.
(A) Representative live-cell images of THP-1_actin-CB derived macrophages cultured on PEM surfaces with varying surface hydrophobicity or on tissue culture plate untreated (M0), stimulated with LPS/IFN-γ (M1) or treated with IL-4/IL-13 (M2) for 24 h, 48 h, and 72 h. Scale bar: 50 µm. (B) Quantification of cell circularity in >150 cells after 24 h, 48 h, and 72 h. Values are presented as mean ± S.D. from at least two independent experiments. (B) Quantification of cells with podosomes. >100 THP-1 derived macrophages were analyzed for each condition. Values are presented as mean ± S.D. from at least two independent experiments.

In addition to cellular morphologies, actin arrangements in THP-1 derived macrophages were assessed manually. As previously described in section 5.3.2, the percentage of THP-1 derived macrophages with podosomes was chosen as a readout parameter. While after 24 h an increase of cells exhibiting podosomes could be observed in THP-1 derived M1 macrophages, the percentage of cells with podosomes decreased after 72 h compared to M0 macrophages (**Figure 28 C**). More interestingly, cultivation on PEM 3 resulted in an increased number of podosome-positive cells after 24 h, 48 h and 72 h. Moreover, whereas THP-1 derived macrophages cultured on PEM 4 had decreased podosomes after 48 h and 72 h compared to M0 macrophages.

Next, secretion pro-inflammatory and anti-inflammatory cytokines was analyzed by multiplexed the developed cytokine panel to assess macrophage polarization states (**Figure 29**). Quantification of cytokine secretion showed overall increased levels of the pro-inflammatory cytokine IL-8. Nevertheless, pro-inflammatory and anti-inflammatory responses of THP-1_actin-CB derived M0 macrophages were overall low. As expected, a significant upregulation of pro-inflammatory cytokines (IL-8, MCP-1 and MIP-1 β) was observed after LPS/IFNγ stimulation (M1 activation) for 72 h. In parallel, M2 activation (IL-4/IL-13 treatment) resulted in an upregulated expression of the anti-inflammatory markers IL-10 and IL-1RA, whereas VEGF was downregulated.

Evaluating the cytokine responses of THP-1_actin-CB derived macrophages cultured on PEM coatings with different surface wettability, differences in pro-inflammatory cytokine levels were observed: Expression of the cytokines IL-8 and MIP-1 β were notably higher on the most hydrophobic coating PEM 4 compared to M0 control, an observation which was not found with PEM 1 - 3. Notably, no differences were found in the expression of anti-inflammatory cytokines IL 10 and IL 1Ra or the wound healing factor VEGF following cultivation of the THP-1_actin-CB derived macrophages on any of the PEM-coated TCP.

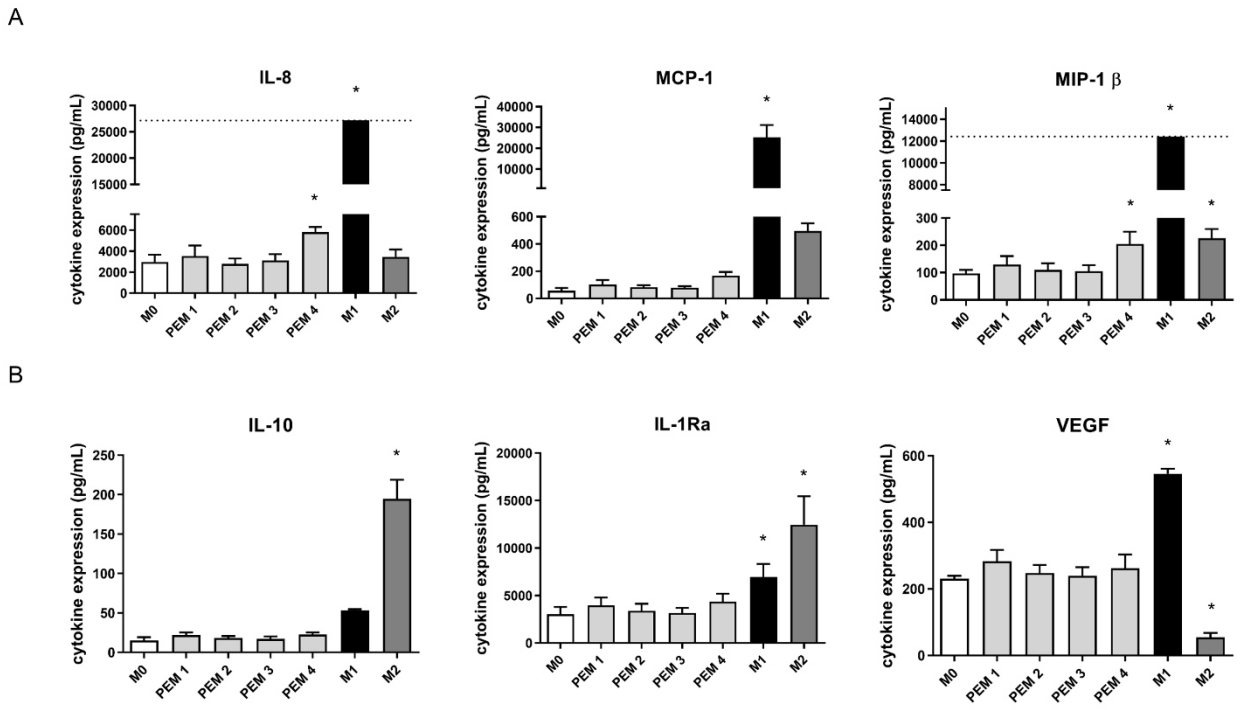

Figure 29: Pro- and anti-inflammatory cytokine response from THP-1_actin-CB derived macrophages cultured on polyelectrolyte multilayer (PEM) substrates with different surface hydrophobicity.
*Bar chart showing the expression levels (pg/mL) of pro-inflammatory (A) and anti-inflammatory (B) cytokines from THP-1_actin-CB derived macrophages cultured for three days on PEM substrates with increasing surface hydrophobicity (from PEM 1 to PEM 4). Macrophages cultured on tissue culture plate (TCP) were left non-treated (M0) or incubated with LPS/IFN-γ (M1) or IL-4/IL-13 (M2) and served as controls. Cytokines were assessed using the multiplexed cytokine detection panel. Data are shown as mean ± standard derivation of at least three biological replicates ($n \geq 3$). For statistical analysis ordinary one-way ANOVA followed by a post hoc Dunnett's test was performed. * $p < 0.05$ vs. M0. Cytokine expression was measured by Meike Jakobi.*

To summarize, the chromobody cell line THP-1_actin-CB can be applied for studies of cellular morphology and endogenous actin in living cells, thus allowing a reliable model to follow their dynamics. However, morphological readouts were not suited for a high throughput approach to predict the immune response. Pro-inflammatory cytokine expression could not be correlated to cellular morphologies directly. Although the percentage of cells with podosomes, on the other hand, was inversely linked to the pro-inflammatory cytokine responses observed, levels of pro-inflammatory cytokine expression was not reflected by values of podosome-positive cells.

5.5 Influencing biomaterial-induced immune responses using PEM coatings

Having observed low pro-inflammatory effects of PEM 1 coating, the next question was whether this coating can potentially be applied to modulate the elicited pro-inflammatory response of biomaterials. For this purpose, a set of three surfaces was analyzed: (i) PEM 1 coating on TCP, (ii)

material F_1, and (iii) PEM 1-coated material F_1. PEM coating of surfaces and its confirmation was carried out independently by the group of Dr. Hanna Hartmann.

To analyze the influence of PEM 1 coating on the induced cytokine secretion of biomaterials, THP-1_actin-CB derived macrophages were cultured on the different surfaces mentioned above. After 72 h of culture, secretion of pro-inflammatory and anti-inflammatory cytokines was assessed in the supernatant (**Figure 30**).

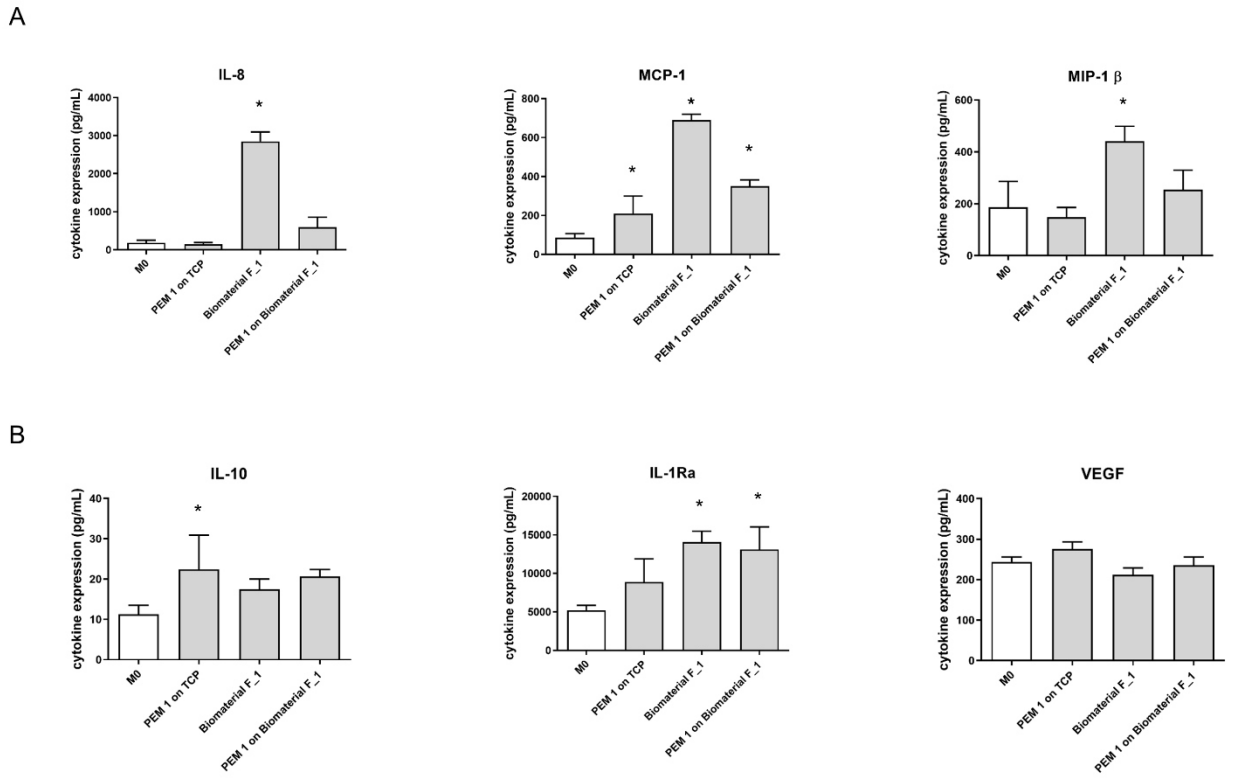

Figure 30: Pro- and anti-inflammatory cytokine production from THP-1_actin-CB derived macrophages cultured on PEM 1-coated TCP and material F_1 or uncoated material F_1.
*THP-1_actin-CB derived macrophages were cultured for 72 h on the different surfaces, after which (A) pro-inflammatory and (B) anti-inflammatory cytokine release was analyzed using multiplexed sandwich immunoassays. The dotted line represents the Upper Limit of Quantification (ULoQ). Results are presented as mean cytokine concentration (pg/mL) ± S.D. of three biological replicates (n = 3). For statistical analysis ordinary one-way ANOVA followed by a post hoc Dunnett's test was performed. * p < 0.05 vs. M0. Cytokine expression was measured by Meike Jakobi.*

Quantification of pro-inflammatory cytokines IL-8, MCP-1 and MIP-1 β revealed a significant decrease of cytokine expression on PEM 1-coated material F_1 compared to the uncoated material F_1 (**Figure 30 A**). Furthermore, no significant differences in pro-inflammatory cytokine response

between PEM 1 coating on TCP and material F_1 were observed. The anti-inflammatory cytokine secretion showed no significant differences on all three surfaces analyzed.

Taken together, these results suggest that the application of coating PEM 1 on inflammation-associated biomaterials dampens the elicited pro-inflammatory immune response. Based on these results it can be considered that the employment of the coating PEM 1 for modulation of the immune response is a versatile tool to improve the immunological results of existing biomaterial implants. Nevertheless, it has to be demonstrated that PEM coating is applicable for other biomaterials as well.

6 DISCUSSION

The analysis of biomaterial-induced cellular responses significantly contributes to a better understanding regarding the influence of surface properties on cell function, thus improving implant functionality and survival rate. Especially the impact on immune cells is of interest because they predominantly orchestrate the overall biological response to implants. Generally, macrophage responses to implant biomaterials are evaluated utilizing the production of pro-and anti-inflammatory cytokines or surface marker expression. Moreover, it was noticed that macrophage polarization is also accompanied by changes in cellular morphology and cytoskeleton formation of macrophages (Cougoule et al., 2012; Malheiro, Lehner, Dinca, Hoffmann, & Maniura-Weber, 2016; Vereyken et al., 2011).

In this thesis, the postulated correlation between cellular morphology and macrophage polarization state was demonstrated in an *in vitro* model employing THP-1 derived macrophages. The secretion of pro- and anti-inflammatory cytokines, surface marker expression and immune-associated protein expression confirmed polarization of THP-1 derived macrophages into the pro-inflammatory M1 and anti-inflammatory M2 phenotype following LPS/IFN-γ treatment or IL-4/IL-13 treatment, respectively. Given the fact that THP-1 cells have been employed to assess immune responses to biomaterial surfaces by other groups (Alfarsi et al., 2014; Buser et al., 1991; Fernandes et al., 2017), this cellular *in vitro* model was used to measure the immune reaction in response to biomaterials with varying physicochemical surface properties. Cytokine data revealed a strong influence of physical properties on macrophages. Furthermore, surface chemistry played a determinant role in how the immune response was modulated since some materials, such as polyurethane, did not affect cytokine secretion at all. Subsequently, it was addressed whether surface properties induce distinct morphologies and actin cytoskeleton arrangements that represent a specific inflammatory response. Admittedly, observed biomaterial-induced morphology did not correlate with cytokine response. Nevertheless, organization of actin cytoskeleton tendentially indicates whether a pro-inflammatory reaction occurs. Since biomaterial-induced biological responses are mainly assessed by endpoint assays, the spatial dynamic changes of inflammation in the human body cannot be displayed. To overcome this pitfall, stable THP-1 cell lines expressing the actin-biosensors actin-CB or LifeAct were generated to trace cytoskeletal and morphological changes in living cells. By analyzing the intracellular expressed fluorescence signal, THP-1 cells expressing the actin-CB (THP-1_actin-

CB) were identified to display actin structures with lower background signal. Employing the newly generated THP-1_actin-CB cell line, responses to polyelectrolyte multilayers (PEMs) with varying surface wettability were determined in living cells. As shown in cytokine expression levels, high degrees of hydrophobicity are related to increased pro-inflammatory responses. While macrophage morphologies did not reflect the observed immune response, actin cytoskeleton organization tended to indicate the corresponding immune response. Additionally, by applying the most hydrophilic PEM coating could dampen reactions to biomaterials eliciting pro-inflammatory responses.

In the following sections the obtained results and observations will be critically discussed in the context of the current state of knowledge in assessment of biomaterial-associated responses, modulation of (immune) cell responses through surface properties and the relation between macrophage polarization morphology. Finally, an outlook regarding possible expansions and application opportunities of macrophage reporter cell lines will be given.

6.1 Assessment of biomaterial-induced immune responses

To ensure the long-time survival and functionality of biomaterials in the patient, it is necessary to understand the inflammatory and subsequent cellular processes, such as fibrosis, following implantation. The biological evaluation of medical devices is based on ISO 10993, which evaluates the compatibility of the materials used with the body. Especially for the assessment of immunotoxicology and local effects following implantation animal models are mandatory ((ISO, 2006, 2017)). Nevertheless, physiological differences between organisms cause low correlation with the outcome in human patients (Bailey, Thew, & Balls, 2014). I*n vitro* tests based on human cells represent an interesting alternative, since they represent the human organism more closely (Seok et al., 2013). Furthermore, the application of such *in vitro* assays would reduce the number of animal testing needed. However, there is currently no standardly accepted *in vitro* model. They only allow to evaluate biocompatibility of new and existing biomaterials in an initial step.

Within the research campus “system immunology at biological-technical interfaces”, to which also the results generated in this study also contributed, the immune response to biomaterials was investigated with different *in vitro* models differing in their complexity. In addition to the THP-1 derived macrophage model, peripheral blood mononuclear cells (PBMCs) and human whole blood were employed which provide greater biological complexity and resemble the *in vivo* situation

more closely. In these experiments it was revealed that the reductionist THP-1 derived macrophage model showed similar responses to the more complex models (Segan et al., 2020).

In general, complex *in vitro* models allow to take more factors into account. For example, whole blood models also include the responses of granulocytes which represent a significant source of immunoregulatory signals following biomaterial implantation (reviewed in Franz et al. (2011). Further improvements of *in vitro* models could be to simulate the environment during surgical procedures, for instance by the addition of LPS during biomaterial testing. Moreover, multicellular approaches utilizing fibroblasts and endothelial cells in addition to macrophages mimic the complexity of the host response more closely, thus predicting the *in vivo* responses in a better way (Boersema, Grotenhuis, Bayon, Lange, & Bastiaansen-Jenniskens, 2016).

Despite these possible improvements for *in vitro* models, THP-1 derived macrophages still present a promising model to assess biomaterial-induced immune responses. For instance, (Alfarsi et al., 2014) observed that in vivo observations can be confirmed with THP-1 cells.

6.2 Biomaterial-induced modulation of immune responses

Within this study a number of varying biomaterials were assessed regarding the elicited immune response. The biomaterials ranged from materials with defined surface property changes to different classes of materials intended for commercial applications. Generally, cytokine results showed that all surface properties (such as stiffness, pore size, topography, and surface chemistry) of biomaterials allow the induction of different macrophage polarization states. This phenomenon can be applied to design biomaterials which alter immune responses in a desired way (reviewed in (Mariani et al., 2019)). To this end, it is necessary to get a better understanding which modifications have beneficial inflammatory effects.

The impact of surface topography on the immune response has been described for a number of materials, including glass (Shayan et al., 2018), polivinylidene fluoride (Paul et al., 2008) and polytetrafluoroethylene (Bota et al., 2010). Thus, to systematically study the effect of surface topography on the immune response, polyurethane specimens with defined roughness were investigated. Unexpectedly, grad of roughness did not influence the elicited response as cytokine secretion was low on all polyurethane specimens. Accordingly, it can be speculated that polyurethane itself triggers such low immune responses that the effects of roughness cannot be

measured. These observations can be further confirmed by the broad in vivo application of polyurethane in artificial heart valves and arteries (Burke & Hasirci, 2004) or insulation of pacemakers (Hayes, 1992).

Titanium has generally been described to show high levels of biocompatibility, which is why it is a prominent material for implants (L. C. Zhang & Chen, 2019). Nevertheless, previous studies have shown that surface modifications resulted in an improved implant success rate (Hotchkiss et al., 2016; Wennerberg & Albrektsson, 2009). Out of such modifications, surface wettability and roughness have caught attention as they were linked to high success rates. Since hydrophilic and rough titanium samples have been reported to decrease pro-inflammatory responses in murine and human *in vitro* models (Hamlet et al., 2012; Hotchkiss et al., 2016), it can be postulated that this success is also due to the controlled anti-inflammatory activation of macrophages. The results generated within this study are not completely consistent with these findings. Albeit not significantly for most pro-inflammatory cytokines, hydrophilized sandblasted and acid etched titanium 5 showed elevated levels of pro-inflammatory cytokines compared to the polished titanium 1. The responses to titanium 5 overall tended to be lower compared to sand blasted and acid etched titanium 4. This discrepancy compared to the literature described above is not entirely at odds. For example, in a study employing THP-1 derived macrophages titanium surface alterations did not induce alterations in immune response (Miao et al., 2017). Thus, source and processing protocols of titanium may also be considered as deciding factors for the elicited biological responses.

The creation of implant devices is a very complex and lengthy process. Various aspects such as technical functionality, stability and longevity of the implant must be ensured. Instead of creating new biomaterials, surface property modification of existing materials could be a versatile tool to improve immunological outcome. For this application, PEMs present a promising coating system. In accordance with relevant literature, increased hydrophobicity on PEMs was associated with elevated levels of pro-inflammatory markers (Lv et al., 2018; Visalakshan et al., 2019). Moreover, applying the most hydrophilic PEM coating on biomaterials eliciting pro-inflammatory responses dampened the inflammatory reactions. A comparable strategy could be the incorporation of bioactive molecules on the biomaterial surface to mitigate the foreign body reaction, which, however, would result in the subject of extensive clinical trials. A solution solely based on chemical composition is thus advantageous.

In summary, the *in vitro* model consisting of THP-1 derived macrophages allows the measurement of biomaterial-induced immune responses. The observed effects tend to be displayed *in vivo* as well, making the model an interesting tool for the preliminary examination of the materials.

6.3 Studying macrophage polarization using cellular morphology

The primary focus of this thesis was to study the relationship between cellular morphology and the associated cytokine production in macrophages to evaluate biomaterial-induced responses. Consequently, to quantitatively describe the different morphologies observed in THP-1 derived macrophages, an automated readout was generated utilizing the parameters cell shape, cell elongation and cell spreading. The same parameters have already been applied in other *in vitro* studies analyzing macrophage morphology, which underlines their suitability for describing the morphology (Malheiro et al., 2016; McWhorter et al., 2013).

Following chemical stimulation of THP-1 derived macrophages, the quantitative analysis of the cell shape factor showed an evident correlation between changes in cellular morphology and macrophage polarization state: M1 macrophage polarization (LPS/IFN-γ treatment) induced a roundish morphology compared to the more elongated morphology in M0 and M2 macrophages. Such relationships between macrophage polarization state and morphology have been described in a number of studies (Malheiro et al., 2016; McWhorter et al., 2013; Nishio et al., 2016; F. Zhang et al., 2015). However, opposing observations were made. For instance, McWhorter et al. (2013) reported in murine macrophages that M1 polarization led to a circular phenotype whereas M2 polarization resulted in macrophage elongation. Correspondingly, similar observations have been reported in human cells (Nishio et al., 2016). On the contrary, others observed macrophage elongation in the M1 phenotype of THP-1 derived macrophages (F. Zhang et al., 2015) or cell irregularities but not elongation in M2 THP-1 derived macrophages (Malheiro et al., 2016). The corresponding discrepancies between the morphological adaptions in the different studies may result from different reasons. On one hand, precise culture conditions have a major impact on macrophage morphology. As described by Rey-Giraud, Hafner, and Ries (2012) both composition of culture media and stimulants used influenced the observed morphology in primary human M1 and M2 macrophages. On the other hand, different experimental concepts (cell line vs. primary cells, interspecies differences, culture period) might be a reason. Thus, before using a

morphological readout for macrophages, the M1 and M2 macrophage morphology of one' s model must be carefully examined.

In addition to morphological differences, alterations in the actin cytoskeleton arrangement were observed in THP-1 derived macrophages following chemical stimulation. Whereas M1 polarization resulted in the formation of cortical actin structures, M0 and M2 macrophages showed actin throughout the cytoplasm with enrichment in podosomal structures. As already seen for cell morphology, such observations seem to be concentrated on individual studies rather than apply to a larger population. In accordance with the findings of this study, it has been reported that M2 polarization induced podosome formation while M1 macrophages were devoid of them (Cougoule et al., 2012). Other studies, however, observed actin enrichment close to the nucleus in murine M2 macrophages (Pelegrin & Surprenant, 2009; Vereyken et al., 2011).

Macrophage morphological responses to surface properties have been reported convincingly in a number of studies (Bartneck, Schulte, et al., 2010; Lee et al., 2013; Luu, Gott, Woo, Rao, & Liu, 2015; Lv et al., 2018; Malheiro et al., 2016; McWhorter et al., 2013). The focus of these studies was on the influence of surface topography, especially structured features, to induce certain cellular morphologies. In light of these studies it was rather expected to observe an impact of varying surface topographies of polyurethane or titanium specimens as well as different surface wettability of PEMs on cellular morphology. Nevertheless, the differences in biomaterial surface-induced morphology did not correlate to the expression levels of pro- and anti-inflammatory cytokines. Accordingly, a predominantly elongated phenotype observed on titanium 2 or PEM 4 was not associated with decreased levels of pro-inflammatory cytokines. Instead they were even elevated. Also in literature, observed morphologies could only be related to the corresponding immune response to a limited extent. Whereas McWhorter et al. (2013) and Luu et al. (2015) reported that surface grooves influencing cell elongation affect inflammatory response, Malheiro et al. (2016) did not observe that topography-induced morphologies promote significant expression of pro- and anti-inflammatory markers. Furthermore, not all studies include chemically induced M1 and M2 macrophages as controls. Thus, it is possible that certain morphologies in association with specific inflammatory responses are induced on materials, but these correlations are not present in M1 and M2 macrophages upon chemical stimulation.

Since cellular morphology of THP-1 derived macrophages cultured on different biomaterials was not associated with specific inflammatory immune responses in this thesis, the hypothesis that the induction of certain morphologies promotes significant changes in immune responses could not be confirmed. The adaption of macrophages to physical cues most likely occurs to facilitate their ability to migrate or phagocyte, functions associated with the actin cytoskeleton. Therefore, it was hypothesized that changes in the cell cytoskeleton arrangements lead to the inflammatory reactions observed. In contrast to most motile cell models, such as mesenchymal cells, macrophage motility is not based on large focal adhesions. Instead, they employ focal complexes and podosomes for adhesion and migration (Linder & Aepfelbacher, 2003). Podosomes are mechanosensing cell structures, that sense the substrate stiffness and increase their force in response (Labernadie et al., 2014). Based on these studies, the formation of podosomes on biomaterials was employed as an additional readout. It was observed that a pro-inflammatory response tended to result in a reduced number of podosome-forming cells. The differences in the organization of the actin cytoskeleton constitute a possible link between the sensing of the biomaterial and the induced inflammatory reaction. Nevertheless, other mechanisms also may be included ultimately leading to macrophage responses to biomaterial surface properties.

Taken together, cell morphology is not suited as sole readout to predict the immune reaction to biomaterials. Besides the formation of the actin cytoskeleton, cell sensitivity to surface properties most likely also occurs through other

6.4 Further optimizations and possibilities for macrophage reporter cell lines

To trace cytokine re-arrangements and cell morphology a stable THP-1 cell line expressing the actin-binder actin-CB (THP-1_actin-CB) was established. The actin-CB has been applied to visualize actin in plant and mammalian cells as well as zebrafish without affecting actin dynamics or cellular responses (Panza et al., 2015; Rocchetti, Hawes, & Kriechbaumer, 2014), which could be further confirmed in this study. Visualization of actin structures in living THP-1 derived macrophages was already accomplished in previous studies utilizing GFP-actin or LifeAct, respectively (Lee et al., 2013; Van Audenhove et al., 2015). Not influencing the formation of actin filaments (Doyle & Botstein, 1996) or limited visualization of actin filaments (Melak et al., 2017; Spracklen et al., 2014) the actin-CB provides distinct benefits.

Utilizing the THP-1_actin-CB cell line to assess biomaterial-induced responses allow only limited conclusion regarding the inflammatory response based on the readouts morphology and actin cytoskeleton organization. Additionally, it was not possible to implement an automated readout for assessing the actin formation. Thus, automated machine learning may present an alternative readout system. In this context, an image based machine learning tool has been published which was able to identify chemically induced macrophage subsets in primary human macrophages (Rostam, Reynolds, Alexander, Gadegaard, & Ghaemmaghami, 2017). However, the applicability of such approaches for biomaterials as well as THP-1 derived macrophages would have to be checked first.

Generally, stable cell lines expressing CBs are generated by random genomic integration of the CMV-driven CB expression plasmid and subsequent antibiotic selection (Keller et al., 2019), a technique also used in this thesis. However, this technique suffers from several drawbacks. First off, the CMV promotor has been shown to be susceptible to silencing (Balleza, Kim, & Cluzel, 2018) which leads to heterogeneous cell populations over several passages. Recently, it has been shown that the usage of the EF1-α promotor result in strong CB transgene expression (Keller et al., 2019) while also being applicable for long-term cultures (Qin et al., 2010). Moreover, random genomic integration does not allow to control site of integration nor the number of transgene copies integrated. To overcome these disadvantages, CRISPR/Cas9 presents a promising tool. By applying the CRISPR/Cas9 technology, transgenes can be introduced into the AAVS1 safe harbor locus (Gaj et al., 2017; Keller et al., 2019).

The main advantage of reporter cell lines is to generate a fast and reliable readout tool, representing the cellular responses. For the investigation of biomaterial-induced immune responses, cell lines are conceivable which directly indicate the inflammatory macrophage phenotype. For example, a transcriptional fluorescent reporter system based on the human monocytic THP-1 cell line has been reported recently. By introducing a transgene comprising GFP under the control of NF-κB, inflammatory reactions could be detected by following the fluorescence signal (Battin et al., 2017). Fluorescent protein tagging of endogenous genes of interest, such as immune associated proteins, represents another possibility. As demonstrated by Schmid-Burgk, Honing, Ebert, and Hornung (2016) CRISPR/Cas9 technology allows tagging of different proteins of interest, even in the difficult-to-transfect cell line THP-1. However, it has to be considered that most biomaterials are non-transparent, thus limiting the application of reporter cell lines which monitor responses under the microscope over time.

6.5 Conclusion

In this dissertation, an *in vitro* macrophage model based on the human monocytic cell line THP-1 has been demonstrated. Subsequently, the application to assess biomaterial-induced immune responses was successfully demonstrated. Moreover, the induction of distinct cell morphologies in adaption to biomaterial surface properties was observed. These changes could not be correlated to a specific macrophage polarization state. However, cultivation on biomaterials also induced changes in actin cytoskeleton formation which tended to correlate with inflammatory reactions. Lastly, a stable THP-1 cell line expressing the actin-CB was developed which enables tracing changes in cell morphology and actin cytoskeleton in live macrophages.

7 REFERENCES

Alfarsi, M. A., Hamlet, S. M., & Ivanovski, S. (2014). Titanium surface hydrophilicity modulates the human macrophage inflammatory cytokine response. *J Biomed Mater Res A, 102*(1), 60-67. doi:10.1002/jbm.a.34666

Anderson, J. M. (2000). Multinucleated giant cells. *Curr Opin Hematol, 7*(1), 40-47. doi:10.1097/00062752-200001000-00008

Anderson, J. M., & McNally, A. K. (2011). Biocompatibility of implants: lymphocyte/macrophage interactions. *Semin Immunopathol, 33*(3), 221-233. doi:10.1007/s00281-011-0244-1

Anderson, J. M., Rodriguez, A., & Chang, D. T. (2008). Foreign body reaction to biomaterials. *Semin Immunol, 20*(2), 86-100. doi:10.1016/j.smim.2007.11.004

Atri, C., Guerfali, F. Z., & Laouini, D. (2018). Role of Human Macrophage Polarization in Inflammation during Infectious Diseases. *Int J Mol Sci, 19*(6). doi:10.3390/ijms19061801

Badylak, S. F., Freytes, D. O., & Gilbert, T. W. (2009). Extracellular matrix as a biological scaffold material: Structure and function. *Acta Biomater, 5*(1), 1-13. doi:10.1016/j.actbio.2008.09.013

Badylak, S. F., & Gilbert, T. W. (2008). Immune response to biologic scaffold materials. *Semin Immunol, 20*(2), 109-116. doi:10.1016/j.smim.2007.11.003

Bailey, J., Thew, M., & Balls, M. (2014). An analysis of the use of animal models in predicting human toxicology and drug safety. *Altern Lab Anim, 42*(3), 181-199. doi:10.1177/026119291404200306

Balleza, E., Kim, J. M., & Cluzel, P. (2018). Systematic characterization of maturation time of fluorescent proteins in living cells. *Nat Methods, 15*(1), 47-51. doi:10.1038/nmeth.4509

Barth, K. A., Waterfield, J. D., & Brunette, D. M. (2013). The effect of surface roughness on RAW 264.7 macrophage phenotype. *J Biomed Mater Res A, 101*(9), 2679-2688. doi:10.1002/jbm.a.34562

Bartneck, M., Keul, H. A., Singh, S., Czaja, K., Bornemann, J., Bockstaller, M., . . . Groll, J. (2010). Rapid uptake of gold nanorods by primary human blood phagocytes and immunomodulatory effects of surface chemistry. *ACS Nano, 4*(6), 3073-3086. doi:10.1021/nn100262h

Bartneck, M., Schulte, V. A., Paul, N. E., Diez, M., Lensen, M. C., & Zwadlo-Klarwasser, G. (2010). Induction of specific macrophage subtypes by defined micro-patterned structures. *Acta Biomater, 6*(10), 3864-3872. doi:10.1016/j.actbio.2010.04.025

Battin, C., Hennig, A., Mayrhofer, P., Kunert, R., Zlabinger, G. J., Steinberger, P., & Paster, W. (2017). A human monocytic NF-kappaB fluorescent reporter cell line for detection of

microbial contaminants in biological samples. *PLoS One, 12*(5), e0178220. doi:10.1371/journal.pone.0178220

Belin, B. J., Goins, L. M., & Mullins, R. D. (2014). Comparative analysis of tools for live cell imaging of actin network architecture. *Bioarchitecture, 4*(6), 189-202. doi:10.1080/19490992.2014.1047714

Bird, R. E., Hardman, K. D., Jacobson, J. W., Johnson, S., Kaufman, B. M., Lee, S. M., . . . Whitlow, M. (1988). Single-chain antigen-binding proteins. *Science, 242*(4877), 423-426. doi:10.1126/science.3140379

Boersema, G. S., Grotenhuis, N., Bayon, Y., Lange, J. F., & Bastiaansen-Jenniskens, Y. M. (2016). The Effect of Biomaterials Used for Tissue Regeneration Purposes on Polarization of Macrophages. *Biores Open Access, 5*(1), 6-14. doi:10.1089/biores.2015.0041

Bota, P. C., Collie, A. M., Puolakkainen, P., Vernon, R. B., Sage, E. H., Ratner, B. D., & Stayton, P. S. (2010). Biomaterial topography alters healing in vivo and monocyte/macrophage activation in vitro. *J Biomed Mater Res A, 95*(2), 649-657. doi:10.1002/jbm.a.32893

Brodbeck, W. G., Nakayama, Y., Matsuda, T., Colton, E., Ziats, N. P., & Anderson, J. M. (2002). Biomaterial surface chemistry dictates adherent monocyte/macrophage cytokine expression in vitro. *Cytokine, 18*(6), 311-319. doi:10.1006/cyto.2002.1048

Brown, B. N., Sicari, B. M., & Badylak, S. F. (2014). Rethinking regenerative medicine: a macrophage-centered approach. *Front Immunol, 5*, 510. doi:10.3389/fimmu.2014.00510

Brown, B. N., Valentin, J. E., Stewart-Akers, A. M., McCabe, G. P., & Badylak, S. F. (2009). Macrophage phenotype and remodeling outcomes in response to biologic scaffolds with and without a cellular component. *Biomaterials, 30*(8), 1482-1491. doi:10.1016/j.biomaterials.2008.11.040

Burke, A., & Hasirci, N. (2004). Polyurethanes in biomedical applications. *Adv Exp Med Biol, 553*, 83-101. doi:10.1007/978-0-306-48584-8_7

Buser, D., Schenk, R. K., Steinemann, S., Fiorellini, J. P., Fox, C. H., & Stich, H. (1991). Influence of surface characteristics on bone integration of titanium implants. A histomorphometric study in miniature pigs. *J Biomed Mater Res, 25*(7), 889-902. doi:10.1002/jbm.820250708

Campo, G. M., Avenoso, A., Campo, S., Ferlazzo, A., Altavilla, D., Micali, C., & Calatroni, A. (2003). Aromatic trap analysis of free radicals production in experimental collagen-induced arthritis in the rat: protective effect of glycosaminoglycans treatment. *Free Radic Res, 37*(3), 257-268. doi:10.1080/1071576021000046640

Cattaneo, A., & Biocca, S. (1999). The selection of intracellular antibodies. *Trends Biotechnol, 17*(3), 115-121. doi:10.1016/s0167-7799(98)01268-2

Chanput, W., Mes, J. J., & Wichers, H. J. (2014). THP-1 cell line: an in vitro cell model for immune modulation approach. *Int Immunopharmacol, 23*(1), 37-45. doi:10.1016/j.intimp.2014.08.002

Chanput, W., Peters, V., & Wichers, H. (2015). THP-1 and U937 Cells. In K. Verhoeckx, P. Cotter, I. Lopez-Exposito, C. Kleiveland, T. Lea, A. Mackie, T. Requena, D. Swiatecka, & H. Wichers (Eds.), *The Impact of Food Bioactives on Health: in vitro and ex vivo models* (pp. 147-159). Cham (CH).

Clark, A. G., Dierkes, K., & Paluch, E. K. (2013). Monitoring actin cortex thickness in live cells. *Biophys J, 105*(3), 570-580. doi:10.1016/j.bpj.2013.05.057

Cougoule, C., Van Goethem, E., Le Cabec, V., Lafouresse, F., Dupre, L., Mehraj, V., . . . Maridonneau-Parini, I. (2012). Blood leukocytes and macrophages of various phenotypes have distinct abilities to form podosomes and to migrate in 3D environments. *Eur J Cell Biol, 91*(11-12), 938-949. doi:10.1016/j.ejcb.2012.07.002

Cui, K., Ardell, C. L., Podolnikova, N. P., & Yakubenko, V. P. (2018). Distinct Migratory Properties of M1, M2, and Resident Macrophages Are Regulated by alphaDbeta2 and alphaMbeta2 Integrin-Mediated Adhesion. *Front Immunol, 9*, 2650. doi:10.3389/fimmu.2018.02650

D'Este, E., Kamin, D., Gottfert, F., El-Hady, A., & Hell, S. W. (2015). STED nanoscopy reveals the ubiquity of subcortical cytoskeleton periodicity in living neurons. *Cell Rep, 10*(8), 1246-1251. doi:10.1016/j.celrep.2015.02.007

DeFife, K. M., Jenney, C. R., McNally, A. K., Colton, E., & Anderson, J. M. (1997). Interleukin-13 induces human monocyte/macrophage fusion and macrophage mannose receptor expression. *J Immunol, 158*(7), 3385-3390.

Doyle, T., & Botstein, D. (1996). Movement of yeast cortical actin cytoskeleton visualized in vivo. *Proc Natl Acad Sci U S A, 93*(9), 3886-3891. doi:10.1073/pnas.93.9.3886

Ducheyne, P. (1994). Bioactive ceramics. *J Bone Joint Surg Br, 76*(6), 861-862.

Elshal, M. F., & McCoy, J. P. (2006). Multiplex bead array assays: performance evaluation and comparison of sensitivity to ELISA. *Methods, 38*(4), 317-323. doi:10.1016/j.ymeth.2005.11.010

Fernandes, K. R., Zhang, Y., Magri, A. M. P., Renno, A. C. M., & van den Beucken, J. (2017). Biomaterial Property Effects on Platelets and Macrophages: An in Vitro Study. *ACS Biomater Sci Eng, 3*(12), 3318-3327. doi:10.1021/acsbiomaterials.7b00679

Franz, S., Rammelt, S., Scharnweber, D., & Simon, J. C. (2011). Immune responses to implants - a review of the implications for the design of immunomodulatory biomaterials. *Biomaterials, 32*(28), 6692-6709. doi:10.1016/j.biomaterials.2011.05.078

Gaj, T., Staahl, B. T., Rodrigues, G. M. C., Limsirichai, P., Ekman, F. K., Doudna, J. A., & Schaffer, D. V. (2017). Targeted gene knock-in by homology-directed genome editing using Cas9 ribonucleoprotein and AAV donor delivery. *Nucleic Acids Res, 45*(11), e98. doi:10.1093/nar/gkx154

Garg, K., Pullen, N. A., Oskeritzian, C. A., Ryan, J. J., & Bowlin, G. L. (2013). Macrophage functional polarization (M1/M2) in response to varying fiber and pore dimensions of electrospun scaffolds. *Biomaterials, 34*(18), 4439-4451. doi:10.1016/j.biomaterials.2013.02.065

Genin, M., Clement, F., Fattaccioli, A., Raes, M., & Michiels, C. (2015). M1 and M2 macrophages derived from THP-1 cells differentially modulate the response of cancer cells to etoposide. *BMC Cancer, 15*, 577. doi:10.1186/s12885-015-1546-9

Geutjes, P. J., Daamen, W. F., Buma, P., Feitz, W. F., Faraj, K. A., & van Kuppevelt, T. H. (2006). From molecules to matrix: construction and evaluation of molecularly defined bioscaffolds. *Adv Exp Med Biol, 585*, 279-295. doi:10.1007/978-0-387-34133-0_19

Gifford, R., Batchelor, M. M., Lee, Y., Gokulrangan, G., Meyerhoff, M. E., & Wilson, G. S. (2005). Mediation of in vivo glucose sensor inflammatory response via nitric oxide release. *J Biomed Mater Res A, 75*(4), 755-766. doi:10.1002/jbm.a.30359

Gilroy, D. W. (2004). The endogenous control of acute inflammation–from onset to resolution. *Drug Discovery Today: Therapeutic Strategies, 1*(3), 313-319.

Ginhoux, F., & Jung, S. (2014). Monocytes and macrophages: developmental pathways and tissue homeostasis. *Nat Rev Immunol, 14*(6), 392-404. doi:10.1038/nri3671

Ginhoux, F., Schultze, J. L., Murray, P. J., Ochando, J., & Biswas, S. K. (2016). New insights into the multidimensional concept of macrophage ontogeny, activation and function. *Nat Immunol, 17*(1), 34-40. doi:10.1038/ni.3324

Gower, R. M., Boehler, R. M., Azarin, S. M., Ricci, C. F., Leonard, J. N., & Shea, L. D. (2014). Modulation of leukocyte infiltration and phenotype in microporous tissue engineering scaffolds via vector induced IL-10 expression. *Biomaterials, 35*(6), 2024-2031. doi:10.1016/j.biomaterials.2013.11.036

Gross, G. G., Junge, J. A., Mora, R. J., Kwon, H. B., Olson, C. A., Takahashi, T. T., . . . Arnold, D. B. (2013). Recombinant probes for visualizing endogenous synaptic proteins in living neurons. *Neuron, 78*(6), 971-985. doi:10.1016/j.neuron.2013.04.017

Hamers-Casterman, C., Atarhouch, T., Muyldermans, S., Robinson, G., Hamers, C., Songa, E. B., . . . Hamers, R. (1993). Naturally occurring antibodies devoid of light chains. *Nature, 363*(6428), 446-448. doi:10.1038/363446a0

Hamlet, S., Alfarsi, M., George, R., & Ivanovski, S. (2012). The effect of hydrophilic titanium surface modification on macrophage inflammatory cytokine gene expression. *Clin Oral Implants Res, 23*(5), 584-590. doi:10.1111/j.1600-0501.2011.02325.x

Hayes, D. L. (1992). The next 5 years in cardiac pacemakers: a preview. *Mayo Clin Proc, 67*(4), 379-384. doi:10.1016/s0025-6196(12)61556-0

He, H., Buckley, M., Britton, B., Mu, Y., Warner, K., Kumar, S., & Cory, T. J. (2018). Polarized macrophage subsets differentially express the drug efflux transporters MRP1 and BCRP,

resulting in altered HIV production. *Antivir Chem Chemother, 26*, 2040206617745168. doi:10.1177/2040206617745168

Hench, L. L. (1980). Biomaterials. *Science, 208*(4446), 826-831. doi:10.1126/science.6246576

Hench, L. L., & Polak, J. M. (2002). Third-generation biomedical materials. *Science, 295*(5557), 1014-1017. doi:10.1126/science.1067404

Hench, L. L., & Thompson, I. (2010). Twenty-first century challenges for biomaterials. *J R Soc Interface, 7 Suppl 4*, S379-391. doi:10.1098/rsif.2010.0151.focus

Herman, I. M. (1993). Actin isoforms. *Curr Opin Cell Biol, 5*(1), 48-55. doi:10.1016/s0955-0674(05)80007-9

Hetrick, E. M., Prichard, H. L., Klitzman, B., & Schoenfisch, M. H. (2007). Reduced foreign body response at nitric oxide-releasing subcutaneous implants. *Biomaterials, 28*(31), 4571-4580. doi:10.1016/j.biomaterials.2007.06.036

Hoffman, A. S. (2002). Hydrogels for biomedical applications. *Adv Drug Deliv Rev, 54*(1), 3-12. doi:10.1016/s0169-409x(01)00239-3

Hotchkiss, K. M., Reddy, G. B., Hyzy, S. L., Schwartz, Z., Boyan, B. D., & Olivares-Navarrete, R. (2016). Titanium surface characteristics, including topography and wettability, alter macrophage activation. *Acta Biomater, 31*, 425-434. doi:10.1016/j.actbio.2015.12.003

Huber, F., Boire, A., Lopez, M. P., & Koenderink, G. H. (2015). Cytoskeletal crosstalk: when three different personalities team up. *Curr Opin Cell Biol, 32*, 39-47. doi:10.1016/j.ceb.2014.10.005

ISO/TS 10993-20:2006-08 Biological evaluation of medical devices - Part 20: Principles and methods for immunotoxicology testing of medical devices, (2006).

DIN EN ISO 10993-6:2017-09 Biological evaluation of medical devices - Part 6: Tests for local effects after implantation (ISO 10993-6:2016), (2017).

Jain, N., & Vogel, V. (2018). Spatial confinement downsizes the inflammatory response of macrophages. *Nat Mater, 17*(12), 1134-1144. doi:10.1038/s41563-018-0190-6

Janeway Jr, C. A., Travers, P., Walport, M., & Shlomchik, M. J. (2001). *Immunobiology: The Immune System in Health and Disease.* (5 ed.): Garland Science.

Jekely, G. (2014). Origin and evolution of the self-organizing cytoskeleton in the network of eukaryotic organelles. *Cold Spring Harb Perspect Biol, 6*(9), a016030. doi:10.1101/cshperspect.a016030

Jones, J. A., Chang, D. T., Meyerson, H., Colton, E., Kwon, I. K., Matsuda, T., & Anderson, J. M. (2007). Proteomic analysis and quantification of cytokines and chemokines from biomaterial surface-adherent macrophages and foreign body giant cells. *J Biomed Mater Res A, 83*(3), 585-596. doi:10.1002/jbm.a.31221

Kaiser, P. D., Maier, J., Traenkle, B., Emele, F., & Rothbauer, U. (2014). Recent progress in generating intracellular functional antibody fragments to target and trace cellular components in living cells. *Biochim Biophys Acta, 1844*(11), 1933-1942. doi:10.1016/j.bbapap.2014.04.019

Kao, W. J., & Lee, D. (2001). In vivo modulation of host response and macrophage behavior by polymer networks grafted with fibronectin-derived biomimetic oligopeptides: the role of RGD and PHSRN domains. *Biomaterials, 22*(21), 2901-2909. doi:10.1016/s0142-9612(01)00037-0

Kao, W. J., & Liu, Y. (2001). Utilizing biomimetic oligopeptides to probe fibronectin-integrin binding and signaling in regulating macrophage function in vitro and in vivo. *Front Biosci, 6*, D992-999. doi:10.2741/kao

Kao, W. J., McNally, A. K., Hiltner, A., & Anderson, J. M. (1995). Role for interleukin-4 in foreign-body giant cell formation on a poly(etherurethane urea) in vivo. *J Biomed Mater Res, 29*(10), 1267-1275. doi:10.1002/jbm.820291014

Keller, B. M., Maier, J., Weldle, M., Segan, S., Traenkle, B., & Rothbauer, U. (2019). A Strategy to Optimize the Generation of Stable Chromobody Cell Lines for Visualization and Quantification of Endogenous Proteins in Living Cells. *Antibodies (Basel), 8*(1). doi:10.3390/antib8010010

Kilic, C., Girotti, A., Rodriguez-Cabello, J. C., & Hasirci, V. (2014). A collagen-based corneal stroma substitute with micro-designed architecture. *Biomater Sci, 2*(3), 318-329. doi:10.1039/c3bm60194c

Koestler, S. A., Rottner, K., Lai, F., Block, J., Vinzenz, M., & Small, J. V. (2009). F- and G-actin concentrations in lamellipodia of moving cells. *PLoS One, 4*(3), e4810. doi:10.1371/journal.pone.0004810

Krastev, R., Rudt, A., Xiong, X., & Hartmann, H. (2018). Polyelectrolyte coatings for surface modification of medical implants. *Current Directions in Biomedical Engineering, 4*(1), 217-220.

Labernadie, A., Bouissou, A., Delobelle, P., Balor, S., Voituriez, R., Proag, A., . . . Maridonneau-Parini, I. (2014). Protrusion force microscopy reveals oscillatory force generation and mechanosensing activity of human macrophage podosomes. *Nat Commun, 5*, 5343. doi:10.1038/ncomms6343

Lazarides, E., & Weber, K. (1974). Actin antibody: the specific visualization of actin filaments in non-muscle cells. *Proc Natl Acad Sci U S A, 71*(6), 2268-2272. doi:10.1073/pnas.71.6.2268

Le Saux, G., Magenau, A., Bocking, T., Gaus, K., & Gooding, J. J. (2011). The relative importance of topography and RGD ligand density for endothelial cell adhesion. *PLoS One, 6*(7), e21869. doi:10.1371/journal.pone.0021869

Lee, H. S., Stachelek, S. J., Tomczyk, N., Finley, M. J., Composto, R. J., & Eckmann, D. M. (2013). Correlating macrophage morphology and cytokine production resulting from biomaterial contact. *J Biomed Mater Res A, 101*(1), 203-212. doi:10.1002/jbm.a.34309

Lehto, V. P., Hovi, T., Vartio, T., Badley, R. A., & Virtanen, I. (1982). Reorganization of cytoskeletal and contractile elements during transition of human monocytes into adherent macrophages. *Lab Invest, 47*(4), 391-399.

Li, X., Huang, Q., Elkhooly, T. A., Liu, Y., Wu, H., Feng, Q., . . . Hu, T. (2018). Effects of titanium surface roughness on the mediation of osteogenesis via modulating the immune response of macrophages. *Biomed Mater, 13*(4), 045013. doi:10.1088/1748-605X/aabe33

Linder, S., & Aepfelbacher, M. (2003). Podosomes: adhesion hot-spots of invasive cells. *Trends Cell Biol, 13*(7), 376-385. doi:10.1016/s0962-8924(03)00128-4

Luu, T. U., Gott, S. C., Woo, B. W., Rao, M. P., & Liu, W. F. (2015). Micro- and Nanopatterned Topographical Cues for Regulating Macrophage Cell Shape and Phenotype. *ACS Appl Mater Interfaces, 7*(51), 28665-28672. doi:10.1021/acsami.5b10589

Lv, L., Xie, Y., Li, K., Hu, T., Lu, X., Cao, Y., & Zheng, X. (2018). Unveiling the Mechanism of Surface Hydrophilicity-Modulated Macrophage Polarization. *Adv Healthc Mater, 7*(19), e1800675. doi:10.1002/adhm.201800675

Lynn, A. D., Kyriakides, T. R., & Bryant, S. J. (2010). Characterization of the in vitro macrophage response and in vivo host response to poly(ethylene glycol)-based hydrogels. *J Biomed Mater Res A, 93*(3), 941-953. doi:10.1002/jbm.a.32595

Madden, L. R., Mortisen, D. J., Sussman, E. M., Dupras, S. K., Fugate, J. A., Cuy, J. L., . . . Ratner, B. D. (2010). Proangiogenic scaffolds as functional templates for cardiac tissue engineering. *Proc Natl Acad Sci U S A, 107*(34), 15211-15216. doi:10.1073/pnas.1006442107

Malheiro, V., Lehner, F., Dinca, V., Hoffmann, P., & Maniura-Weber, K. (2016). Convex and concave micro-structured silicone controls the shape, but not the polarization state of human macrophages. *Biomater Sci, 4*(11), 1562-1573. doi:10.1039/c6bm00425c

Mariani, E., Lisignoli, G., Borzi, R. M., & Pulsatelli, L. (2019). Biomaterials: Foreign Bodies or Tuners for the Immune Response? *Int J Mol Sci, 20*(3). doi:10.3390/ijms20030636

Martinez, F. O., & Gordon, S. (2014). The M1 and M2 paradigm of macrophage activation: time for reassessment. *F1000Prime Rep, 6*, 13. doi:10.12703/P6-13

Martinez, F. O., Helming, L., Milde, R., Varin, A., Melgert, B. N., Draijer, C., . . . Gordon, S. (2013). Genetic programs expressed in resting and IL-4 alternatively activated mouse and human macrophages: similarities and differences. *Blood, 121*(9), e57-69. doi:10.1182/blood-2012-06-436212

McNally, A. K., & Anderson, J. M. (1995). Interleukin-4 induces foreign body giant cells from human monocytes/macrophages. Differential lymphokine regulation of macrophage fusion

leads to morphological variants of multinucleated giant cells. *Am J Pathol, 147*(5), 1487-1499.

McNally, A. K., Jones, J. A., Macewan, S. R., Colton, E., & Anderson, J. M. (2008). Vitronectin is a critical protein adhesion substrate for IL-4-induced foreign body giant cell formation. *J Biomed Mater Res A, 86*(2), 535-543. doi:10.1002/jbm.a.31658

McWhorter, F. Y., Davis, C. T., & Liu, W. F. (2015). Physical and mechanical regulation of macrophage phenotype and function. *Cell Mol Life Sci, 72*(7), 1303-1316. doi:10.1007/s00018-014-1796-8

McWhorter, F. Y., Wang, T., Nguyen, P., Chung, T., & Liu, W. F. (2013). Modulation of macrophage phenotype by cell shape. *Proc Natl Acad Sci U S A, 110*(43), 17253-17258. doi:10.1073/pnas.1308887110

Melak, M., Plessner, M., & Grosse, R. (2017). Actin visualization at a glance. *J Cell Sci, 130*(3), 525-530. doi:10.1242/jcs.189068

Miao, X., Wang, D., Xu, L., Wang, J., Zeng, D., Lin, S., . . . Jiang, X. (2017). The response of human osteoblasts, epithelial cells, fibroblasts, macrophages and oral bacteria to nanostructured titanium surfaces: a systematic study. *Int J Nanomedicine, 12*, 1415-1430. doi:10.2147/IJN.S126760

Mills, C. D., Kincaid, K., Alt, J. M., Heilman, M. J., & Hill, A. M. (2000). M-1/M-2 macrophages and the Th1/Th2 paradigm. *J Immunol, 164*(12), 6166-6173. doi:10.4049/jimmunol.164.12.6166

Mokarram, N., Merchant, A., Mukhatyar, V., Patel, G., & Bellamkonda, R. V. (2012). Effect of modulating macrophage phenotype on peripheral nerve repair. *Biomaterials, 33*(34), 8793-8801. doi:10.1016/j.biomaterials.2012.08.050

Morais, J. M., Papadimitrakopoulos, F., & Burgess, D. J. (2010). Biomaterials/tissue interactions: possible solutions to overcome foreign body response. *AAPS J, 12*(2), 188-196. doi:10.1208/s12248-010-9175-3

Mosser, D. M., & Edwards, J. P. (2008). Exploring the full spectrum of macrophage activation. *Nat Rev Immunol, 8*(12), 958-969. doi:10.1038/nri2448

Muyldermans, S. (2013). Nanobodies: natural single-domain antibodies. *Annu Rev Biochem, 82*, 775-797. doi:10.1146/annurev-biochem-063011-092449

Myrna, K. E., Mendonsa, R., Russell, P., Pot, S. A., Liliensiek, S. J., Jester, J. V., . . . Murphy, C. J. (2012). Substratum topography modulates corneal fibroblast to myofibroblast transformation. *Invest Ophthalmol Vis Sci, 53*(2), 811-816. doi:10.1167/iovs.11-7982

Nguyen, V. K., Hamers, R., Wyns, L., & Muyldermans, S. (1999). Loss of splice consensus signal is responsible for the removal of the entire C(H)1 domain of the functional camel IGG2A heavy-chain antibodies. *Mol Immunol, 36*(8), 515-524. doi:10.1016/s0161-5890(99)00067-x

Nilsson, B., Ekdahl, K. N., Mollnes, T. E., & Lambris, J. D. (2007). The role of complement in biomaterial-induced inflammation. *Mol Immunol, 44*(1-3), 82-94. doi:10.1016/j.molimm.2006.06.020

Nishio, M., Urakawa, N., Shigeoka, M., Takase, N., Ichihara, Y., Arai, N., . . . Yokozaki, H. (2016). Software-assisted morphometric and phenotype analyses of human peripheral blood monocyte-derived macrophages induced by a microenvironment model of human esophageal squamous cell carcinoma. *Pathol Int, 66*(2), 83-93. doi:10.1111/pin.12381

Oliver, J. M., & Berlin, R. D. (1982). Cytoskeleton-membrane interaction and the remodeling of the cell surface during phagocytosis and chemotaxis. *Adv Exp Med Biol, 155*, 113-131. doi:10.1007/978-1-4684-4394-3_10

Oshikawa, K., Yamasawa, H., & Sugiyama, Y. (2003). Human lung fibroblasts inhibit macrophage inflammatory protein-1alpha production by lipopolysaccharide-stimulated macrophages. *Biochem Biophys Res Commun, 312*(3), 650-655. doi:10.1016/j.bbrc.2003.10.166

Panza, P., Maier, J., Schmees, C., Rothbauer, U., & Sollner, C. (2015). Live imaging of endogenous protein dynamics in zebrafish using chromobodies. *Development, 142*(10), 1879-1884. doi:10.1242/dev.118943

Parsons, J. T., Horwitz, A. R., & Schwartz, M. A. (2010). Cell adhesion: integrating cytoskeletal dynamics and cellular tension. *Nat Rev Mol Cell Biol, 11*(9), 633-643. doi:10.1038/nrm2957

Patel, N. R., & Gohil, P. P. (2012). A review on biomaterials: scope, applications & human anatomy significance. *International Journal of Emerging Technology and Advanced Engineering, 2*(4), 91-101.

Paul, N. E., Skazik, C., Harwardt, M., Bartneck, M., Denecke, B., Klee, D., . . . Zwadlo-Klarwasser, G. (2008). Topographical control of human macrophages by a regularly microstructured polyvinylidene fluoride surface. *Biomaterials, 29*(30), 4056-4064. doi:10.1016/j.biomaterials.2008.07.010

Pelegrin, P., & Surprenant, A. (2009). Dynamics of macrophage polarization reveal new mechanism to inhibit IL-1beta release through pyrophosphates. *EMBO J, 28*(14), 2114-2127. doi:10.1038/emboj.2009.163

Periz, J., Whitelaw, J., Harding, C., Gras, S., Del Rosario Minina, M. I., Latorre-Barragan, F., . . . Meissner, M. (2017). Toxoplasma gondii F-actin forms an extensive filamentous network required for material exchange and parasite maturation. *Elife, 6*. doi:10.7554/eLife.24119

Pollard, T. D., & Borisy, G. G. (2003). Cellular motility driven by assembly and disassembly of actin filaments. *Cell, 112*(4), 453-465. doi:10.1016/s0092-8674(03)00120-x

Qin, J. Y., Zhang, L., Clift, K. L., Hulur, I., Xiang, A. P., Ren, B. Z., & Lahn, B. T. (2010). Systematic comparison of constitutive promoters and the doxycycline-inducible promoter. *PLoS One, 5*(5), e10611. doi:10.1371/journal.pone.0010611

Rani, R., Jordan, M. B., Divanovic, S., & Herbert, D. R. (2012). IFN-gamma-driven IDO production from macrophages protects IL-4Ralpha-deficient mice against lethality during Schistosoma mansoni infection. *Am J Pathol, 180*(5), 2001-2008. doi:10.1016/j.ajpath.2012.01.013

Ratner, B. D., & Bryant, S. J. (2004). Biomaterials: where we have been and where we are going. *Annu Rev Biomed Eng, 6*, 41-75. doi:10.1146/annurev.bioeng.6.040803.140027

Rey-Giraud, F., Hafner, M., & Ries, C. H. (2012). In vitro generation of monocyte-derived macrophages under serum-free conditions improves their tumor promoting functions. *PLoS One, 7*(8), e42656. doi:10.1371/journal.pone.0042656

Riedl, J., Crevenna, A. H., Kessenbrock, K., Yu, J. H., Neukirchen, D., Bista, M., . . . Wedlich-Soldner, R. (2008). Lifeact: a versatile marker to visualize F-actin. *Nat Methods, 5*(7), 605-607. doi:10.1038/nmeth.1220

Riedl, J., Flynn, K. C., Raducanu, A., Gartner, F., Beck, G., Bosl, M., . . . Wedlich-Soldner, R. (2010). Lifeact mice for studying F-actin dynamics. *Nat Methods, 7*(3), 168-169. doi:10.1038/nmeth0310-168

Rocchetti, A., Hawes, C., & Kriechbaumer, V. (2014). Fluorescent labelling of the actin cytoskeleton in plants using a cameloid antibody. *Plant Methods, 10*, 12. doi:10.1186/1746-4811-10-12

Rostam, H. M., Reynolds, P. M., Alexander, M. R., Gadegaard, N., & Ghaemmaghami, A. M. (2017). Image based Machine Learning for identification of macrophage subsets. *Sci Rep, 7*(1), 3521. doi:10.1038/s41598-017-03780-z

Rőszer, T. (2015). Understanding the mysterious M2 macrophage through activation markers and effector mechanisms. *Mediators of inflammation, 2015*.

Rothbauer, U., Zolghadr, K., Muyldermans, S., Schepers, A., Cardoso, M. C., & Leonhardt, H. (2008). A versatile nanotrap for biochemical and functional studies with fluorescent fusion proteins. *Mol Cell Proteomics, 7*(2), 282-289. doi:10.1074/mcp.M700342-MCP200

Rothbauer, U., Zolghadr, K., Tillib, S., Nowak, D., Schermelleh, L., Gahl, A., . . . Leonhardt, H. (2006). Targeting and tracing antigens in live cells with fluorescent nanobodies. *Nat Methods, 3*(11), 887-889. doi:10.1038/nmeth953

Sachot, N., Mateos-Timoneda, M. A., Planell, J. A., Velders, A. H., Lewandowska, M., Engel, E., & Castano, O. (2015). Towards 4th generation biomaterials: a covalent hybrid polymer-ormoglass architecture. *Nanoscale, 7*(37), 15349-15361. doi:10.1039/c5nr04275e

Saini, M., Singh, Y., Arora, P., Arora, V., & Jain, K. (2015). Implant biomaterials: A comprehensive review. *World J Clin Cases, 3*(1), 52-57. doi:10.12998/wjcc.v3.i1.52

Salek-Ardakani, S., Arrand, J. R., Shaw, D., & Mackett, M. (2000). Heparin and heparan sulfate bind interleukin-10 and modulate its activity. *Blood, 96*(5), 1879-1888.

Schell, M. J., Erneux, C., & Irvine, R. F. (2001). Inositol 1,4,5-trisphosphate 3-kinase A associates with F-actin and dendritic spines via its N terminus. *J Biol Chem, 276*(40), 37537-37546. doi:10.1074/jbc.M104101200

Schmid-Burgk, J. L., Honing, K., Ebert, T. S., & Hornung, V. (2016). CRISPaint allows modular base-specific gene tagging using a ligase-4-dependent mechanism. *Nat Commun, 7*, 12338. doi:10.1038/ncomms12338

Schoen, F. J., Levy, R. J., & Piehler, H. R. (1992). Pathological considerations in replacement cardiac valves. *Cardiovasc Pathol, 1*(1), 29-52. doi:10.1016/1054-8807(92)90006-A

Scopelliti, P. E., Borgonovo, A., Indrieri, M., Giorgetti, L., Bongiorno, G., Carbone, R., . . . Milani, P. (2010). The effect of surface nanometre-scale morphology on protein adsorption. *PLoS One, 5*(7), e11862. doi:10.1371/journal.pone.0011862

Segan, S., Jakobi, M., Khokhani, P., Klimosch, S., Billing, F., Schneider, M., . . . Shipp, C. (2020). Systematic Investigation of Polyurethane Biomaterial Surface Roughness on Human Immune Responses in vitro. *Biomed Res Int, 2020*, 3481549. doi:10.1155/2020/3481549

Seok, J., Warren, H. S., Cuenca, A. G., Mindrinos, M. N., Baker, H. V., Xu, W., . . . Host Response to Injury, L. S. C. R. P. (2013). Genomic responses in mouse models poorly mimic human inflammatory diseases. *Proc Natl Acad Sci U S A, 110*(9), 3507-3512. doi:10.1073/pnas.1222878110

Shayan, M., Padmanabhan, J., Morris, A. H., Cheung, B., Smith, R., Schroers, J., & Kyriakides, T. R. (2018). Nanopatterned bulk metallic glass-based biomaterials modulate macrophage polarization. *Acta Biomater, 75*, 427-438. doi:10.1016/j.actbio.2018.05.051

Sheikh, Z., Brooks, P. J., Barzilay, O., Fine, N., & Glogauer, M. (2015). Macrophages, Foreign Body Giant Cells and Their Response to Implantable Biomaterials. *Materials (Basel), 8*(9), 5671-5701. doi:10.3390/ma8095269

Shen, M., Garcia, I., Maier, R. V., & Horbett, T. A. (2004). Effects of adsorbed proteins and surface chemistry on foreign body giant cell formation, tumor necrosis factor alpha release and procoagulant activity of monocytes. *J Biomed Mater Res A, 70*(4), 533-541. doi:10.1002/jbm.a.30069

Sivaraman, B., Fears, K. P., & Latour, R. A. (2009). Investigation of the effects of surface chemistry and solution concentration on the conformation of adsorbed proteins using an improved circular dichroism method. *Langmuir, 25*(5), 3050-3056. doi:10.1021/la8036814

Spiller, K. L., Nassiri, S., Witherel, C. E., Anfang, R. R., Ng, J., Nakazawa, K. R., . . . Vunjak-Novakovic, G. (2015). Sequential delivery of immunomodulatory cytokines to facilitate the M1-to-M2 transition of macrophages and enhance vascularization of bone scaffolds. *Biomaterials, 37*, 194-207. doi:10.1016/j.biomaterials.2014.10.017

Spracklen, A. J., Fagan, T. N., Lovander, K. E., & Tootle, T. L. (2014). The pros and cons of common actin labeling tools for visualizing actin dynamics during Drosophila oogenesis. *Dev Biol, 393*(2), 209-226. doi:10.1016/j.ydbio.2014.06.022

Stern, R., Asari, A. A., & Sugahara, K. N. (2006). Hyaluronan fragments: an information-rich system. *Eur J Cell Biol, 85*(8), 699-715. doi:10.1016/j.ejcb.2006.05.009

Suarez, C., Carroll, R. T., Burke, T. A., Christensen, J. R., Bestul, A. J., Sees, J. A., . . . Kovar, D. R. (2015). Profilin regulates F-actin network homeostasis by favoring formin over Arp2/3 complex. *Dev Cell, 32*(1), 43-53. doi:10.1016/j.devcel.2014.10.027

Taniguchi, K., Hikiji, H., Okinaga, T., Hashidate-Yoshida, T., Shindou, H., Ariyoshi, W., . . . Nishihara, T. (2015). Essential Role of Lysophosphatidylcholine Acyltransferase 3 in the Induction of Macrophage Polarization in PMA-Treated U937 Cells. *J Cell Biochem, 116*(12), 2840-2848. doi:10.1002/jcb.25230

Tapper, H. (1996). The secretion of preformed granules by macrophages and neutrophils. *J Leukoc Biol, 59*(5), 613-622. doi:10.1002/jlb.59.5.613

Tauber, A. I. (2003). Metchnikoff and the phagocytosis theory. *Nat Rev Mol Cell Biol, 4*(11), 897-901. doi:10.1038/nrm1244

Termeer, C., Benedix, F., Sleeman, J., Fieber, C., Voith, U., Ahrens, T., . . . Simon, J. C. (2002). Oligosaccharides of Hyaluronan activate dendritic cells via toll-like receptor 4. *J Exp Med, 195*(1), 99-111. doi:10.1084/jem.20001858

Turner, N. J., & Badylak, S. F. (2015). The Use of Biologic Scaffolds in the Treatment of Chronic Nonhealing Wounds. *Adv Wound Care (New Rochelle), 4*(8), 490-500. doi:10.1089/wound.2014.0604

Valentin, J. E., Badylak, J. S., McCabe, G. P., & Badylak, S. F. (2006). Extracellular matrix bioscaffolds for orthopaedic applications. A comparative histologic study. *J Bone Joint Surg Am, 88*(12), 2673-2686. doi:10.2106/JBJS.E.01008

Van Audenhove, I., Debeuf, N., Boucherie, C., & Gettemans, J. (2015). Fascin actin bundling controls podosome turnover and disassembly while cortactin is involved in podosome assembly by its SH3 domain in THP-1 macrophages and dendritic cells. *Biochim Biophys Acta, 1853*(5), 940-952. doi:10.1016/j.bbamcr.2015.01.003

van Furth, R., & Cohn, Z. A. (1968). The origin and kinetics of mononuclear phagocytes. *J Exp Med, 128*(3), 415-435. doi:10.1084/jem.128.3.415

van Furth, R., Cohn, Z. A., Hirsch, J. G., Humphrey, J. H., Spector, W. G., & Langevoort, H. L. (1972). The mononuclear phagocyte system: a new classification of macrophages, monocytes, and their precursor cells. *Bull World Health Organ, 46*(6), 845-852.

VandeVondele, S., Voros, J., & Hubbell, J. A. (2003). RGD-grafted poly-L-lysine-graft-(polyethylene glycol) copolymers block non-specific protein adsorption while promoting cell adhesion. *Biotechnol Bioeng, 82*(7), 784-790. doi:10.1002/bit.10625

Varol, C., Mildner, A., & Jung, S. (2015). Macrophages: development and tissue specialization. *Annu Rev Immunol, 33*, 643-675. doi:10.1146/annurev-immunol-032414-112220

Vereyken, E. J., Heijnen, P. D., Baron, W., de Vries, E. H., Dijkstra, C. D., & Teunissen, C. E. (2011). Classically and alternatively activated bone marrow derived macrophages differ in cytoskeletal functions and migration towards specific CNS cell types. *J Neuroinflammation, 8*, 58. doi:10.1186/1742-2094-8-58

Vigano, M. A., Bieli, D., Schaefer, J. V., Jakob, R. P., Matsuda, S., Maier, T., . . . Affolter, M. (2018). DARPins recognizing mTFP1 as novel reagents for in vitro and in vivo protein manipulations. *Biol Open, 7*(11). doi:10.1242/bio.036749

Visalakshan, R. M., MacGregor, M. N., Sasidharan, S., Ghazaryan, A., Mierczynska-Vasilev, A. M., Morsbach, S., . . . Vasilev, K. (2019). Biomaterial Surface Hydrophobicity-Mediated Serum Protein Adsorption and Immune Responses. *ACS Appl Mater Interfaces, 11*(31), 27615-27623. doi:10.1021/acsami.9b09900

Wang, S., Xiao, Y., Zhang, D. D., & Wong, P. K. (2018). A gapmer aptamer nanobiosensor for real-time monitoring of transcription and translation in single cells. *Biomaterials, 156*, 56-64. doi:10.1016/j.biomaterials.2017.11.026

Wegner, A., & Isenberg, G. (1983). 12-fold difference between the critical monomer concentrations of the two ends of actin filaments in physiological salt conditions. *Proc Natl Acad Sci U S A, 80*(16), 4922-4925. doi:10.1073/pnas.80.16.4922

Wennerberg, A., & Albrektsson, T. (2009). Effects of titanium surface topography on bone integration: a systematic review. *Clin Oral Implants Res, 20 Suppl 4*, 172-184. doi:10.1111/j.1600-0501.2009.01775.x

Wheeler, K. C., Jena, M. K., Pradhan, B. S., Nayak, N., Das, S., Hsu, C. D., . . . Nayak, N. R. (2018). VEGF may contribute to macrophage recruitment and M2 polarization in the decidua. *PLoS One, 13*(1), e0191040. doi:10.1371/journal.pone.0191040

Williams, D. F. (2009). On the nature of biomaterials. *Biomaterials, 30*(30), 5897-5909. doi:10.1016/j.biomaterials.2009.07.027

Witt, D. P., & Lander, A. D. (1994). Differential binding of chemokines to glycosaminoglycan subpopulations. *Curr Biol, 4*(5), 394-400. doi:10.1016/s0960-9822(00)00088-9

Wu, J. Q., & Pollard, T. D. (2005). Counting cytokinesis proteins globally and locally in fission yeast. *Science, 310*(5746), 310-314. doi:10.1126/science.1113230

Xia, Z. D., Zhu, T. B., Du, J. Y., Zheng, Q. X., Wang, L., Li, S. P., . . . Fang, S. Y. (1994). Macrophages in degradation of collagen/hydroxylapatite(CHA), beta-tricalcium phosphate ceramics (TCP) artificial bone graft. An in vivo study. *Chin Med J (Engl), 107*(11), 845-849.

Xu, W., Zhao, X., Daha, M. R., & van Kooten, C. (2013). Reversible differentiation of pro- and anti-inflammatory macrophages. *Mol Immunol, 53*(3), 179-186. doi:10.1016/j.molimm.2012.07.005

Yamaguchi, H., & Condeelis, J. (2007). Regulation of the actin cytoskeleton in cancer cell migration and invasion. *Biochim Biophys Acta, 1773*(5), 642-652. doi:10.1016/j.bbamcr.2006.07.001

Yamashiro, S., Kamohara, H., Wang, J. M., Yang, D., Gong, W. H., & Yoshimura, T. (2001). Phenotypic and functional change of cytokine-activated neutrophils: inflammatory neutrophils are heterogeneous and enhance adaptive immune responses. *J Leukoc Biol, 69*(5), 698-704.

Yamawaki, H., Hirohata, S., Miyoshi, T., Takahashi, K., Ogawa, H., Shinohata, R., . . . Ninomiya, Y. (2009). Hyaluronan receptors involved in cytokine induction in monocytes. *Glycobiology, 19*(1), 83-92. doi:10.1093/glycob/cwn109

Yin, H. L., & Hartwig, J. H. (1988). The structure of the macrophage actin skeleton. *J Cell Sci Suppl, 9*, 169-184. doi:10.1242/jcs.1988.supplement_9.9

Zdolsek, J., Eaton, J. W., & Tang, L. (2007). Histamine release and fibrinogen adsorption mediate acute inflammatory responses to biomaterial implants in humans. *J Transl Med, 5*, 31. doi:10.1186/1479-5876-5-31

Zhang, F., Liu, H., Jiang, G., Wang, H., Wang, X., Wang, H., . . . Du, J. (2015). Changes in the proteomic profile during the differential polarization status of the human monocyte-derived macrophage THP-1 cell line. *Proteomics, 15*(4), 773-786. doi:10.1002/pmic.201300494

Zhang, L. C., & Chen, L. Y. (2019). A review on biomedical titanium alloys: recent progress and prospect. *Advanced Engineering Materials, 21*(4), 1801215.

Zhang, Y. H., He, M., Wang, Y., & Liao, A. H. (2017). Modulators of the Balance between M1 and M2 Macrophages during Pregnancy. *Front Immunol, 8*, 120. doi:10.3389/fimmu.2017.00120

Zhuo, R., Siedlecki, C. A., & Vogler, E. A. (2006). Autoactivation of blood factor XII at hydrophilic and hydrophobic surfaces. *Biomaterials, 27*(24), 4325-4332. doi:10.1016/j.biomaterials.2006.04.001

8 ANNEX

8.1 Publications

Parts of this thesis are published in:

Segan, S.; Jakobi, M.; Khokhani, P.; Klimosch, S.; Billing, F.; Schneider, M.; Martin, D.; Metzger, U.; Biesemeier, A.; Xiong, X.; Mukherjee, A; Steuer, H.; Keller, B.-M.; Joos, T.; Schmolz, M.; Rothbauer, U.; Hartmann, H.; Burkhardt, C.; Lorenz, G.; Schneiderhan-Marra, N.; Shipp, C. (2020) Systematic investigation of polyurethane biomaterial surface roughness on human immune responses in vitro. Biomed Research International, DOI: 10.1155/2020/3481549

Billing, F.; **Segan, S.**; Jakobi, M.; Arefaine, E.; Pickarski, L.; Schneiderhan-Marra, N.; Martin, D.; Burkhardt, C.; Rothbauer, U.; Shipp, C.; Hartmann, H. (in preparation): Gradient modification of surface wettability as a tunable tool to control inflammation.

To the following publications was contributed:

Keller, B. M..; Maier, J.; Weldle, M.; **Segan, S.**; Traenkle, B.; Rothbauer, U. (2019): A Strategy to Optimize the Generation of Stable Chromobody Cell Lines for Visualization and Quantification of Endogenous Proteins in Living Cells. Antibodies, DOI: 10.3390/antib8010010

Traenkle, B.; **Segan, S.**; Kaiser; P. D.; Rothbauer, U. (2020): A novel epitope tagging system to visualize and monitor antigens in live cells with chromobodies. Scientific Reports, DOI: 10.1038/s41598-020-71091-x

Ghosh, M.; Hartmann, H.; Jakobi, M.; März, L.; Bichmann, L.; Freudenmann, L. K.; Mühlenbruch, L.; **Segan, S.**; Rammensee, H-G.; Shipp, C.; Schneiderhan-Marra, N.; Stevanović, S.; Joos T. O. (submitted to Frontiers): The impact of biomaterial cell contact on the immunopeptidome

Review article:

Keller, B.; Tränkle, B.; Maier, J.; **Segan, S.**; Rothbauer, U. (2018): Nano- und Chromobodys für High-Content Imaging. BIOSpektrum, DOI: 10.1007/s12268-018-0919-4

8.2 Danksagung

An erster Stelle möchte ich mich besonders bei meinem Doktorvater Prof. Dr. Ulrich Rothbauer bedanken. Vielen Dank für die intensive Betreuung und ständige Unterstützung, sei es im Labor, bei der Datenanalyse, Besprechung der Ergebnisse und beim Schreiben. Danke für deine Mühen, deine Zeit, dein immer offenes Ohr bei Problemen und die ermunternden Worte in schwierigen Situationen.

Des Weiteren möchte ich mich bei Jun. Prof. Peter Loskill für die Begutachtung dieser Arbeit bedanken.

Ein riesiger Dank geht auch an die besten Kollegen der Welt Dr. Julia Maier, Dr. Philipp Kaiser, Dr. Björn Tränkle, Funmilayo Fagbadebo, Yana Parfyonova und Teresa Wagner für die fachliche Unterstützung aber auch die tolle Zeit und Arbeitsatmosphäre. Danke euch allen für die schöne Zeit im Labor aber auch nach der Arbeit.

Auch bedanken möchte ich mich bei meinen Kollegen und den anderen Doktoranden am NMI, die meine Zeit auf der Arbeit bereichert haben. Insbesondere danke ich Ricarda Stock, Pauline Jeckel, Sabrina Vogel, Nicole Anderle, Marius Busche und Florian Billing für eure moralische Unterstützung und die lustige Zeit außerhalb der Arbeit.

Ein Dankeschön für die stetige Unterstützung dieser Arbeit geht an den Forschungscampus „Systemimmunologie an biologisch-technischen Grenzflächen“ und die dortigen Kollegen. Danke hierbei besonders an Dr. Hanna Hartmann und Dr. Christopher Shipp für die gute Organisation der vielen Aufgaben und Teilprojekte.

Ganz besonders möchte ich mich auch bei meiner Familie, insbesondere meinen Eltern bedanken. Danke, dass ihr immer für mich da seid und die uneingeschränkte Unterstützung während des Studiums und dieser Arbeit.

Mein allergrößtes Dankeschön gilt meiner Freundin Janine Thomas. Danke für deine Unterstützung, deine Geduld und dass du ständig an mich geglaubt hast und wenn nötig, mit neuer Motivation versorgt hast.